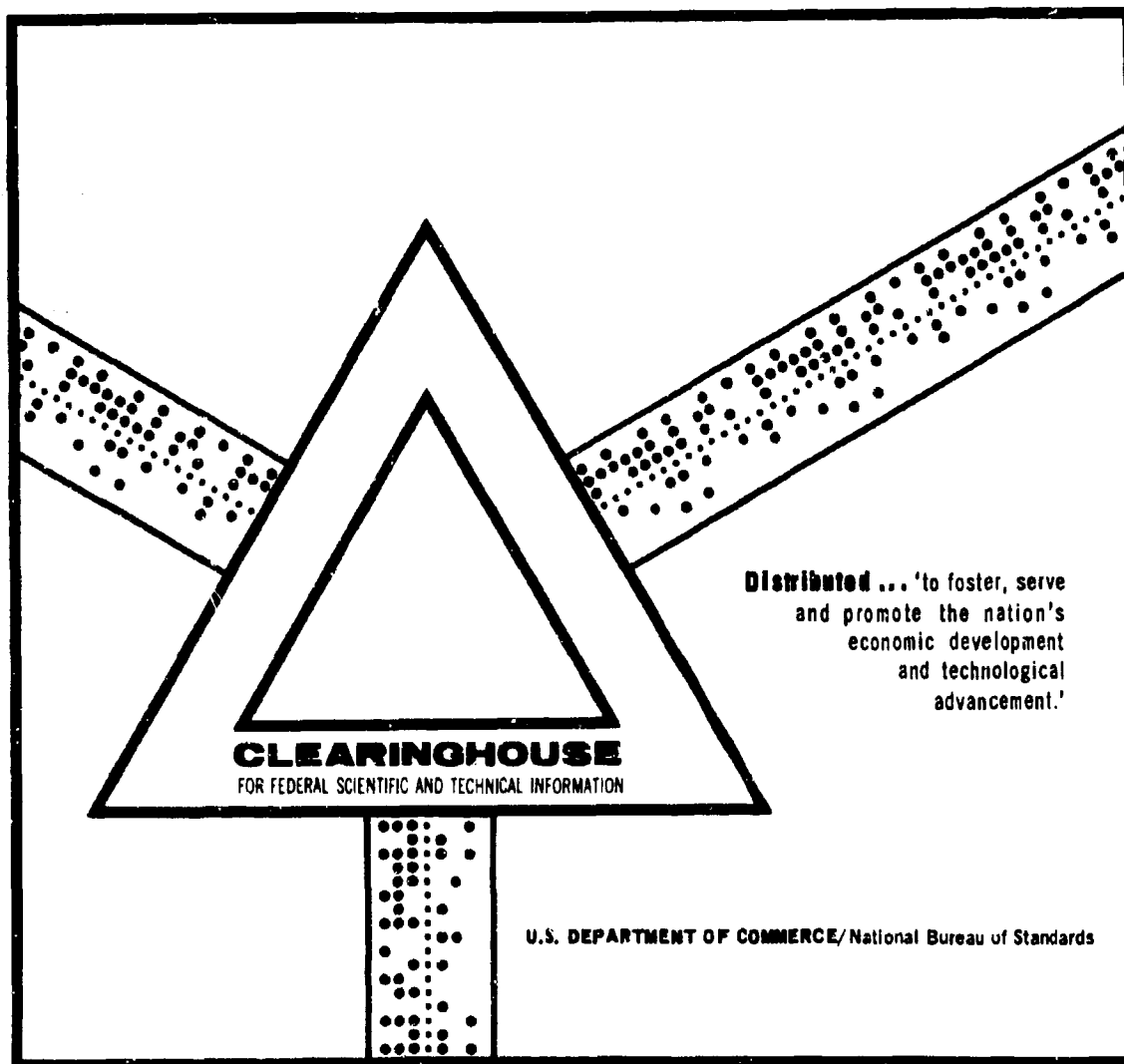# IMPLOSIONS IN PRESSURE VESSELS, EXPERIMENTAL RESULTS

Harold M. Kusano

Naval Civil Engineering Laboratory
Port Hueneme, California

February 1970

CLEARINGHOUSE
FOR FEDERAL SCIENTIFIC AND TECHNICAL INFORMATION

Distributed ... 'to foster, serve
and promote the nation's
economic development
and technological
advancement.'

U.S. DEPARTMENT OF COMMERCE/National Bureau of Standards

This document has been approved for public release and sale.

AD702781

Technical Note N-1059

IMPLOSIONS IN PRESSURE VESSELS,
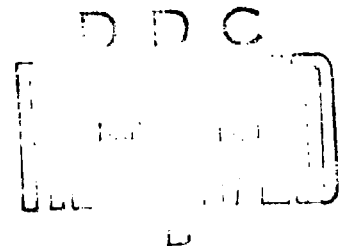
EXPERIMENTAL RESULTS

By

H. M. Kusano

February 1970

This document has been approved for public
release and sale; its distribution is unlimited.

NAVAL CIVIL ENGINEERING LABORATORY
Port Hueneme, California 93041

DDC

88

IMPLOSIONS IN PRESSURE VESSELS, EXPERIMENTAL RESULTS
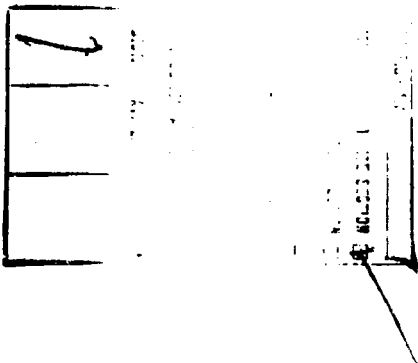
Technical Note N-1059

Y-R009-03-01-004

by

H. M. Kusano

ABSTRACT

Pressure vessels were subjected to implosion-generated hydrodynamic
pressures/impulses. The experimental results indicate the hydrodynamic
pressure and the dynamic response of the pressure vessel vary, depending
upon (1) model size, (2) implosion pressure, and/or (3) distance from
implosion; graphs showing these relationships are presented.

Implosion pressures up to 19,000-psi were obtained. The higher
implosion pressures occurred in the 20,000 psi pressure vessel and
caused damage to O-rings and mounting facilities inside the pressure
vessel, and loosened pipe connections from the top cover plug. High-
speed motion pictures showed that the collapse of air cavities was
generally asymmetric and inconsistent. The critical model sizes for
maximum pressure drop or energy release in pressure vessels were
determined. The effects of implosion on pressure vessels can be reduced
greatly by filling the test sphere with water.

CONTENTS

INTRODUCTION

In connection with deep-ocean studies, there is great interest in the structural behavior of various hollow-shelled objects under high hydrostatic pressure. Testing of these objects is usually performed in pressure vessels, and, because of the dangers to the personnel and equipment involved in such tests, it is essential to determine the effects of implosions on pressure vessel response and structural integrity. The Naval Facilities Engineering Command (NAVFAC) requested that the Naval Civil Engineering Laboratory (NCEL) investigate the problem and provide criteria for implosion testing in pressure vessels.

The objective of this task was to determine the energy release and the impulse function resulting from the collapse of test objects in pressure vessels. The end product desired is an implosion safety criteria for pressure vessels.

SCOPE

The study of implosion effects on pressure vessel response was divided into three areas: (1) energy released in the pressure vessel; (2) hydrodynamic pressure; and (3) dynamic response of the vessel. The factors considered most significant in the implosion effects were varied; the variables were (1) model size, (2) implosion pressure, and (3) distance from implosion. The parameters held constant in the experiments are summarized below:

1. Ordinary tap water was used as the fluid inside the pressure vessel.

2. Temperature of the water was at normal atmospheric conditions.

3. The model content was air at atmospheric pressures.

4. The models were all spherical.

5. All models were positioned centrally in the pressure vessel.

6. The volume of water or inside dimensions of the pressure vessels tested were approximately equal.

1

Although the impulse function was not determined and experimental difficulties (See Appendix) were encountered, significant results on the hydrodynamic pressures generated by the implosion and on the dynamic pressure vessel response were obtained. The experimental data were analyzed in two parts: (1) low-pressure implosion tests (0- to 300-psi) and (2) high-pressure implosion tests (3,000- to 19,000-psi). Theoretical solutions for predicting maximum pressure drop and energy release in pressure vessels were developed.

TEST ITEM DESCRIPTIONS

Low-Pressure Implosion Tests

Test Cylinders. The vessels for low-pressure implosion tests were made of steel, aluminum, and glass (Figure 1); their overall dimensions and capabilities are presented in Table 1. The different cylinders were selected to determine some general principles of their dynamic response to implosions. The load capacity of the steel and aluminum cylinders is based on the maximum sealing pressures, and that for the glass cylinder on maximum burst strength. Two 1-inch-thick by 24-inch-diameter aluminum plates and hard rubber gaskets or O-rings were used to seal the ends of the cylinders. The sealing pressures were attained by connecting the two end plates with sixteen evenly spaced 1/2-inch steel rods, threaded at the ends; constant tension in the steel rods was obtained using a calibrated torque wrench.

Implosion Models. The models tested were Christmas ornaments with diameters ranging from 2-1/4 to 4 inches (Figure 2); the wall thickness in all cases was approximately 1/32 inch. These models were inexpensive and commercially available. The protrusion of the ornaments was sealed with epoxy.

Table 1. Cylinders Used For Low-Pressure Implosion Tests

Cylinders	Length (in.)	Inside Diameter (in.)	Thickness (in.)	Volume (in.^{3})	Maximum Capacity (psi)
Steel	36	17	½	6,167	300
Aluminum	36	17	½	8,167	300
Glass	36	17½	3/16	8,409	80

High-Pressure Implosion Tests

Pressure Vessel. The high-pressure implosion tests were conducted in NCEL's 18-inch-diameter by 36-inch-long (inside dimensions) pressure vessel which has a working capacity of 20,000 psi.

Implosion Models. Glass spheres, with diameters ranging from 3 to 10 inches, were tested (Figure 3). The 3- to 6-inch spheres were fishnet floats; the thickness of the walls was not known and could not be measured because the floats disintegrated at failure. The 10-inch glass spheres with 5/16-inch wall thickness, manufactured by Corning Glass Works, were fabricated by sealing two hemispheres with an adhesive.

INSTRUMENTATION

The oscilloscopes available for recording transient responses were: (1) two Dual Beam, Type 565, (2) two Dual Beam, Type 502A, and (3) one Storage, Type RM564. Four Polaroid cameras were used to photograph oscilloscope displays. The oscilloscopes and the cameras were manufactured by Tektronix, Inc.

The pressure transducers developed by Protocon Research Products were used to measure the hydrodynamic pressure generated by the implosions. These transducers were placed in two water-tight pressure probes, one for low pressures and one for high pressures. The low-pressure probe was made to be positioned directly above and at various distances from the implosion center; the high-pressure probe was limited to one distance (8 inches from the implosion).

Strain measurements for the low-pressure cylinders were obtained using electrical-resistance die-cut foil strain gages manufactured by Dentronics. Strain gages were installed on the top cover (outer surface) to measure the tangential and radial strains at 2 inches from the center. Two other gages were placed at the mid-length of the cylinder wall to measure circumferential and longitudinal strains. For the 20,000-psi pressure vessel, wire-type strain gages (manufactured by Baldwin) were used to measure the circumferential and longitudinal strains at mid-length of the vessel wall.

Accelerometers, manufactured by Endevco, were used to measure the accelerations at center of the top cover and at mid-length of the cylinder wall for the low-pressure tests and the accelerations of the top cover for the high-pressure tests.

3

The approximate response ranges and frequencies for the various transducers are presented below:

Pressure Transducer	Pressure Range (psi)	Diaphram resonant Frequency (cps)
Type 401	0 to 5,000	110,000
Type 402R	0 to 50,000	60,000

Accelerometer Model 2225

Range	0 to ± 10,000 g
Maximum Shock	20,000 g
Frequency Response	0 to 15,000 cps
Mounted Resonant Frequency	80,000 cps

Strain Gages

Resistance	120 ohms
Gage Length	1.0 inch
Capacity	3,000 μ in/in.

ENERGY-RELEASE PREDICTION CURVES

To determine critical implosion parameters, theoretical solutions predicting pressure drop and energy release in pressure vessels were derived as described in this section. The results are presented in the Discussion.

Pressure Drop

The prediction of the hydrostatic pressure after implosion was based on the amount of water added to the pressure vessel because of pressure vessel expansion and on the compressibility of the water and the model contents. The following notations are used:

V_t = volume of the pressure vessel, in.^{3}

V_m = volume of the model, in.^{3}

ΔV_w = added volume of water, in.^{3}

K_t = coefficient of expansion of the pressure vessel, in^3/psi

K = coefficient of compressibility of water, 1/psi

4

P_a = ambient pressure in the model, psi

P_1 = hydrostatic pressure an instant before implosion, psi

P_2 = hydrostatic pressure after implosion, psi

r = ratio of volume of air in model to model volume

With the model in the vessel, the added volume of water necessary to cause implosion can be determined from the following equation:

$$\Delta V_w = K_t P_1 + K(V_t - V_m)P_1 \tag{1}$$

Upon collapse of the model, the added volume of water remains in the system and the compressed water and the pressure vessel expand and contract, respectively, to fill the excess volume created by implosion of the model. The system reaches equilibrium at a lower hydrostatic pressure than that which existed prior to the implosion. The new equilibrium condition can be expressed approximately as:

$$\Delta V_w = K_t P_2 + K(V_t - rV_m)P_2 + \Delta V_a \tag{2}$$

where ΔV_a is the change in volume of air in the model. From Boyle's Law,

$$\Delta V_a = \frac{rV_m P_2}{P_a + P_2} \tag{3}$$

Substituting Equation 3 into 2 and rearranging the terms, the equation for equilibrium becomes:

$$\Delta V_w = P_2 \left[K_t + K\left(V_t - rV_m\right) + \frac{rV_m}{P_a + P_2} \right] \tag{4}$$

Since the added volume of water is the same before and after implosion, Equations 4 and 1 can be combined. Thus, the solution for the final pressure is:

$$P_2 = \frac{-B + \sqrt{B^2 + 4AC}}{2A} \tag{5}$$

where
$$A = K_t + K(V_t - rV_m)$$

$$B = AP_a + rV_m - K_1 P_1$$

$$C = K_1 P_1 P_a$$

$$K_1 = K_t + K(V_t - V_m)$$

5

The pressure drop, pressure ratio, and volume ratio are defined here as $P_1 - P_2$, P_2/P_1, and V_w/V_c, respectively. The pressure drop and pressure ratio are related, as the one increases, the other decreases.

Energy Release

Energy release is defined here as the decrease in the potential energy (P.E.) of the system resulting from the implosion. Essentially, it is the function of the pressure drop. Using previous derivations and notations, the potential energies before and after implosion are, respectively,

$$P.E._1 = 1/2 \left[\Delta V_w P_1 \right] \tag{6}$$

$$P.E._2 = 1/2 \left[\Delta V_w P_2 \right] \tag{7}$$

Subtracting Equation 7 from Equation 6, the energy released is expressed by:

$$P.E. = 1/2 \left[\Delta V_w (P_1 - P_2) \right] \tag{8}$$

Graphically, energy released can be represented by the shaded area in the sketch below:

6
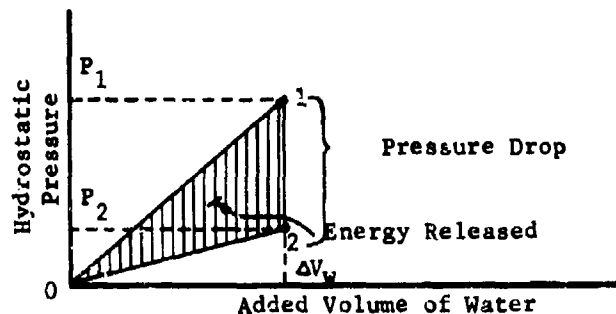
DISCUSSION OF RESULTS

The discussion of results has been divided into three sections:
(I) Energy Release/Pressure Drop, (II) Hydrodynamic Pressure, and
(III) Dynamic Response. Both low (0-300 psi) and high (3,000-19,000 psi)
pressure implosion test results are included in each section.

I. Energy Release/Pressure Drop

Prediction curves based on previous derivations are presented and
experimental results on pressure drop are discussed in this section.
Prediction curves illustrating the effect due to the variation on model
content are also presented. Finally, the critical model parameters
based on the prediction curves are discussed.

Coefficients. The coefficient of compressibility (K) of water at
low pressure was taken to be 3.4×10^{-6} per psi[*] and that at high
pressure was taken to be approximately 2.6×10^{-6} per psi.[**]

The coefficient of expansion (K_t) for the various pressure vessels
was determined from the experimental results of Figures 4 and 5 and
from Equation 1 with V_m equal to zero. The results are tabulated below:

Pressure Vessel	K_t (in. 3/psi)
Glass	0.378
Aluminum	0.179
Steel	0.139
20,000-psi vessel (steel)	0.0023

Prediction Curves. Pressure prediction curves based on the previous
derivations and the above coefficients were determined for the steel
and aluminum cylinders and the 20,000-psi pressure vessel, as shown in
Figures 6, 7, and 8, respectively. The corresponding curve for the
glass cylinder was not computed because no experimental data were
obtained to compare with it. Examples of the energy-release prediction
curves are shown in Figures 9 and 10 for the steel cylinder and the
20,000-psi vessel, respectively.

Since the implosion pressures varied considerably for models of
the same volume, pressure prediction curves (Figures 11, 12, and 13)
were developed for a given model size. These curves were determined
from Figures 6, 7, and 8 for the various models tested by plotting
the pressure ratio P_2/P_1 as a function of the implosion pressure; the
dashed or solid lines represent the semi-empirical solution.

Low-Pressure Test Results. The experimental results for the
pressure drop are shown in Figures 11 and 12, each plotted point
represents the data from one or more tests. Although some scatter was
observed, the correlation between experimental results and the predicted
pressure curves was adequate for implosions of the smaller models that

---

[*] F. W. Sears and M. W. Zemansky, University Physics, 2nd edition,
Massachusetts, Addison-Wesley, 1955, page 187.

[**] V. L. Streeter, Handbook of Fluid Dynamics, 1st edition, New York,
McGraw-Hill, 1961, page 1-4.

collapsed between 100 and 300 psi. However, the correlation for the 4-inch models that collapsed below 50 psi was unsatisfactory because the low values of hydrostatic pressure were not recorded accurately.

High-Pressure Test Results. The correlation between the experimental and predicted results, Figure 13, was unsatisfactory for implosions of the 4-inch and 6-inch models and for the 10-inch models that collapsed beyond 15,000 psi. The volume change of the air void based on Boyle's Law was inadequate for high pressures. The ΔV_a was, therefore, redetermined to be 0.714 V_m using a bulk modulus equal to 1.4 times the pressure.* Substituting the new ΔV_a into Equation 4, the alternate prediction curves are also presented in Figure 13. The latter prediction curves were closer to the experimental values, except for the 10-inch spheres that collapsed beyond 15,000 psi. For these spheres, the error was due to water leakage during the implosion.

Varied Contents in Models. To illustrate the effect of varying the air content of the models, the pressure and energy release prediction curves for the steel cylinder for five values of the air void ratio, r, are shown in Figures 14 and 15. For r <1.00, water was assumed to occupy the remaining void. For these curves, the implosion pressure was arbitrarily selected to be 1,000 psi.

The results of Figures 14 and 15 indicate a significant effect on the pressure drop and the energy release prediction curves when the model void is filled with water. In general, the results show that for a given implosion pressure and a given model size, the pressure ratio increased (or the pressure drop decreased) as the volume of air in the model was decreased. For r = 0 and constant implosion pressure, the pressure ratio (Figure 14) decreased very slightly as the model size increased. In essence, filling the spheres with water reduces the implosion effects on the pressure vessel.

Critical Model Sizes. From the prediction curves, the critical model sizes (or V_m/V_t) generating maximum pressure drop or energy release can be determined for varied implosion pressures. In Figure 9 and 10, the range of critical model sizes occurs when the energy release curve is nearly horizontal; or, essentially, when the model volume is equal to or greater than the added volume of water ($V_m \geq \Delta V_w$). In Figure 10, the slope of the curves changed significantly for high pressure tests as delineated by the dashed line.

The most critical model sizes and implosion pressures causing pressure vessels to fracture have not been determined because the hydrodynamic pressure response data were insufficient in quantity and range.

II. Hydrodynamic Pressure

The pressure-time data were obtained only from the low-pressure tests conducted in the aluminum cylinder; those from the glass and steel cylinders and from the 20,000-psi pressure vessel were not

---

*ibid., page 1-4.

8

obtained, because the pressure transducer was not available and/or was damaged. The theoretical solution for predicting the hydrodynamic pressure was not determined; only experimental results are discussed. The error is estimated to be as high as $\pm$ 15 percent; data beyond the average trend were discarded.

Pressure Magnitudes. The maximum hydrodynamic pressure* and pressure amplitude** as functions of the implosion pressure, distance from implosion, and model size are presented in Figures 16, 17, and 18, respectively. The latter two figures, which required some extrapolation, were determined directly from Figure 16. Each data point (Figure 16) represents the result of a single test; the solid lines indicate the approximate trend of the hydrodynamic pressure and pressure amplitude at three different distances from the implosion center. The hydrodynamic factor (D.F.) represented by dashed lines (Figure 16) is defined as the ratio of the hydrodynamic pressure to the implosion pressure.

The results of Figure 16 indicates that the hydrodynamic pressure increases as the implosion pressure and distance from implosion increase and decrease, respectively; the model size is constant. For example, the D.F. for the hydrodynamic pressure increased from 2.0 to 3.0 for the 2-1/4-inch models that collapsed at from 180 to 235 psi with an implosion distance of 3 inches; in contrast, the D.F. decreased slightly with an implosion distance of 8 and 14-5/8 inches. The D.F. varied similarly for the other model spheres. The pressure amplitudes (Figure 16) were also similarly affected as the implosion pressure increased.

The hydrodynamic pressure and pressure amplitude versus distance from the implosion are shown in Figure 17; the three constant implosion pressures indicated are within the collapse range of that particular model. The results indicate the maximum hydrodynamic pressure and amplitude decreased as the distance from the implosion center increased, and they decreased more rapidly as the implosion pressure increased.

Finally, Figure 18 indicates the maximum pressure magnitude increased as the model size increased from 2-1/4- to 3-1/4 inches in diameter with an implosion pressure of 200 psi. The cause for the lower results from the 2-5/8-inch spheres is not known. For implosion pressures other than 200 psi, similar relations can be determined.

Frequencies. Approximate values of the hydrodynamic pressure frequency from implosions of the 2-1/4- and 2-5/8-inch spheres were obtained. The results, presented later, were compared with the dynamic strain frequencies. Those from implosions of the larger-size models were not determined since the pressure oscillation records were not distinct.

III. Dynamic Response

Theoretical solutions for predicting dynamic response of pressure vessels were not determined; experimental results are discussed for

---

* Difference between zero static pressure and peak hydrodynamic pressure.
** Difference between maximum and minimum hydrodynamic pressures.

(1) low-pressure implosion tests (0- to 300-psi) and (2) high-pressure implosion tests (3,000- to 19,000-psi). Static pressure-strain curves were also determined for comparison with the dynamic strains.

Static Pressure-Strain Curves. The pressure-strain calibration curves for the steel, aluminum, and glass cylinders and the 20,000-psi pressure vessels are shown in Figures 19 through 23. The effect of pretension of the sixteen 1/2-inch steel rods on the three test cylinders appears to be negligible; in Figure 20, the effect is enhanced because of the larger horizontal scale.

The longitudinal strains (Figure 20), after some slight increase, decreased as the hydrostatic pressure increased; this may have been caused by reversed strain gage electrical leads, pretensioned effect of the steel rods, and/or large deflection effect of the end-plates. Although the static results (Figure 20) are presented, they were not used for comparison with the dynamic strains because the longitudinal dynamic strain data records were not distinct enough to reduce.

The tangential and radial strains of the top cover, shown in Figures 21 and 22, were probably affected by the elastic properties of the cylinders even though the same cover was used on all cylinders.

The static strains for the 20,000-psi pressure vessel (Figure 23) were calibrated to 14,000-psi and then extrapolated to 20,000-psi.

Low-Pressure Implosion Test Results. The data analyzed were obtained from the tests in the steel and aluminum cylinders; the tests in the glass cylinder did not provide any reducible data. The experimental error is estimated to be as high as $\pm$ 10 percent. The dynamic response analysis included: (a) dynamic strain magnitudes, (b) frequencies, and (c) accelerations.

A. Dynamic Strain Magnitudes. The dynamic strain analysis was divided into two parts: (1) the maximum dynamic strain[*] and (2) the maximum strain amplitude.[**] These two parameters were plotted as functions of the implosion pressure, shown in Figures 24 through 27; each point represents the result of a single test, while the dashed lines indicate the approximate trend. The dynamic strain factor, D.F., (ratio of the dynamic strain to static strain) is also indicated on the same figures. The circumferential dynamic strain (Figures 24 and 25) was slightly influenced by the variation in the implosion pressure for models of the same size. For example, the maximum D.F. of the 2-1/4-inch models with a collapse range of from 180 to 280 psi was approximately constant at 1.5 for the aluminum cylinder and 1.8 for the steel cylinder. For the 3-1/4-inch models collapsing at less than 100 psi in the aluminum cylinder, the D.F. was less than 1.0; however, when extrapolated to 250 psi, the D.F. increased to 2.0. The D.F.'s varied similarly for the other models of different sizes and collapse pressure ranges.

---

[*] Measurements from zero strain to peak strains.
[**] Measurements between two opposite peaks.

10

The tangential and radial dynamic strains of the top cover (Figures 26 and 27) were less affected than those of the cylinder walls: the D.F.'s were generally less than 1.0.

The maximum dynamic strain amplitudes, also plotted in Figures 24 through 27, were included to provide data for determining minimum or negative dynamic strains (maximum dynamic strain minus strain amplitude). The results of the 2-5/8-inch models indicated slight negative strains in the steel cylinder wall; the others indicated minimum dynamic strains. Negative strains may indicate possible stability failure of thin-shelled cylinders.

Plots of circumferential dynamic strain versus the model size (Figure 28) were obtained from Figures 24 and 25 for an implosion pressure of 200 psi. For the model sizes tested, the dynamic strain of the aluminum cylinder increased as the model size increased; whereas, the dynamic strain of the steel cylinder decreased slightly. For implosion pressures other than 200 psi, the effect from the variation in the model sizes may be similarly determined.

B. Frequencies. The plots of circumferential strain frequency versus implosion pressure for models of the same size did not yield meaningful results. However, if the implosion pressures had been more consistent, for example, at 100 and 300 psi, the results might have been more obvious.

The variation in the model size affected significantly the strain frequency (Figure 29); average results were plotted for models of the same size. The frequencies of the top cover (Table 2) were approximately equal to the dynamic strain frequencies of the cylinder. In general, the frequencies of the cylinder wall and top cover strains decreased as the model size increased.

The frequency of the pressure oscillations, based on two model sizes, also decreased as the model size increased (Table 2). Thus, the pressure and strain data indicate that the cylinder oscillations were caused by the hydrodynamic pressure generated by the implosion. This seems reasonable since the frequencies of the smaller oscillating air cavities are generally higher than those of the larger cavities.

The high frequency of the aluminum cylinder wall caused by the implosion of the 3-1/4-inch models (Table 2) is probably the natural frequency of the cylinder. Although the same size models were tested, the frequencies of the steel cylinder were higher than those of the aluminum cylinder; this is probably because of the difference in their elastic properties and/or sealing methods.

C. Accelerations. The average peak-to-peak acceleration versus the implosion pressure for models of the same size are shown in Figures 30 and 31; each data point represents the result of a single test. The error is estimated to be as high as $\pm$ 15 percent.

The variation in the implosion pressure affected significantly the lateral acceleration of the cylinder wall. In Figure 30, for example, the maximum acceleration of the aluminum cylinder ranged from 1400 to 3000 g for the 2-1/4-inch models that collapsed between 160 and 250 psi.

11

Table 2. Frequency Results (Average)

Model Diameters (in.)	Frequency, cps				
	Aluminum Cylinder			Steel Cylinder	
	SGH [1]	SGT & SGR [2]	Pressure	SGH	SGT & SGR
2-1/4	479	473	491	569	-
2-1/2	-	-	-	524	575
2-5/8	465	463	467	487	-
3	-	-	-	416	417
3-1/4	617	297	-	314	310
4	102	110	-	212	212

1/ SGH - circumferential strain gage on cylinder walls

2/ SGT - tangential strain gage on top cover plate
   SGR - radial strain gage on top cover plate

12

For the 3-1/4-inch models that collapsed between 75 and 150 psi, the acceleration ranged from 80 to 360 g. Similar effects are also found for the steel cylinder. In general, for models of the same size the acceleration increased as the implosion pressure increased.

For a given implosion pressure, the variation in model size appears also to affect the lateral accelerations of the cylinder wall. For example, when the acceleration curve is extrapolated to 200 psi for the 3-1/4-inch models, the results indicate acceleration increases as the model size decreases (Figure 30).

High-Pressure Implosion Test Results. Hydrodynamic pressure and acceleration data were not obtained because the severe shock of the implosion damaged the transducers. The dynamic strain data were analyzed in a manner similar to that used in the low-pressure implosion tests. Experimental error is estimated at $\pm$ 10 percent. In the implosions of the 10-inch spheres, there was considerable scatter in the data.

A. Dynamic Strains. The results of the longitudinal and circumferential dynamic strains of the pressure vessel walls, shown in Figures 32 through 35, were generally similar to those in the low-pressure tests. From Figure 32, for example, the D.F. increased from 1.0 to 3.0 for the 6- and 10-inch spheres that collapsed between 2,000 to 4,000 psi and 3,000 to 19,000 psi, respectively. In contrast, the D.F. ranged from 2.0 to 1.6 for the 3-inch spheres that collapsed from 6,000 to 15,000 psi (Figure 32).

The variation in the model size also appears to affect the dynamic strains. At 3,000 psi, for example, the D.F. decreased from 4.0 to 1.0 as the diameter of the models increased from 4 to 10 inches (Figure 32). At higher implosion pressures, no definite relation can be determined because there are not sufficient data.

The D.F.'s for the circumferential strains were less than 2.0, as shown in Figure 33. The greater effect on the longitudinal strains was probably caused by the high inertia force of the massive end covers.

The strain amplitude, Figures 34 and 35, indicate the presence of high negative dynamic strains. For example, the negative strains were approximately 420 in./in. for the 10-inch spheres that collapsed at 18,000 psi (longitudinal strain).

B. Frequencies. The frequency varied between 1,550 to 1,750 cps for the longitudinal strains and 2,000 to 2,600 cps for the circumferential strains. The relationship between the frequency, model size, and implosion pressure could not be established because of insufficient data.

INCIDENTAL INFORMATION

Implosion Models

The collapse strength of the models varied considerably, even for models of the same size and brand, as shown in Table 3. Although different implosion pressures for each model size were desired, the

13

Table 3. Collapse Pressures of Models

Tests	Model Diameters (in.)	Collapse Pressure Range (psi)
Low-Pressure Implosion	2-1/4	165 - 300
	2-1/2	210 - 305
	2-5/8	120 - 310
	3	75 - 195
	3-1/4	65 - 150
	4	14 - 66
High-Pressure Implosion	3	6,150 - 15,450
	4	1,550 - 2,650
	6	2,210 - 3,750
	10	3,050 - 19,200

considerable variation made it difficult to predict accurately the
implosion pressure and to orient the oscilloscope's triggering system;
thus, many data were not recorded.

High-Speed Motion Pictures of Implosions

High-speed motion pictures (16-mm Fastax movie camera) were taken
of the collapse of the 4-inch spheres tested in the glass cylinder. The
speed was varied from 1,000 to 5,000 frames per second. Of the many
attempts, seven implosions were filmed successfully. A series of
photographs for a typical collapse is shown in Figure 36. From the
films, various observations of the implosions were made; these are
discussed in the following paragraphs.

One significant observation was that the 4-inch spheres did not
collapse symmetrically. Some of the spheres imploded initially from
one side and caused the inflow of water to be unidirectional (Figure 37).
Others collapsed initially inward along the diameter, causing the top
and bottom halves of the spheres to burst. These asymmetrical implosions
were undesirable, since the hydrodynamic pressure distributions would be
non-uniform and/or inconsistent.

The cause of these asymmetrical implosions of the low-pressure
models (Christmas ornaments) was attributed primarily to the poor
quality of the model construction. These models were not perfect spheres,
and the shell thickness was not uniform. The models failed initially at
the weakest section before the entire sphere collapsed, resulting in
the asymmetrical collapse of the air cavity.

Other observations included the presence of numerous tiny bubbles
(possibly cavitation bubbles) and shell fragments after the implosion
occurred. The air bubbles were produced primarily by the high-speed
turbulent motion of the water flowing toward a low-pressure center,
causing the original air cavity to disintegrate into numerous tiny
bubbles. The fragments of the models were also put into high-speed
turbulent motions (Figure 38). Both the air bubbles and the high-
velocity fragments are undesirable since they may produce cavitation or
pitting damages to the cylinder wall and erroneous pressure measurements.

Attempts were made to measure the initial collapse rate of the air
cavity and the period or frequency of the cavity oscillation. However,
because of the lack of symmetry of the collapses, the presence of air
bubbles and shell fragments, and the lack of timing marks on the high-
speed film, the collapse rate and frequency were not determined.

High-Pressure Implosion Damages

The 50,000-psi pressure transducer and the accelerometers were
damaged by the severe implosion-generated shock. The shock from the
implosion loosened the pipe connections attached to the top cover,
causing water to leak (Figure 39). In several tests, water squirted
from the pipe connection. The O-rings for the top and bottom cover of
the pressure vessel were frequently damaged (Figure 40). In the first
test the O-ring for the pressure probe was severely damaged (Figure 41).

15

The mounting system for the spheres was frequently damaged by the implosions. The mounting system shown in Figure 42 was not used after the first test because the 1/2-inch aluminum rods sheared from the top cover. An alternate system (Figure 43) was used throughout the tests although it required frequent repairs. The bottom plate was warped by the tremendous suction forces of the implosions. Most of the above damages occurred when the 10-inch models collapsed at pressure greater than 10,000 psi. However, implosions of the 3-inch models that collapsed at pressures from 10,000 to 15,000 psi did not cause any obvious damage.

The inside surface of the pressure vessel was slightly pitted, but this was not detrimental. Severe pitting would have occurred if the models had been imploded adjacent to the pressure vessel wall.

FINDINGS

1. For the range of tests conducted, the pressure drop prediction curves were satisfactorily determined for implosions of glass spheres in pressure vessels.

2. The critical model size (that which causes maximum pressure drop or energy release in pressure vessels) can be determined for different implosion pressures.

3. The implosion-generated hydrodynamic pressure and the low pressure vessel dynamic strains generally increased as the model size and collapse pressure increased and distance from implosion decreased.

4. The frequency of the cylinder response and the hydrodynamic pressure oscillation decreased as the model size increased; the effect of variation in the implosion pressure on the frequency was negligible and/or indeterminable.

5. The lateral acceleration of the cylinder increased as the implosion pressure increased and model size decreased; the distance from the implosion was constant.

6. The dynamic response of the high-pressure vessel increased as the implosion pressure increased and model size decreased.

7. High-speed motion pictures showed that the spherical models did not collapse symmetrically or consistently, thus indicating a non-uniform hydrodynamic pressure distribution.

8. The 10-inch glass spheres collapsing above 10,000 psi damaged O-rings and mounting facilities inside the pressure vessel and caused the top cover pipe connections to loosen.

9. The implosion effects on pressure vessels can be greatly reduced by filling the test spheres with water.

CONCLUSIONS

1. Although significant results were obtained, the data presented should be used only for rough or preliminary analysis.

2. Further theoretical studies and experimental data are necessary before implosion safety criteria for pressure vessel can be determined with reliability.
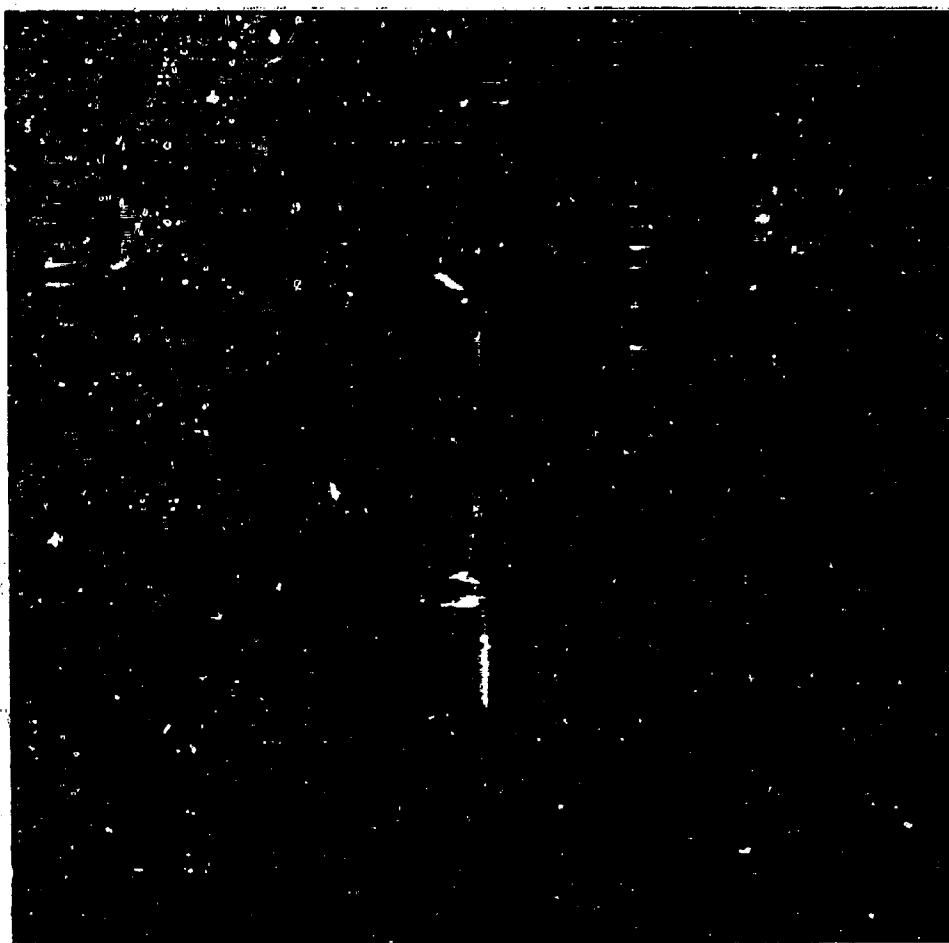
Figure 1. Cylinders for low-pressure implosion tests.

18
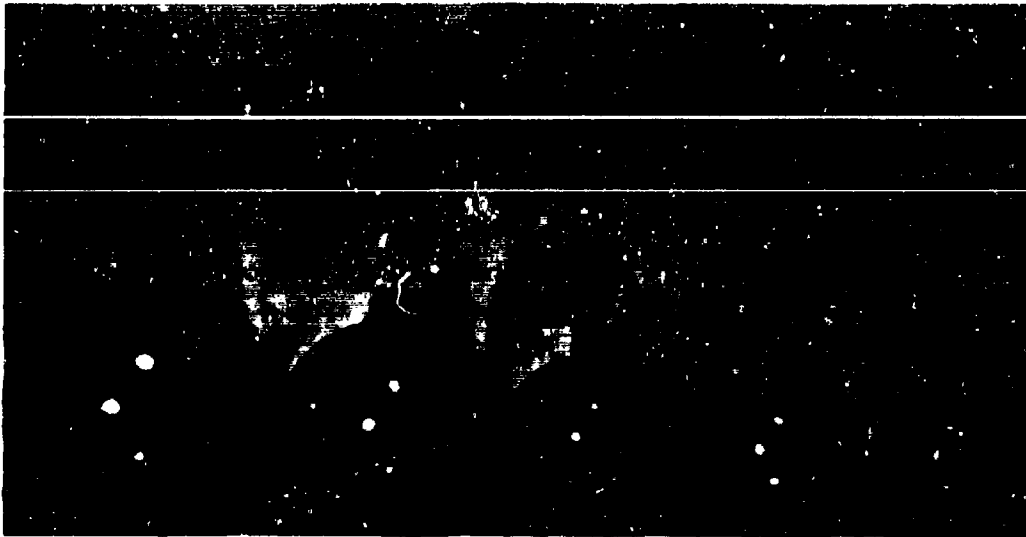
Figure 2. Models for low-pressure implosion tests. Size
range from 4-inch to 2½-inch diameters.
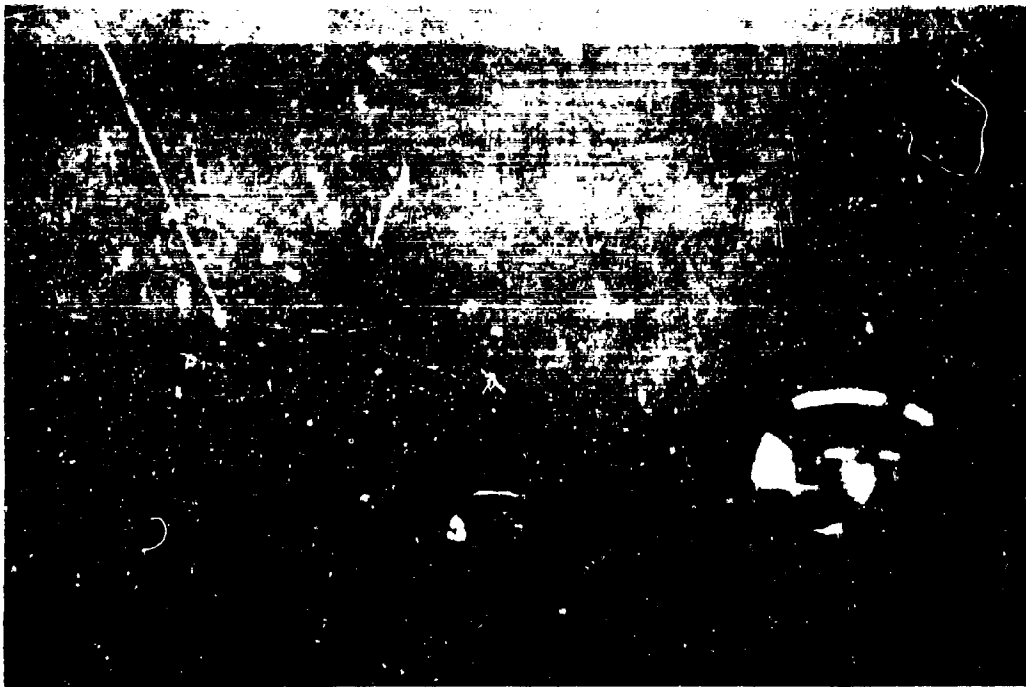
Figure 3. Glass spheres for high-pressure implosion tests.
Size range from 3-inch to 10-inch diameters.
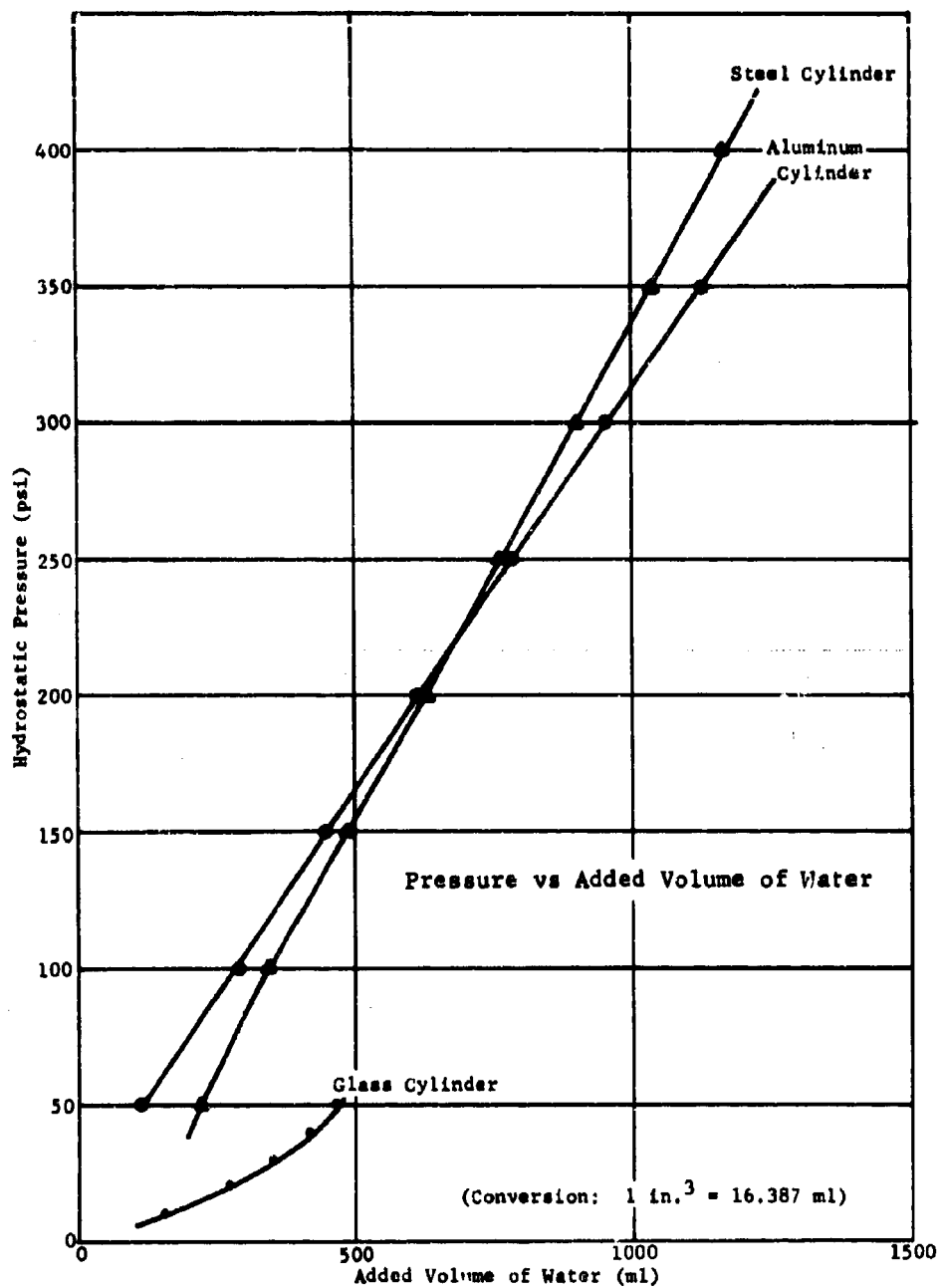
Figure 4. Pressure versus added volume of water for the low-pressure test cylinders.
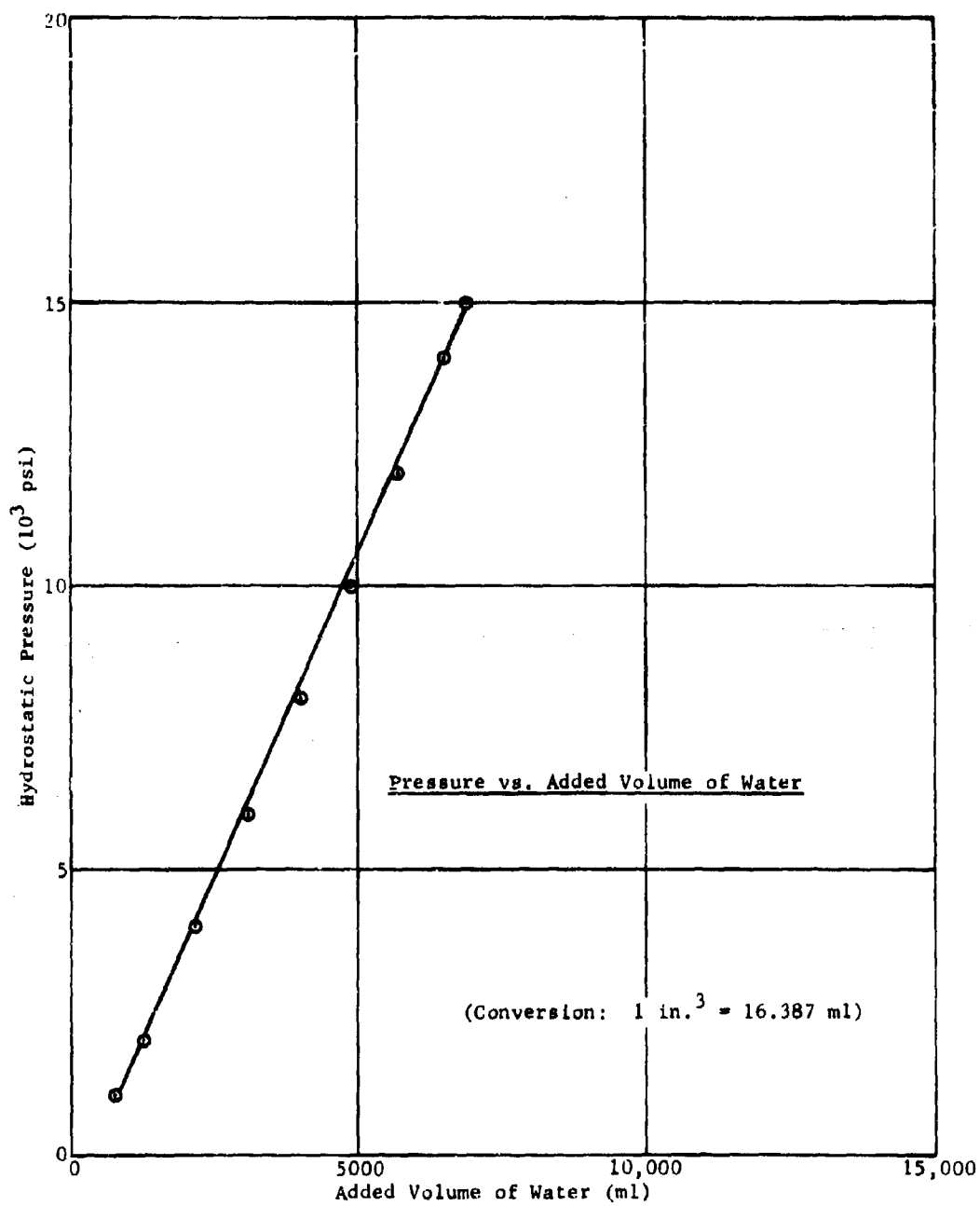
Figure 5. Pressure versus added volume of water for the 20,000-psi
pressure vessel.
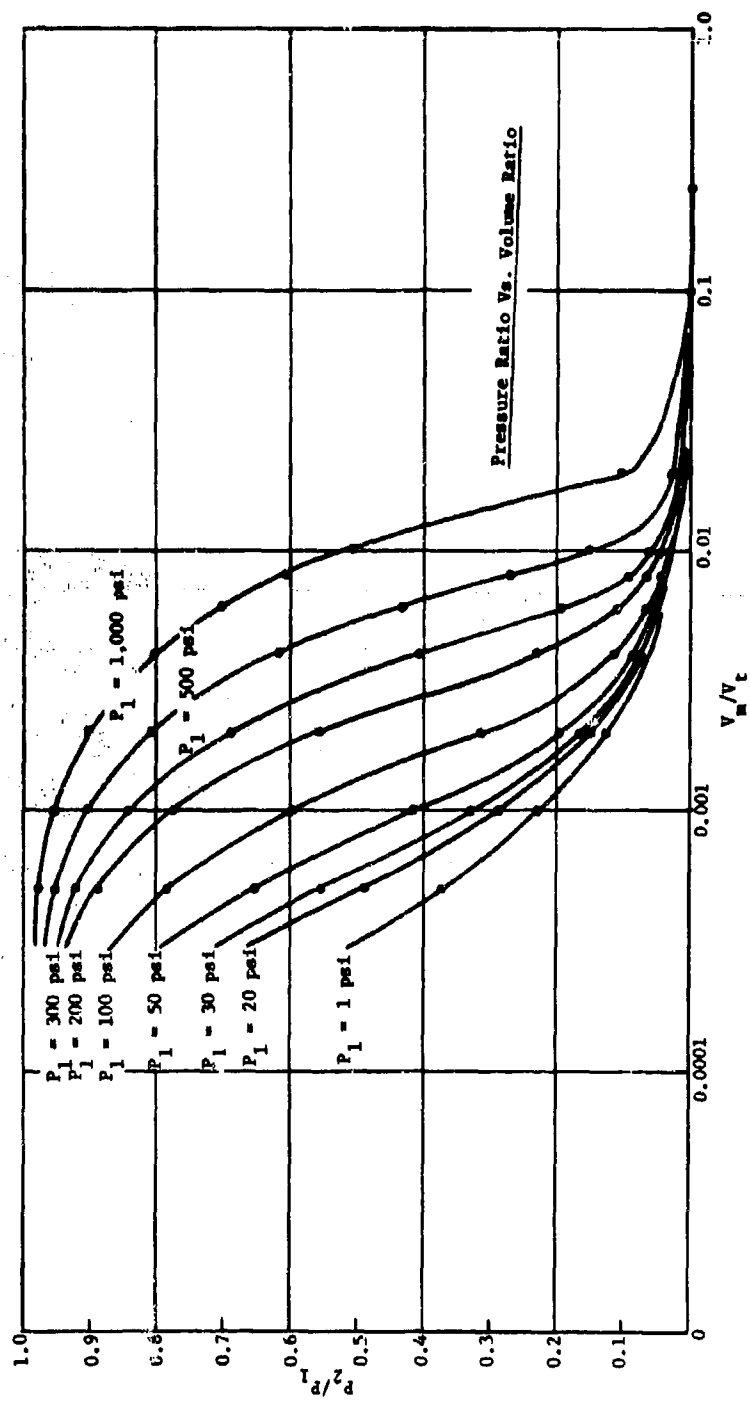
Figure 6. Pressure prediction curves for the steel cylinder.
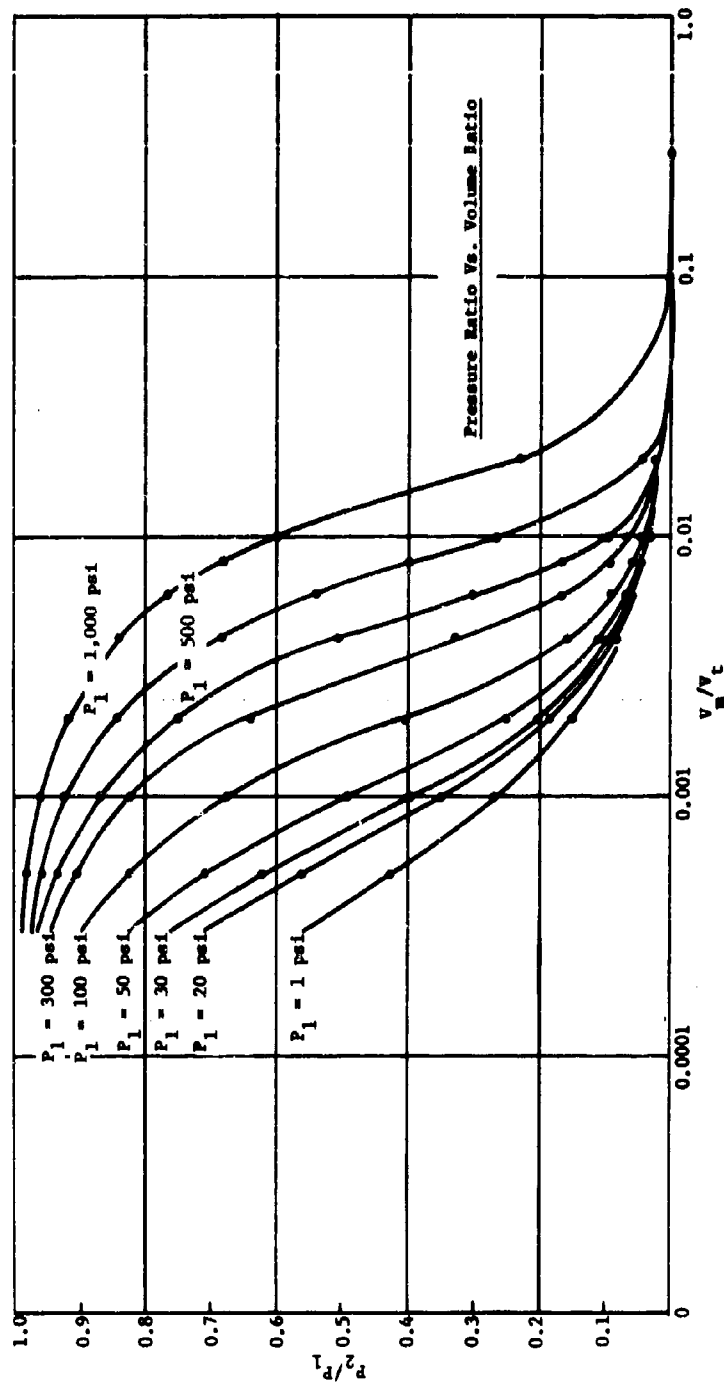
Figure 7. Pressure prediction curves for the aluminum cylinder.
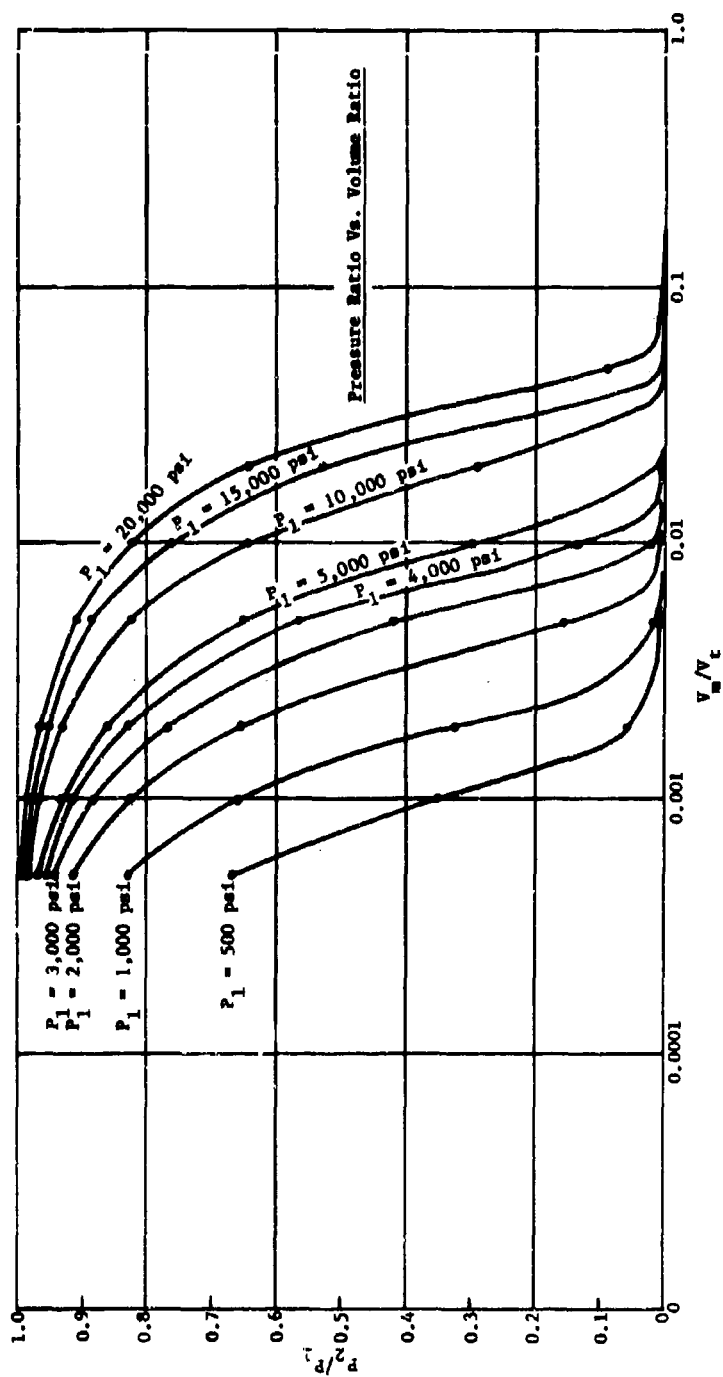
Figure 8. Pressure prediction curves for the 20,000-psi pressure vessel.

24
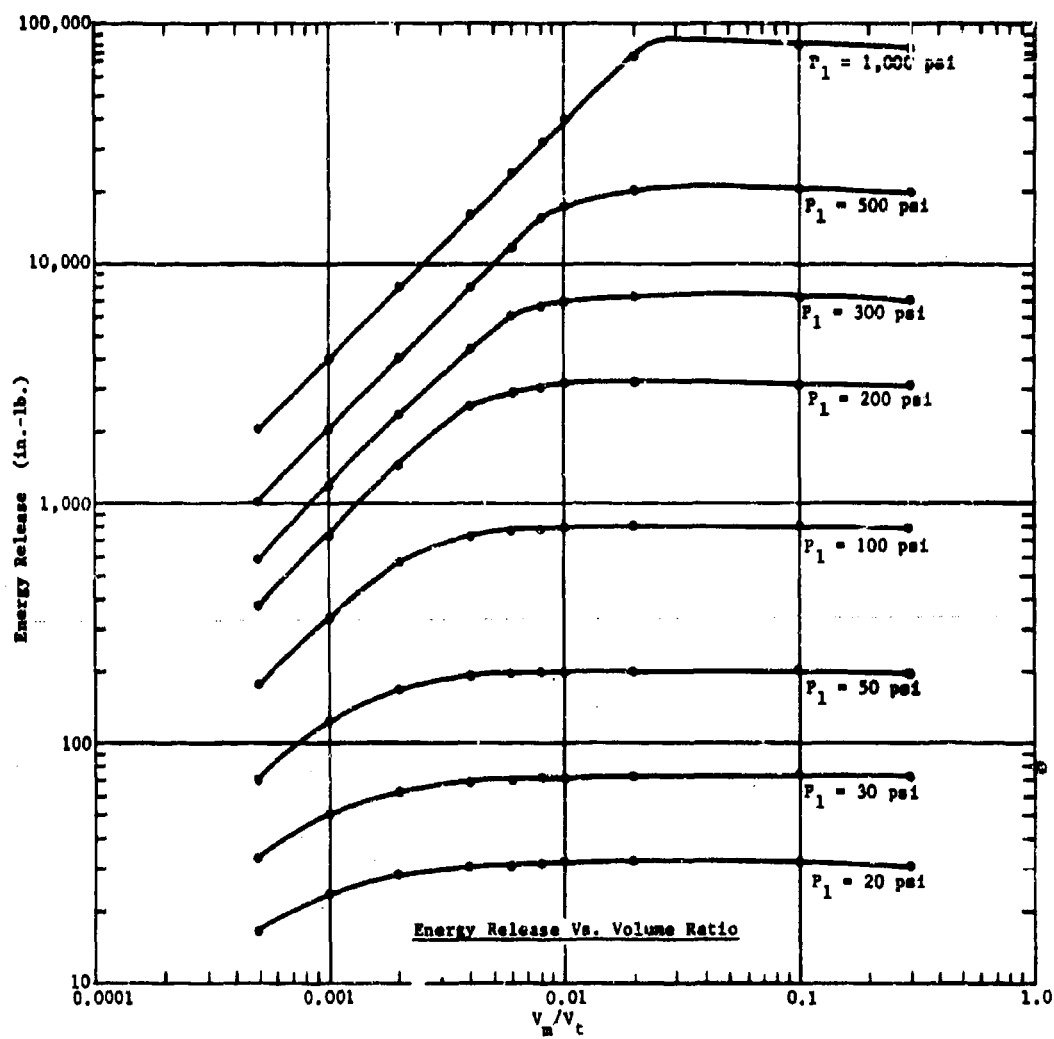
Figure 9. Energy-release prediction curves for the steel cylinder.

25
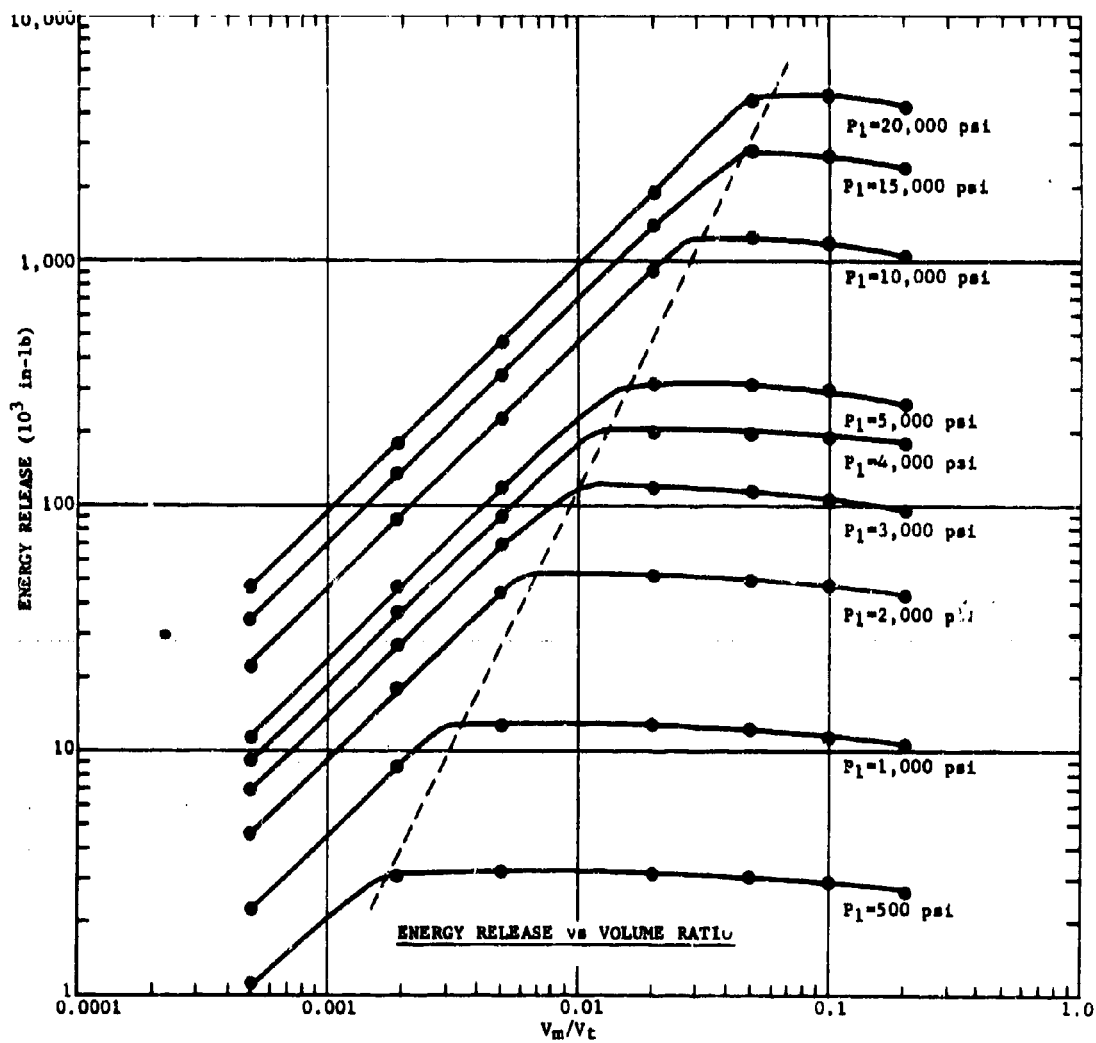
Figure 10. Energy-release prediction curves for the 20,000 psi capacity pressure vessel.
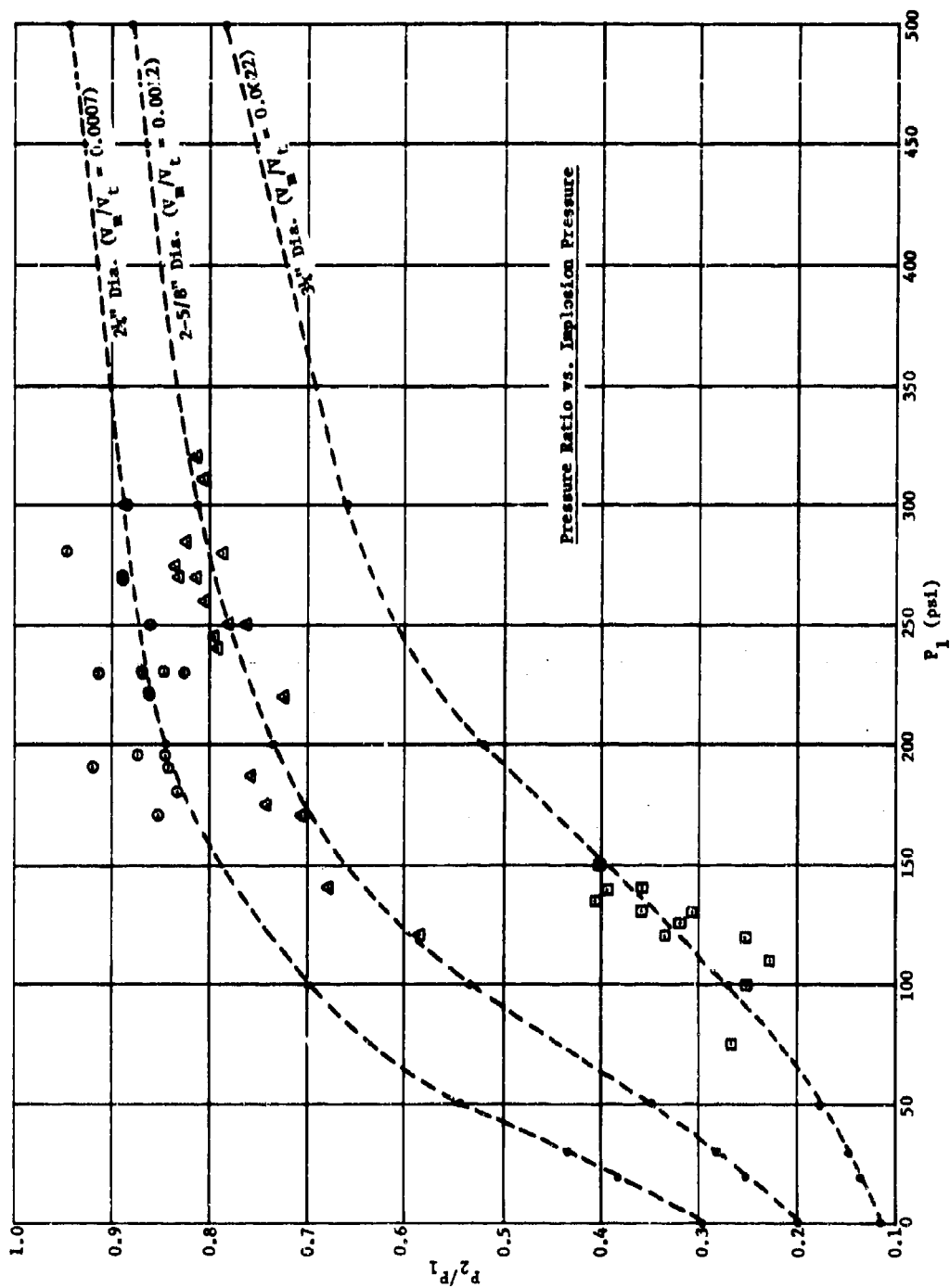
Figure 11a. Pressure-prediction curves for the steel cylinder for various models tested.
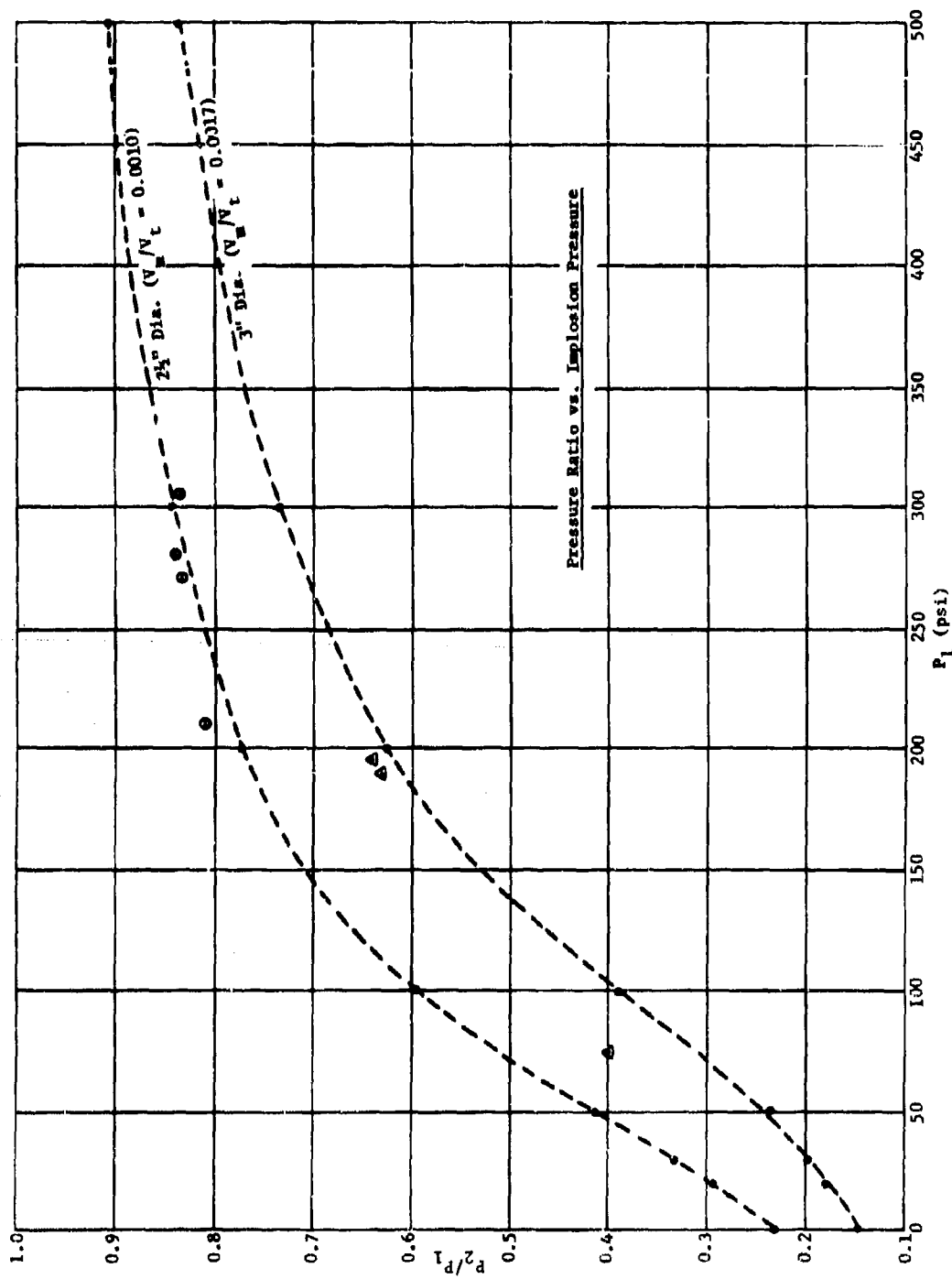
Figure 11b. Pressure-prediction curves for the steel cylinder for various models tested.

28
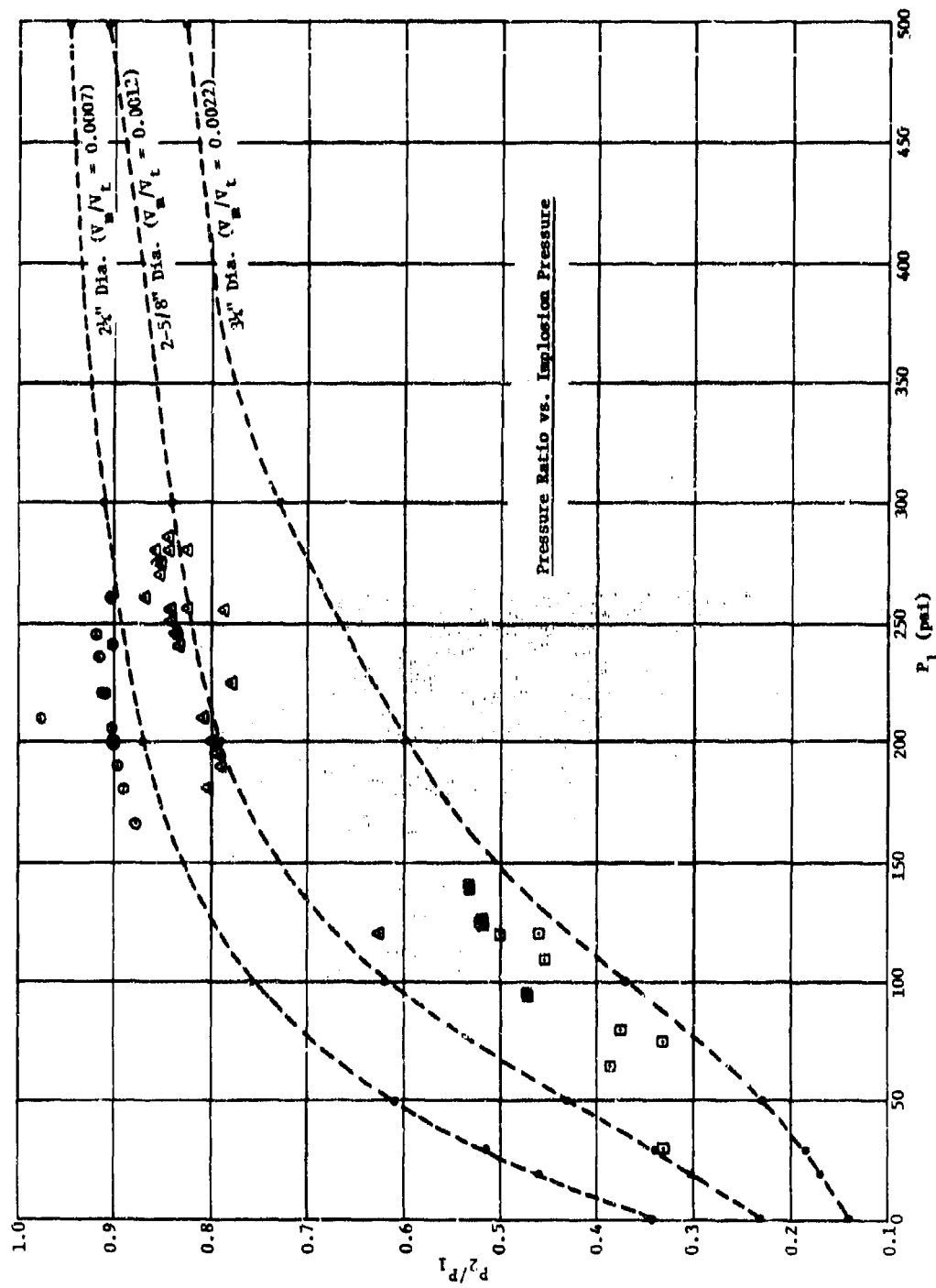
Figure 12a. Pressure-prediction curves for the aluminum cylinder for various models tested.

29
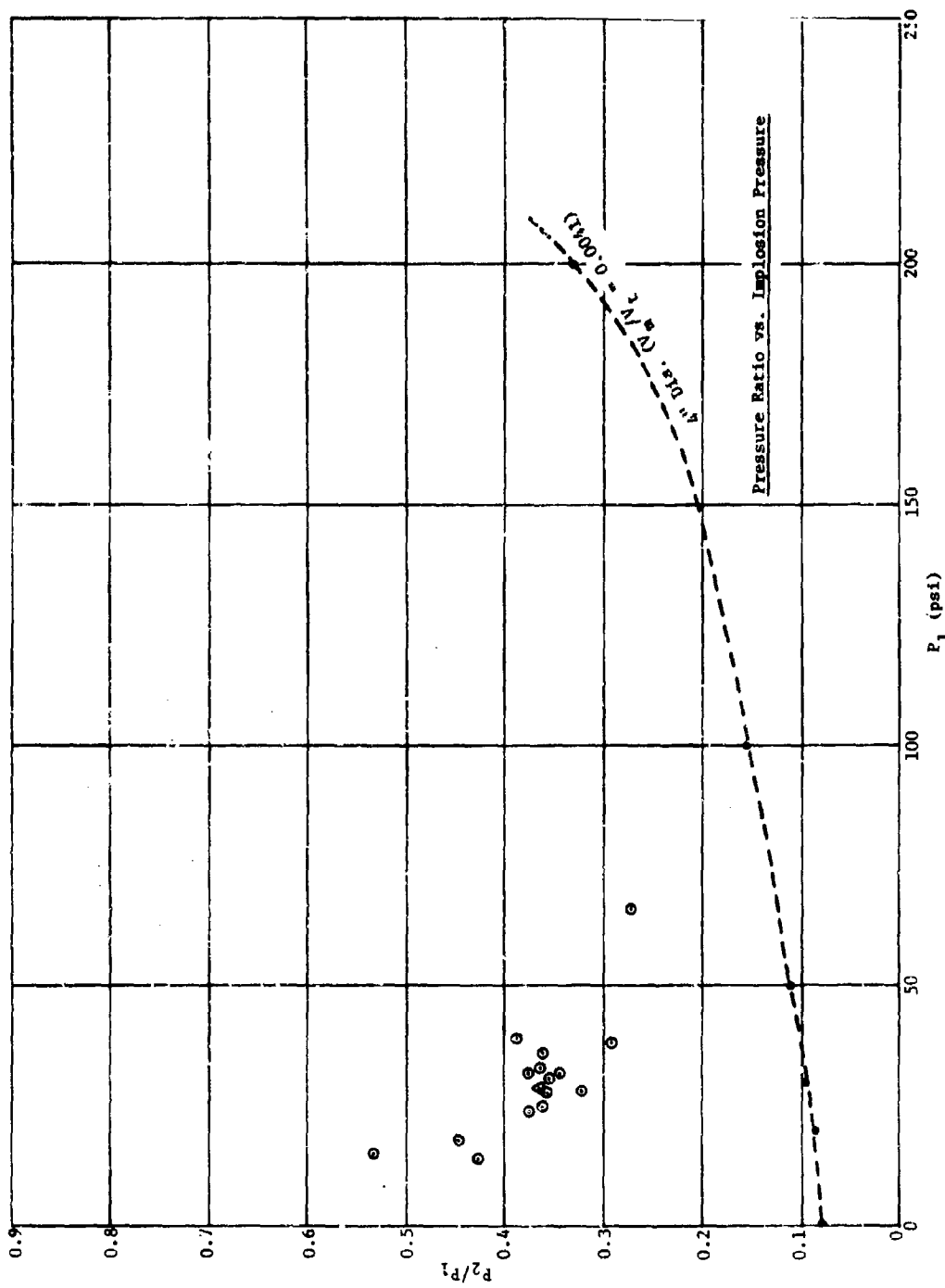
Figure 12b. Pressure-prediction curves for the aluminum cylinder for various models tested.
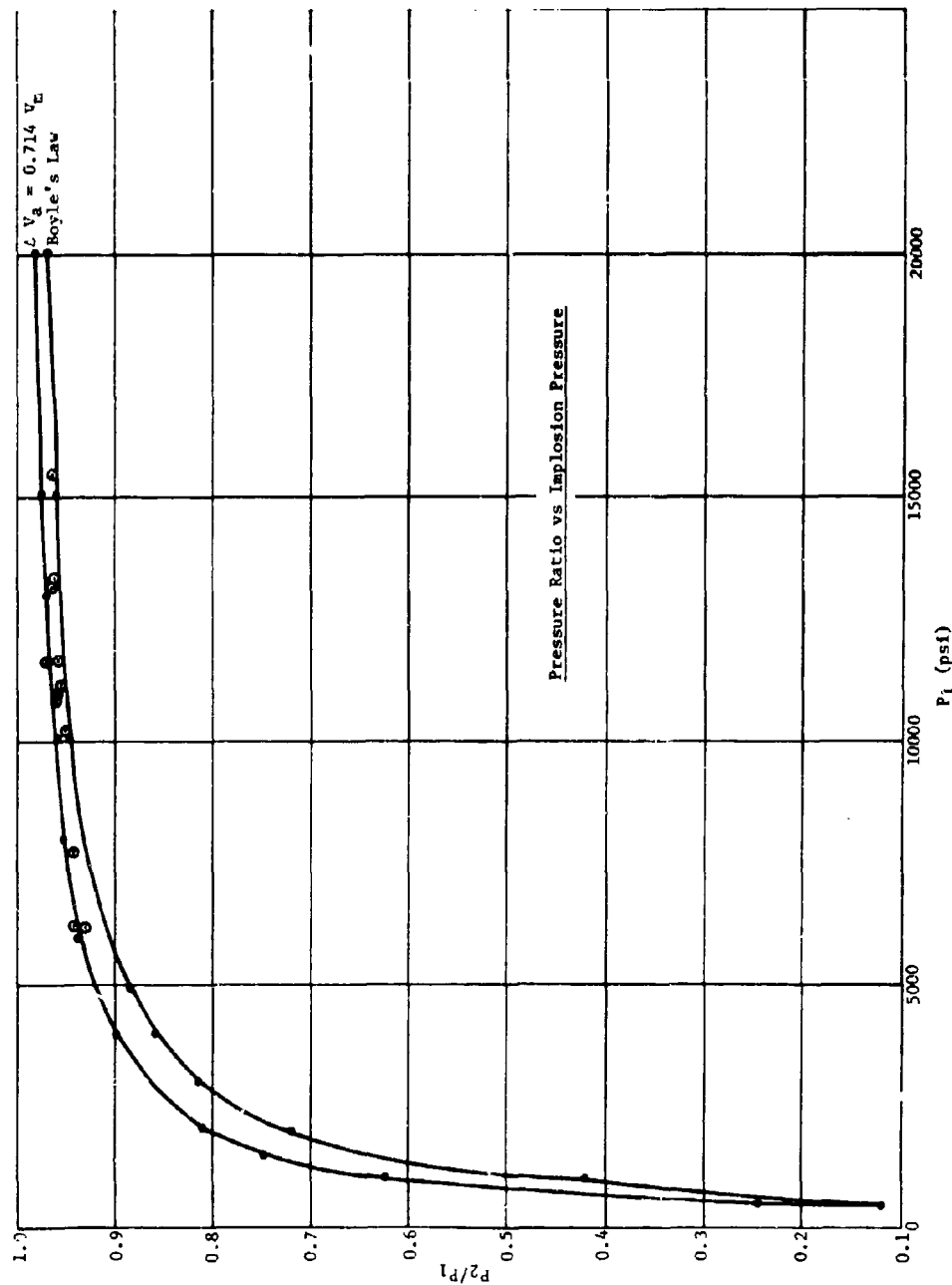
Figure 13a. Pressure-prediction curves for the 20,000-psi vessel for 3" dia. sphere ($V_m/V_t = 0.0015$).

31
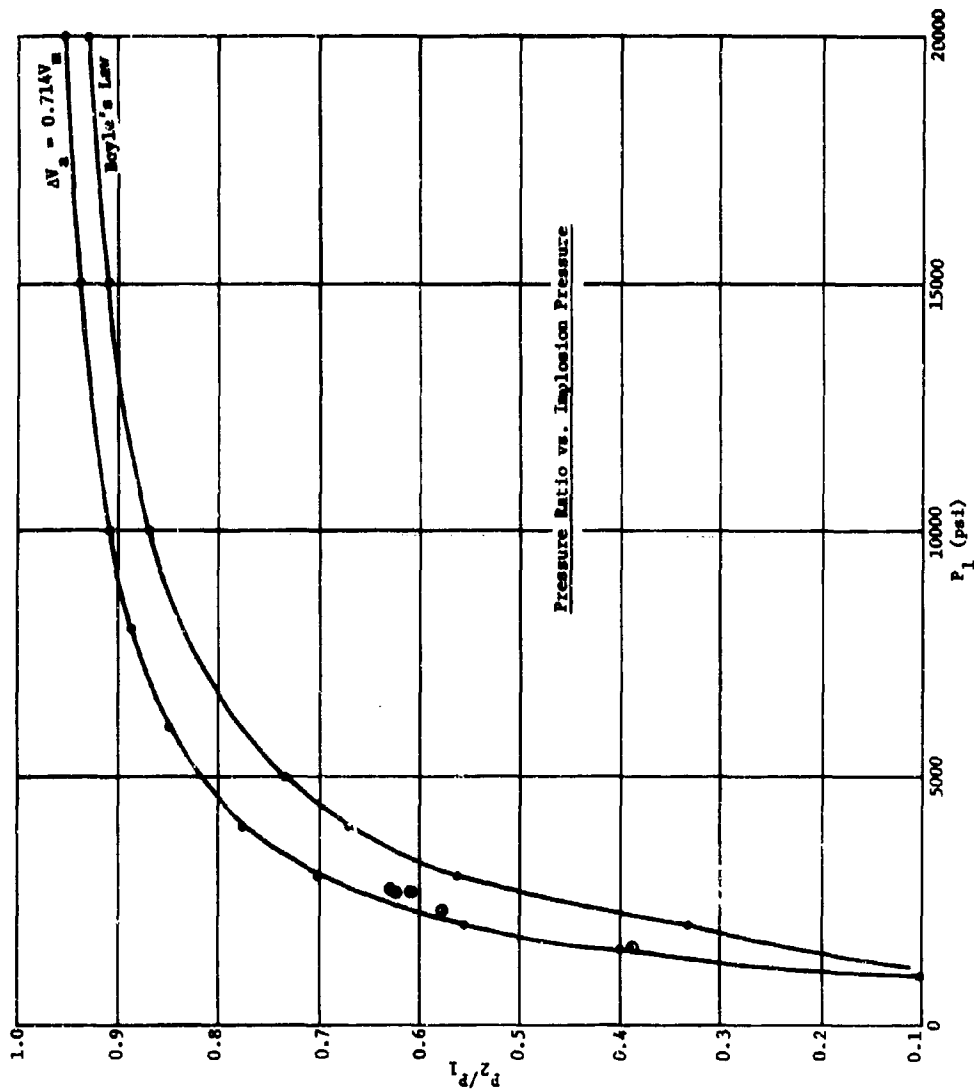
Figure 13b. Pressure-prediction curves for the 20,000-psi vessel for 4" dia. sphere ($V_m/V_t = 0.0037$).

32
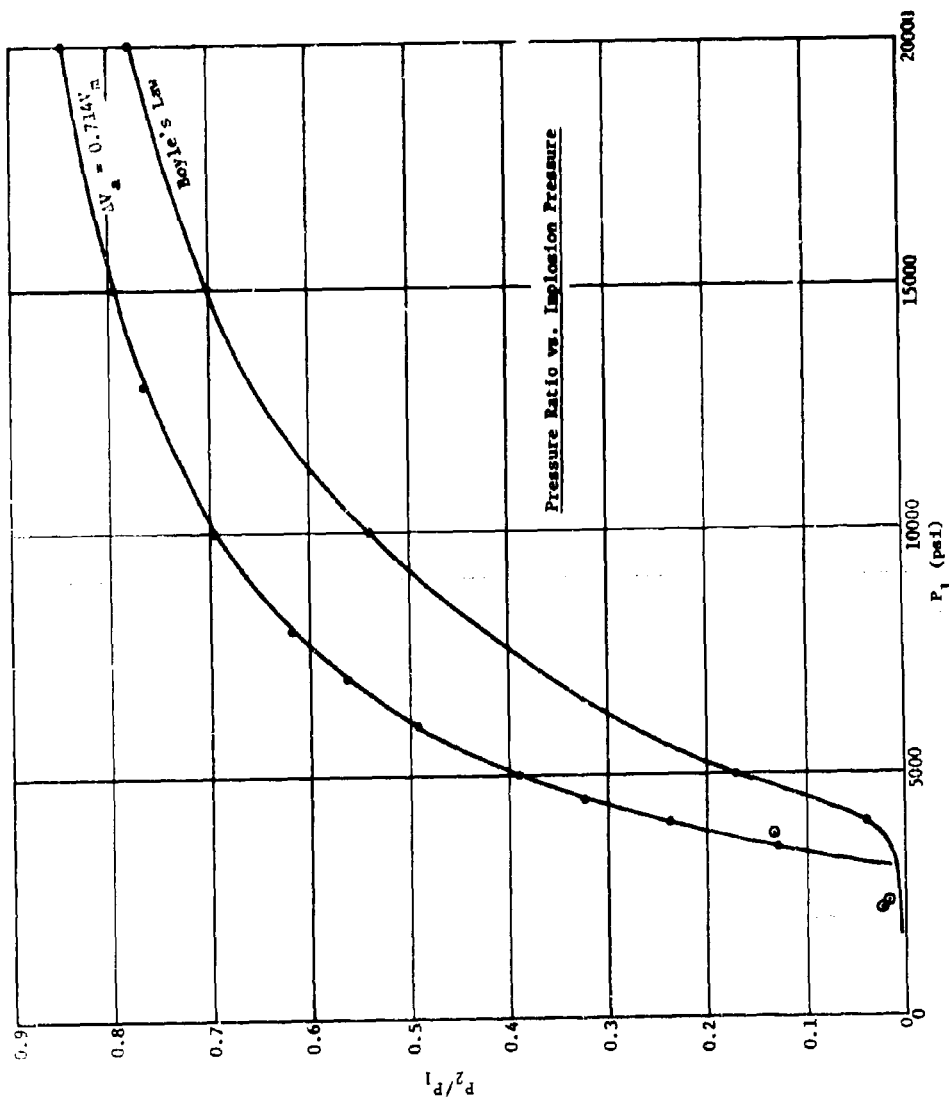
Figure 13c. Pressure-prediction curves for the 20,000-psi vessel for 6" dia. $(V_m/V_t = 0.0123)$.

33
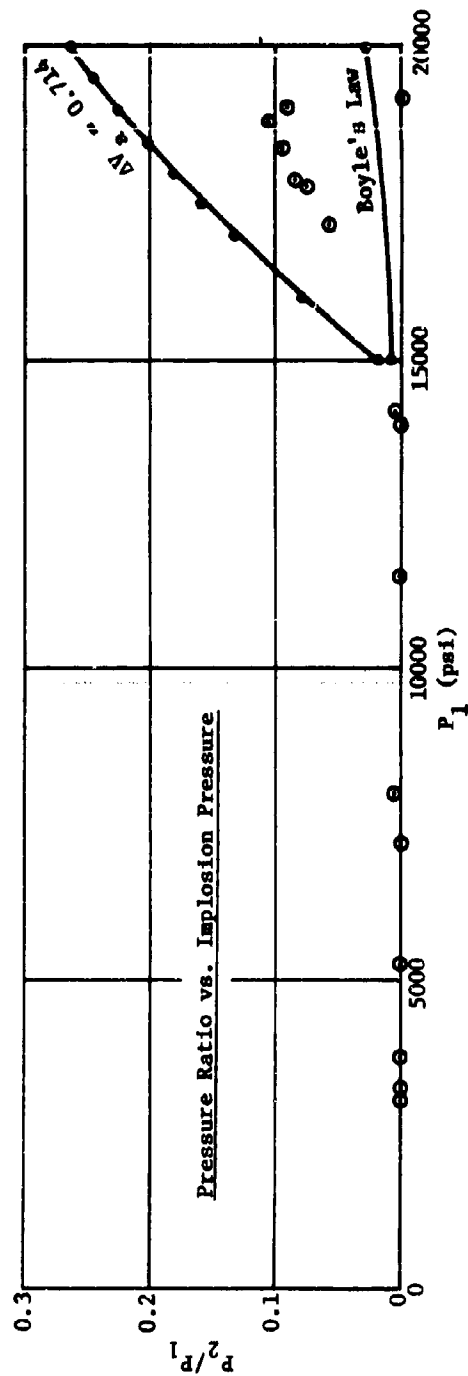
Figure 13d. Pressure-prediction curves for the 20,000-psi vessel for 10" dia. sphere (V_m/V_t = 0.0572).

34
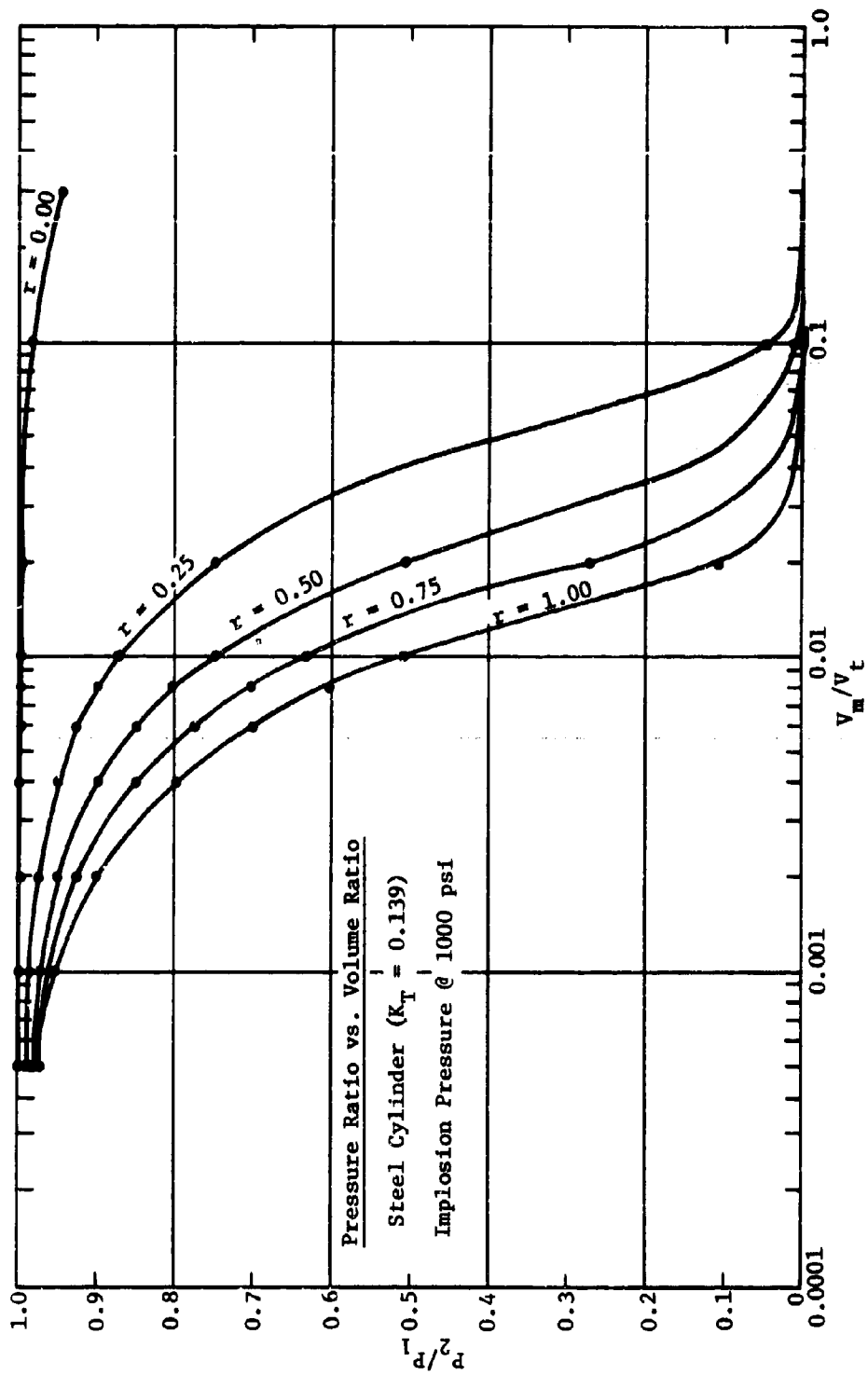
Figure 14. Pressure-prediction curves for the steel cylinder with varied amounts of air in the model.
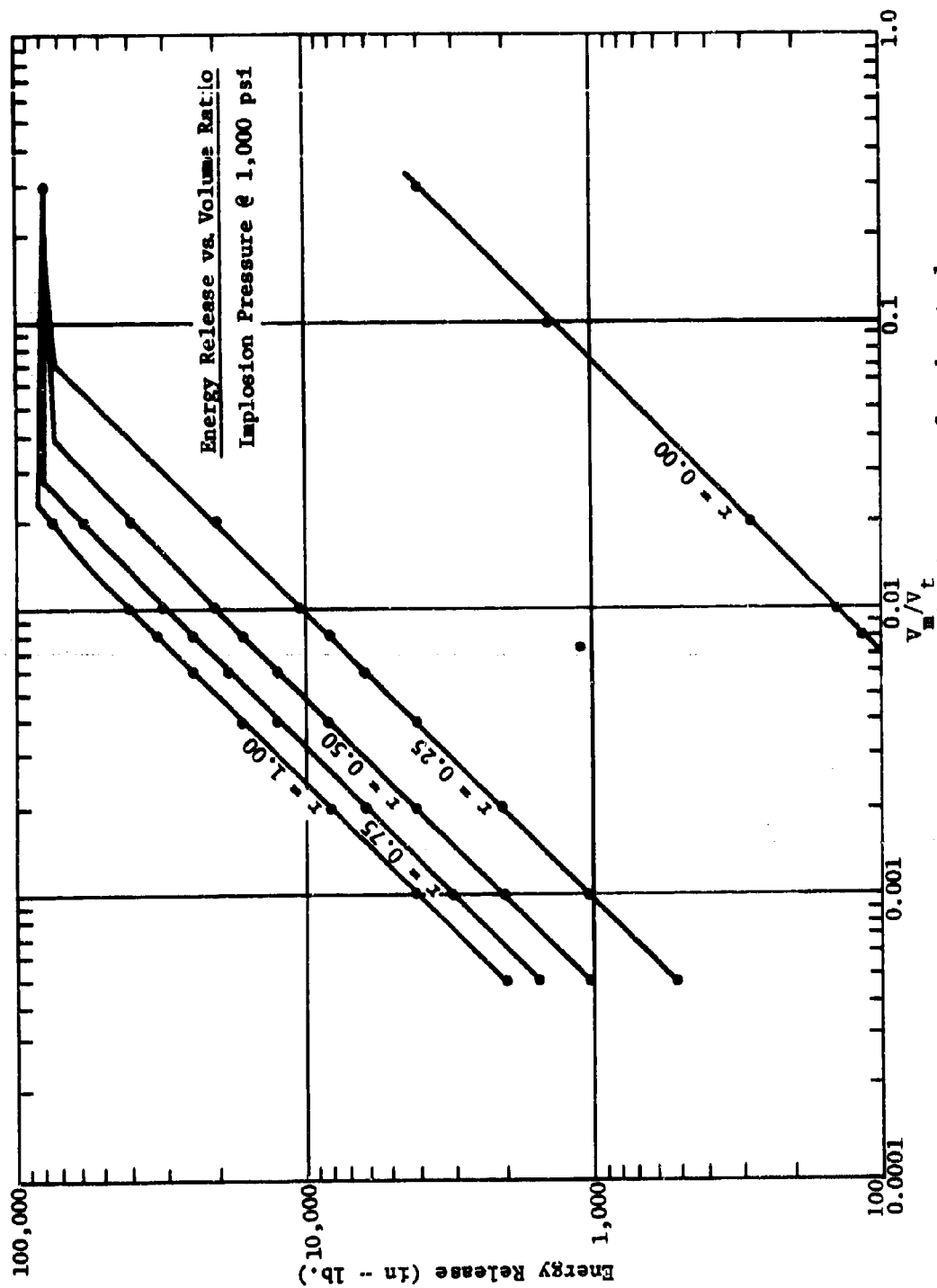
Figure 15. Energy-release prediction curves for the steel
cylinder with varied amounts of air in the model.

36
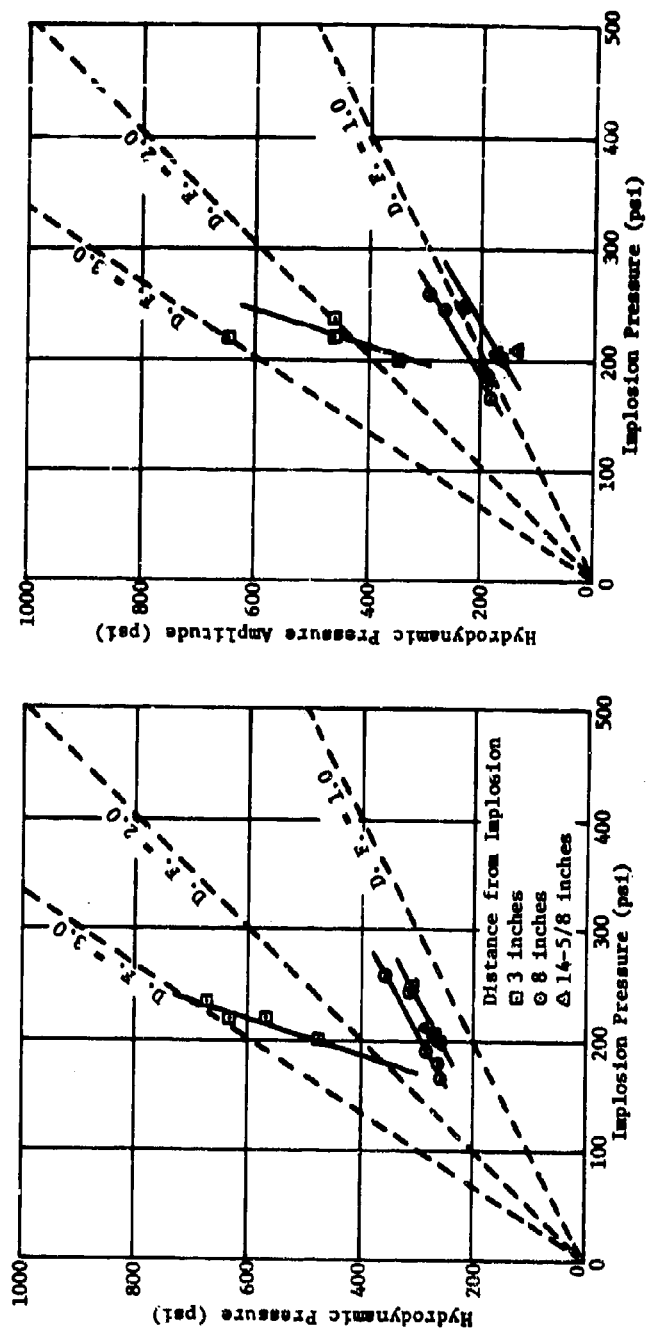
Figure 16a. Maximum hydrodynamic pressure and pressure amplitude versus implosion pressure for 2¾-inch spheres.
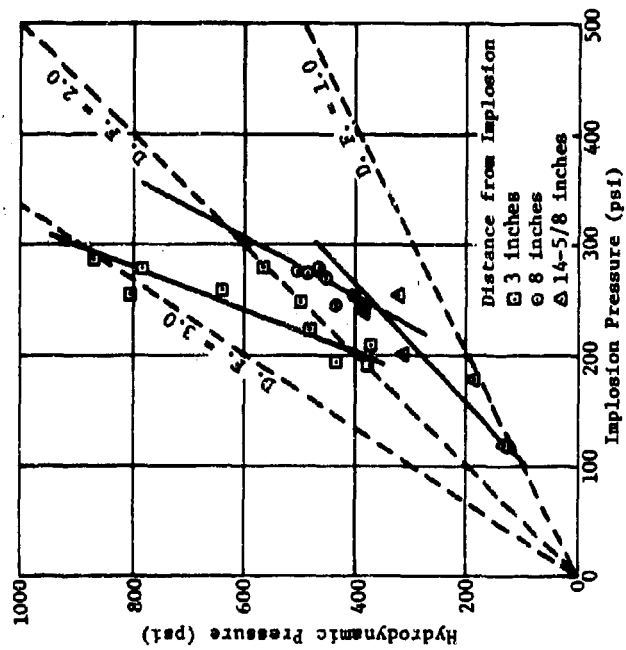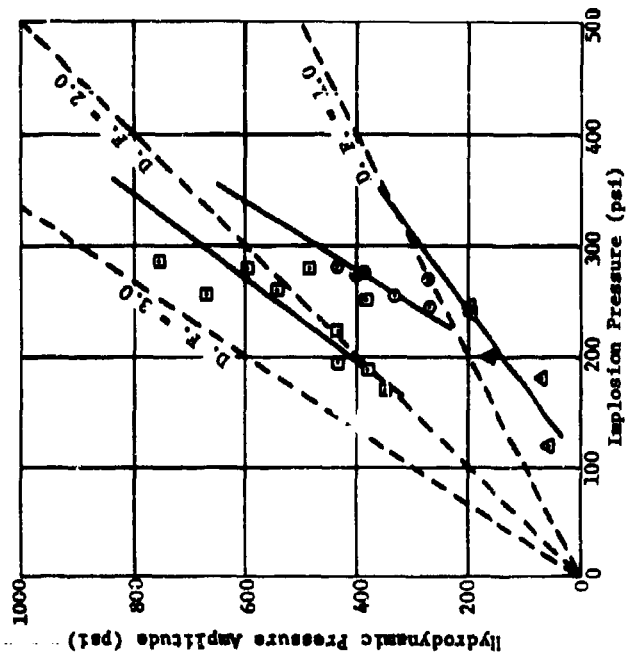
Figure 16b. Maximum hydrodynamic pressure and pressure amplitude
versus implosion pressure for 2-5/8-inch spheres.

38
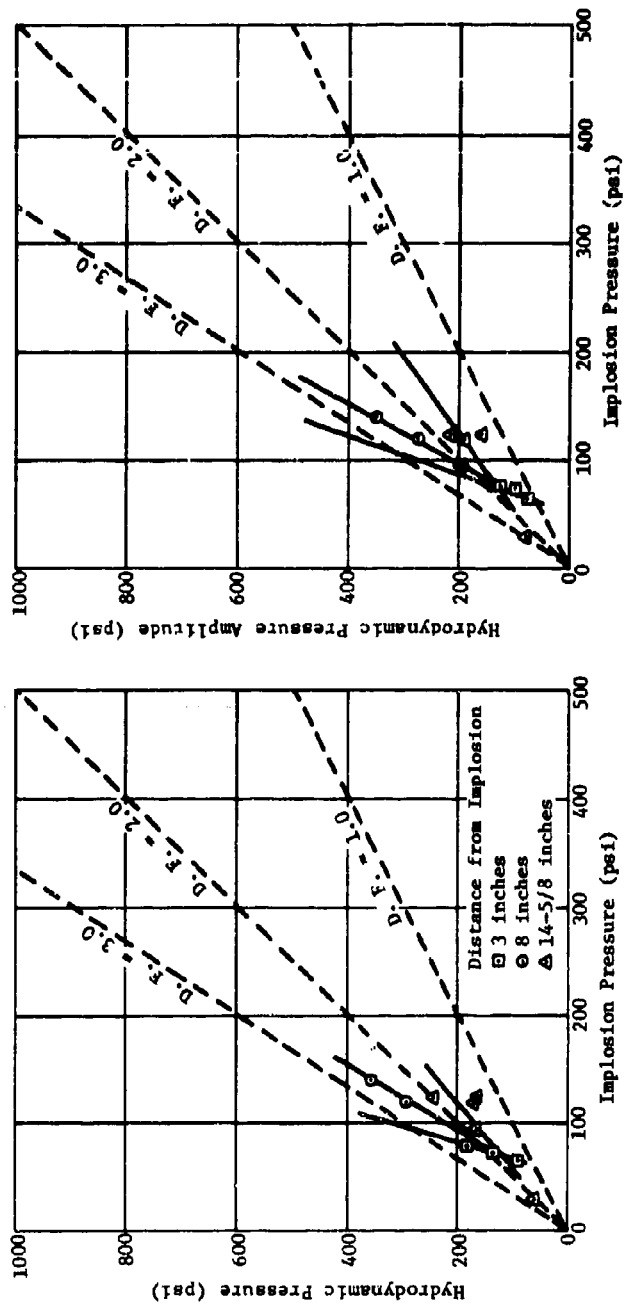
Figure 16c. Maximum hydrodynamic pressure and pressure amplitude versus implosion pressure for 3¼-inch spheres.

39
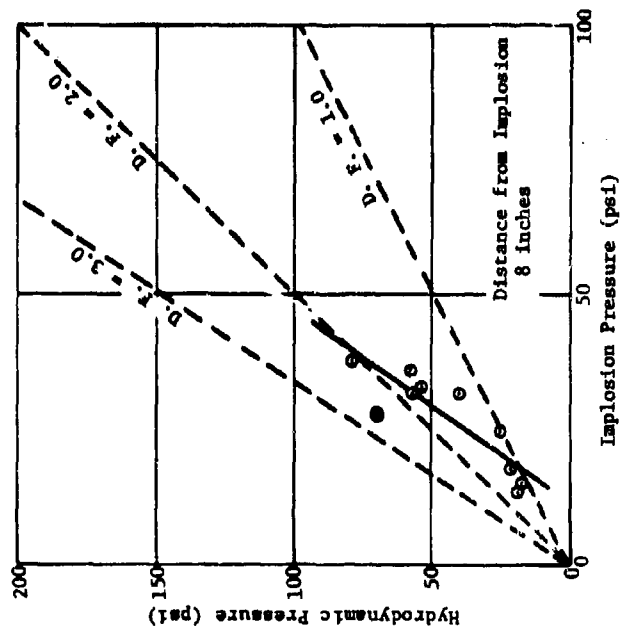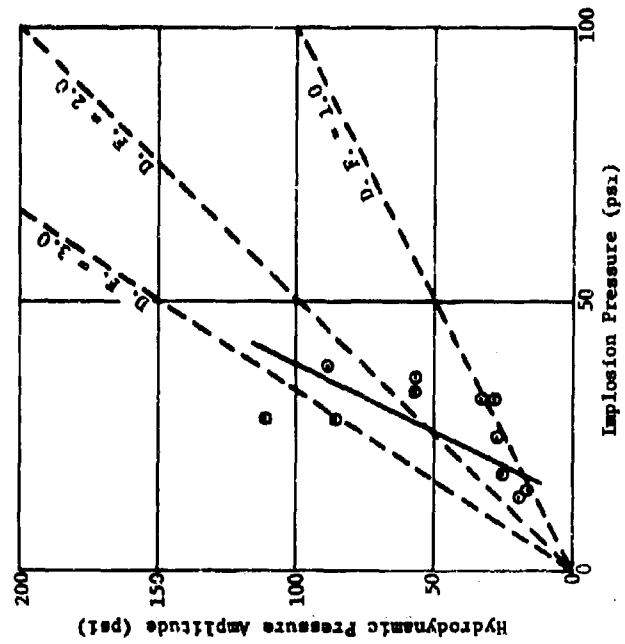
Figure 16d. Maximum hydrodynamic pressure and pressure amplitude
versus implosion pressure for 4-inch spheres.

40
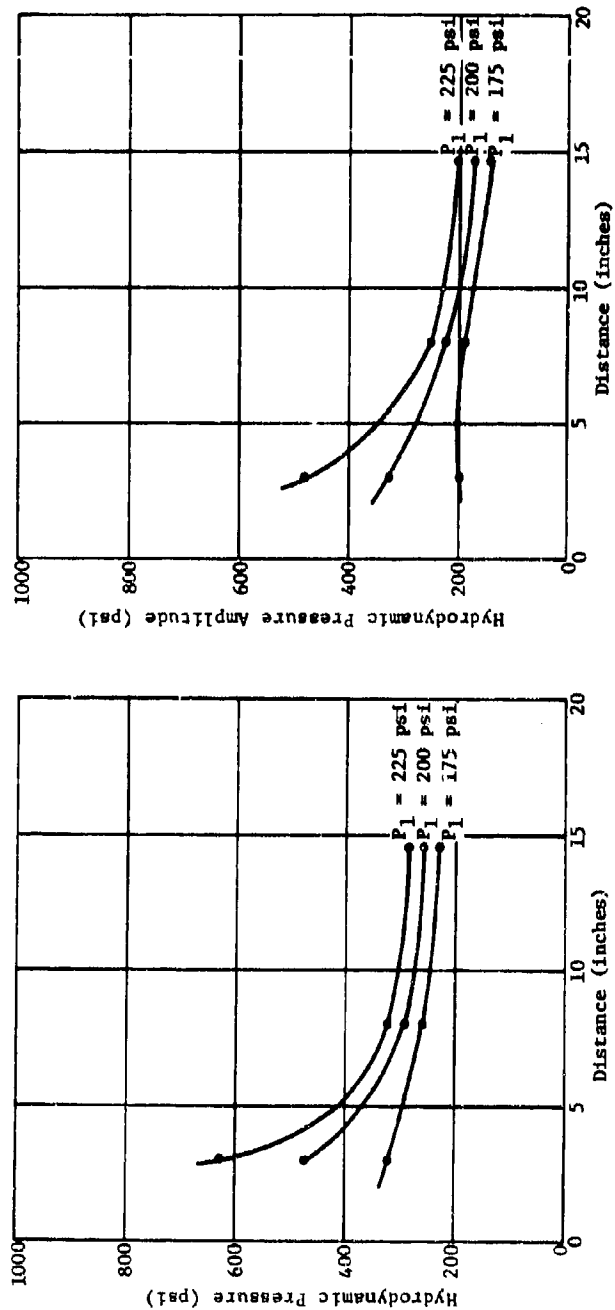
Figure 17a. Maximum hydrodynamic pressure and pressure amplitude versus distance from implosion for 2½-inch spheres.

41
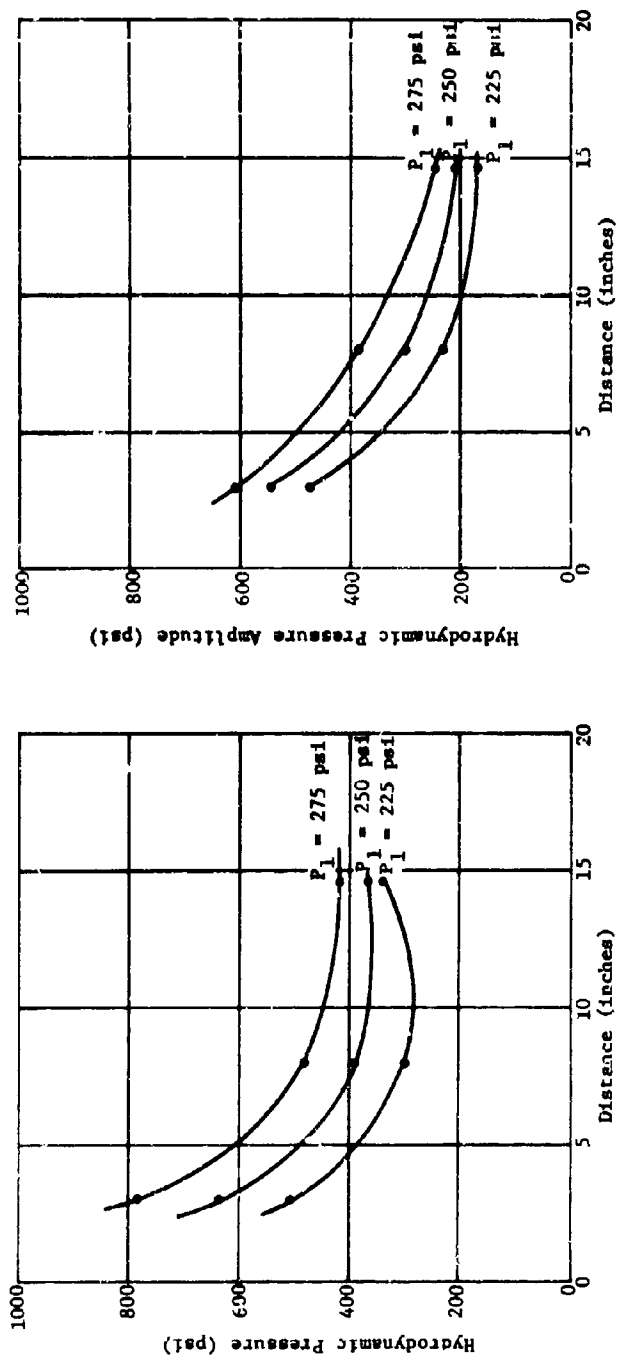
Figure 17b. Maximum hydrodynamic pressure and pressure amplitude versus distance from implosion for 2-5/8-inch spheres.

42
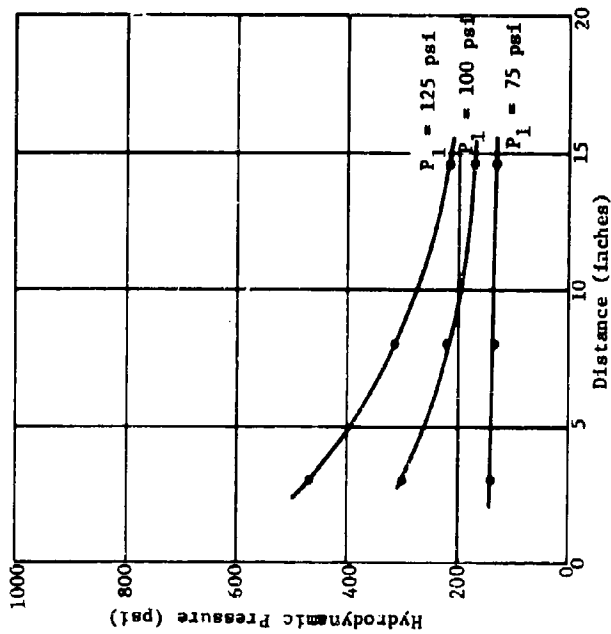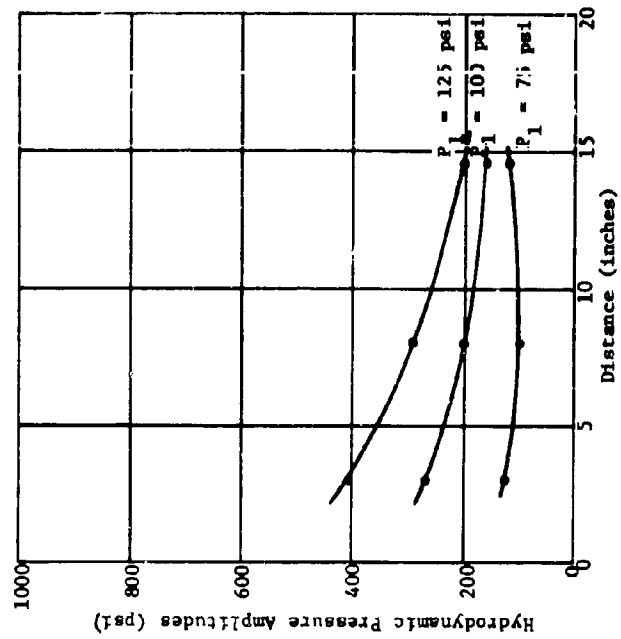
Figure 17c. Maximum hydrodynamic pressure and pressure amplitude versus distance from implosion for 3¼-inch spheres.

43
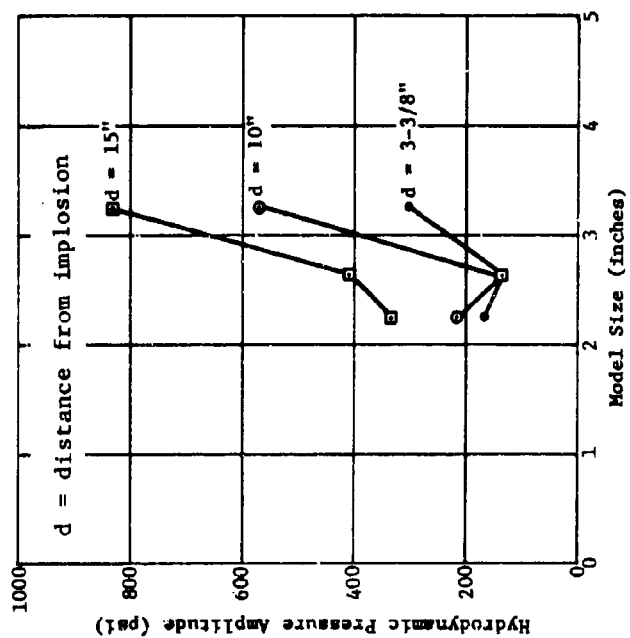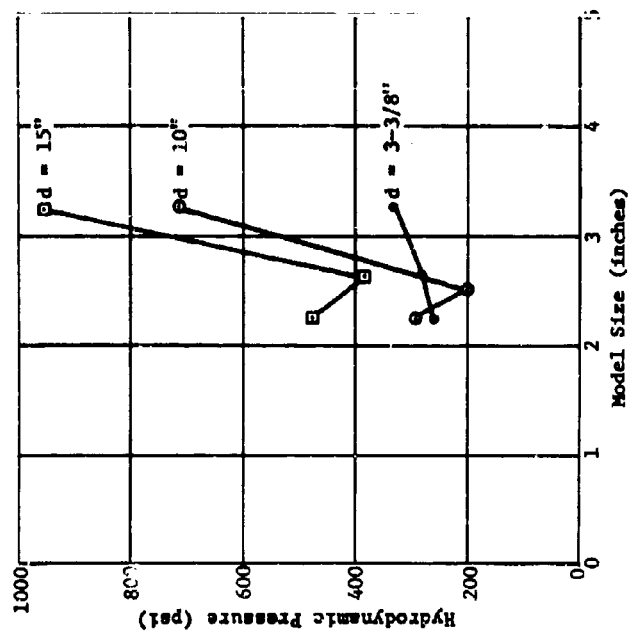
Figure 18. Maximum hydrodynamic pressure and pressure amplitude versus model size for implosion pressure of 200 psi.

44
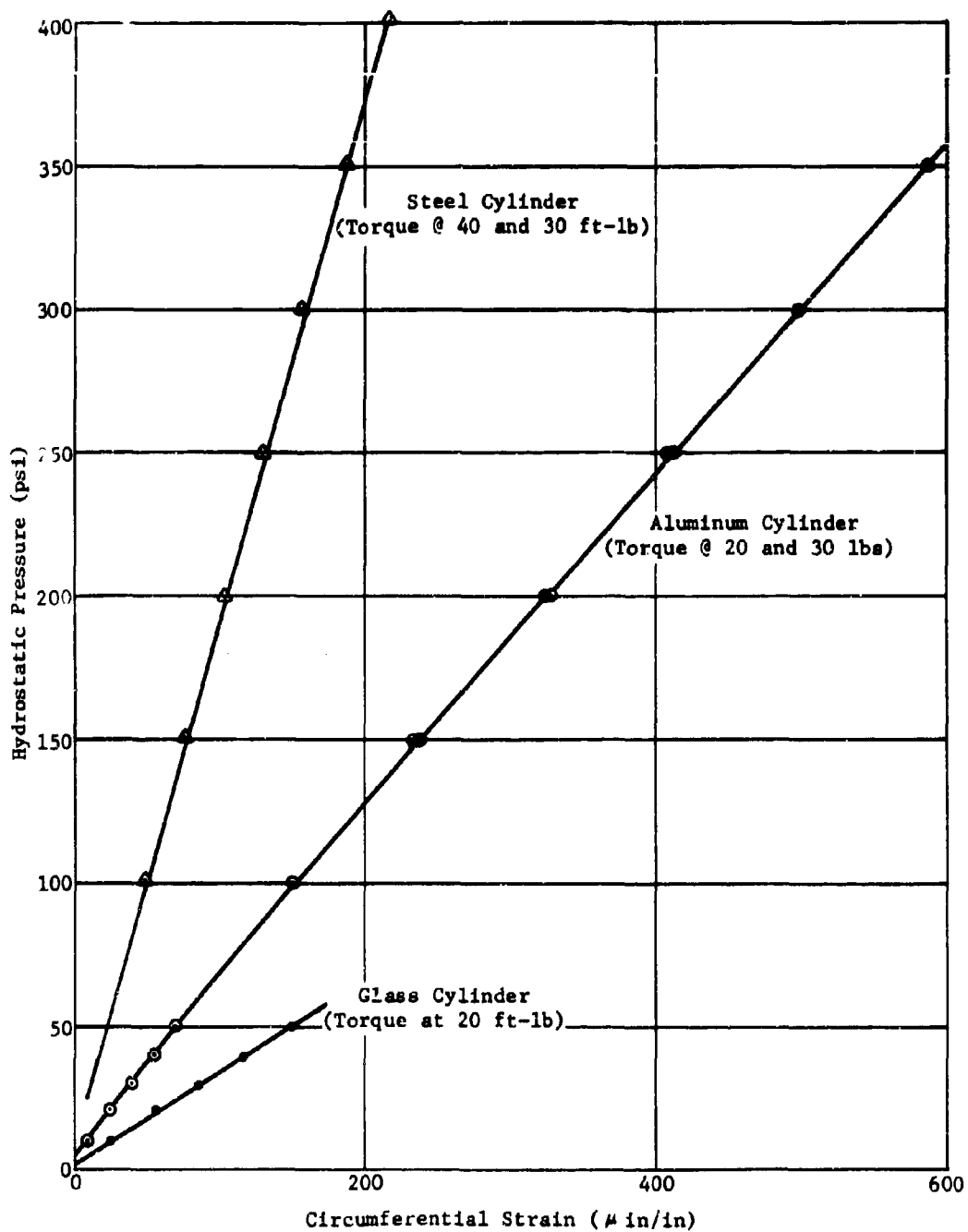
Figure 19. Circumferential static strain versus hydrostatic pressure for the low-pressure cylinders.
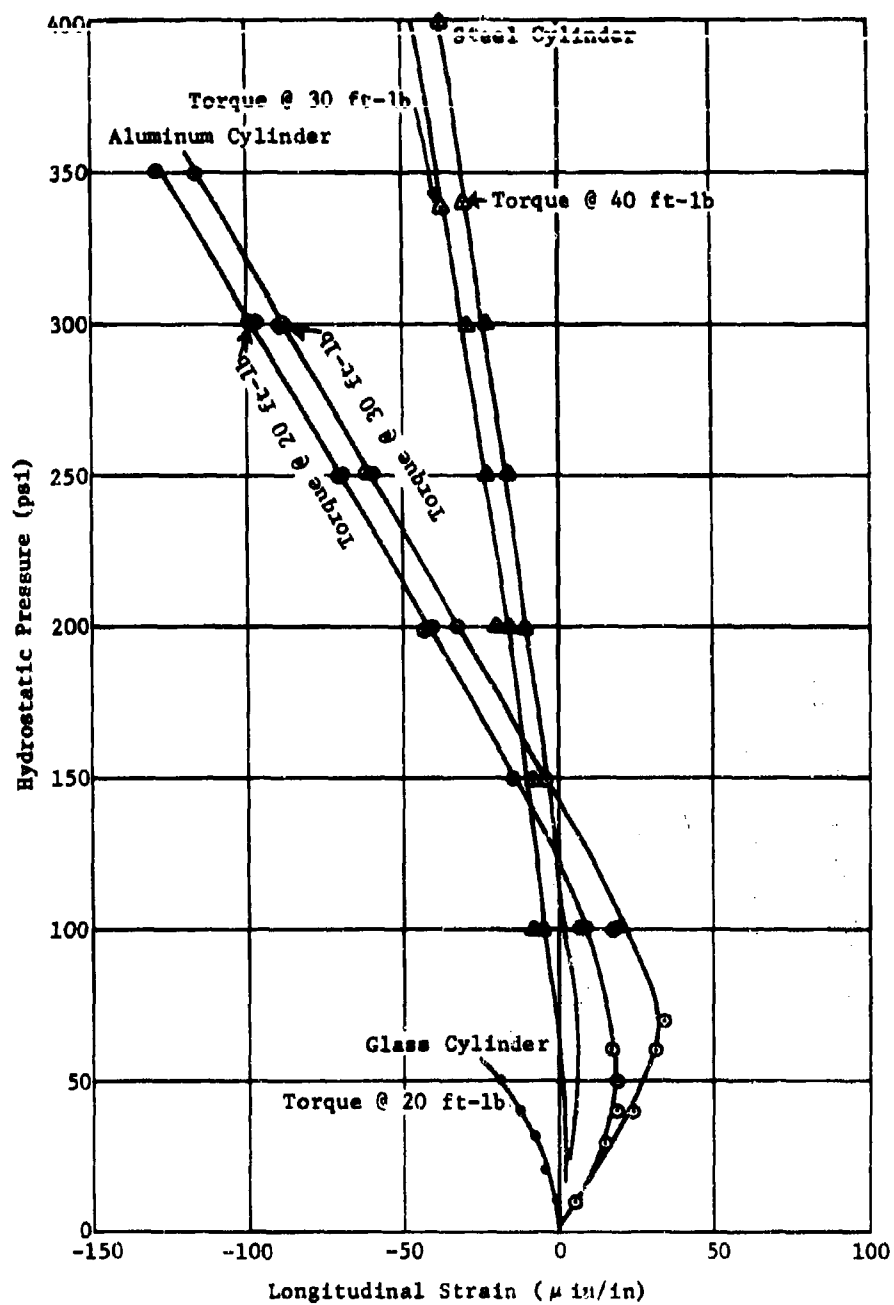
Figure 20. Longitudinal static strain versus hydrostatic pressure for the low-pressure cylinders.

46
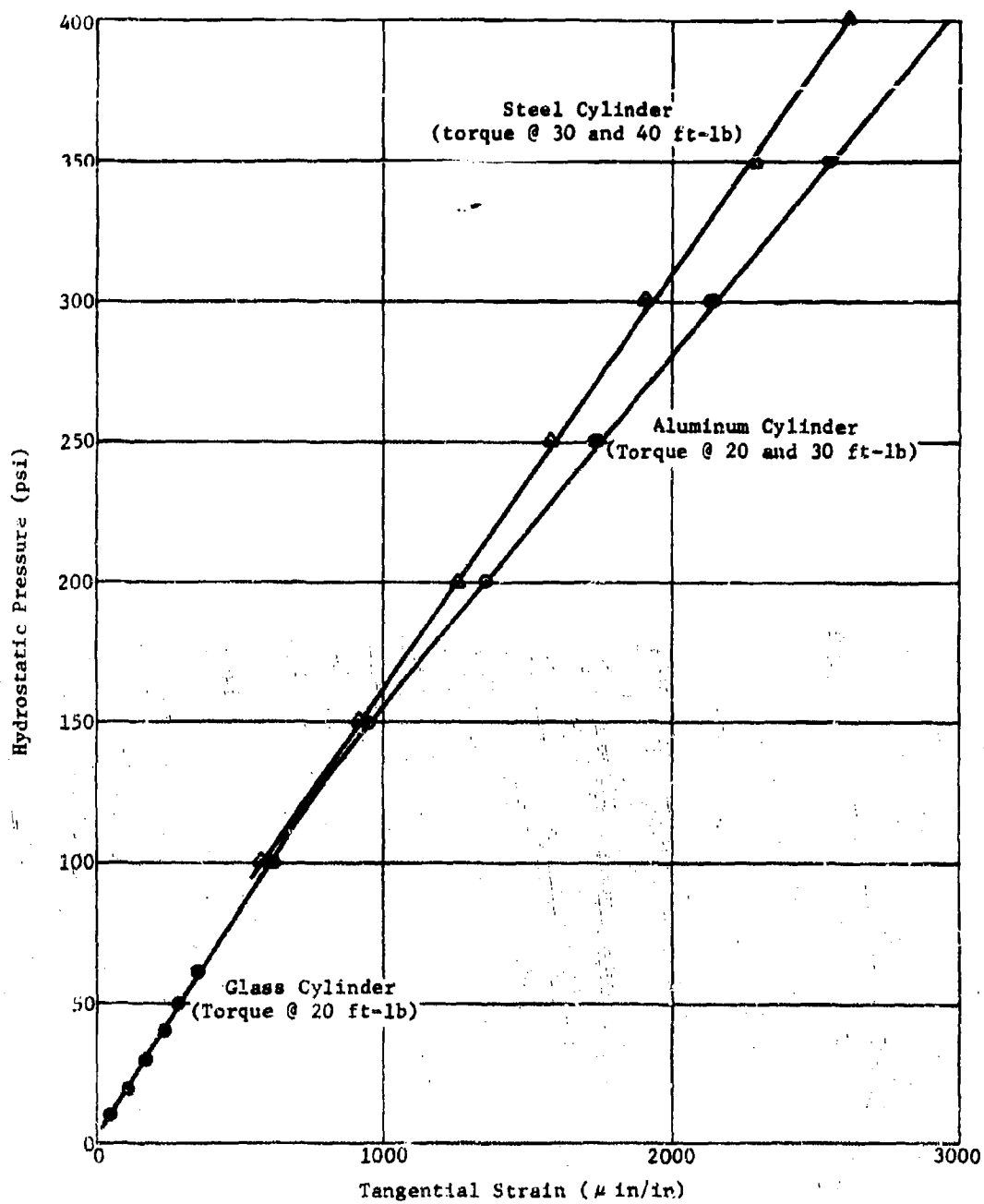
Figure 21. Tangential static strain versus hydrostatic
pressure for the low-pressure cylinders.

47
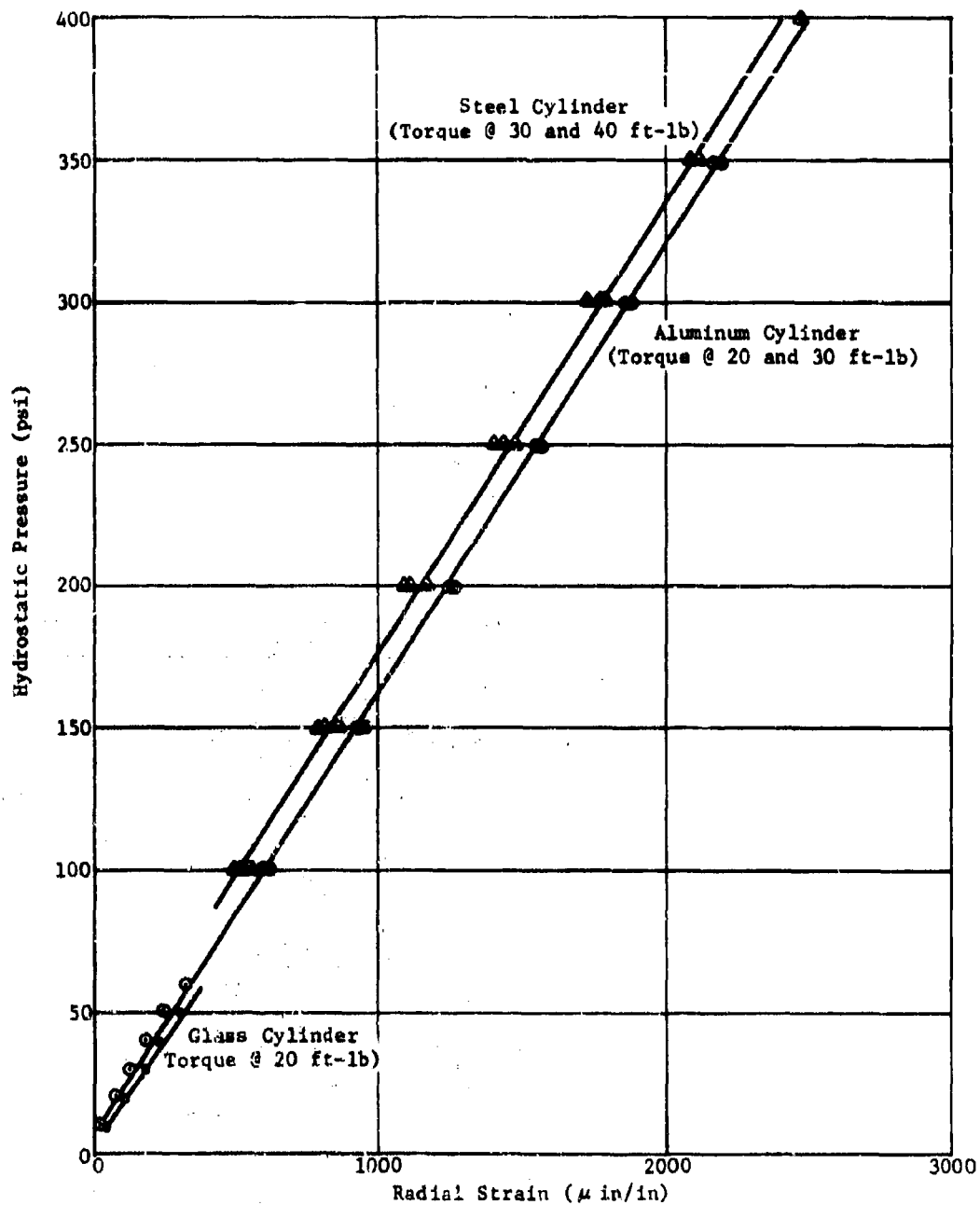
Figure 22. Radial static strain versus hydrostatic
pressure for the low-pressure cylinders.

48
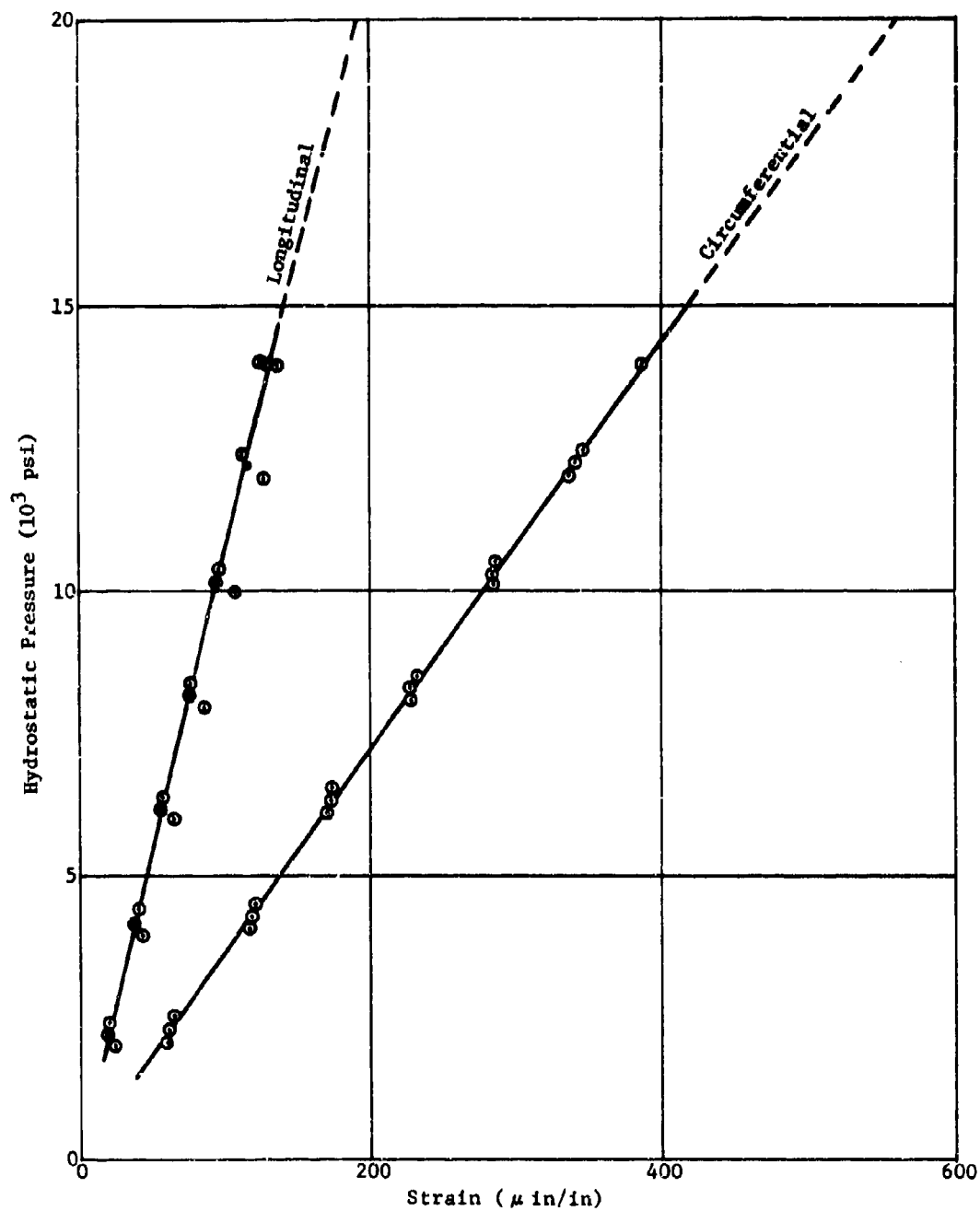
Figure 23. Static strain versus hydrostatic pressure for
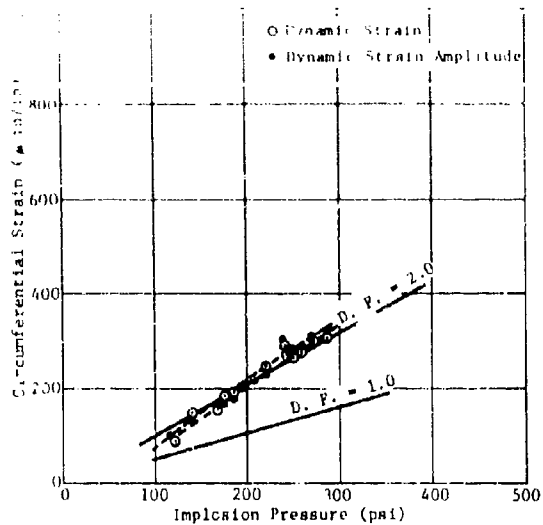the 20,000-psi pressure vessel.

49
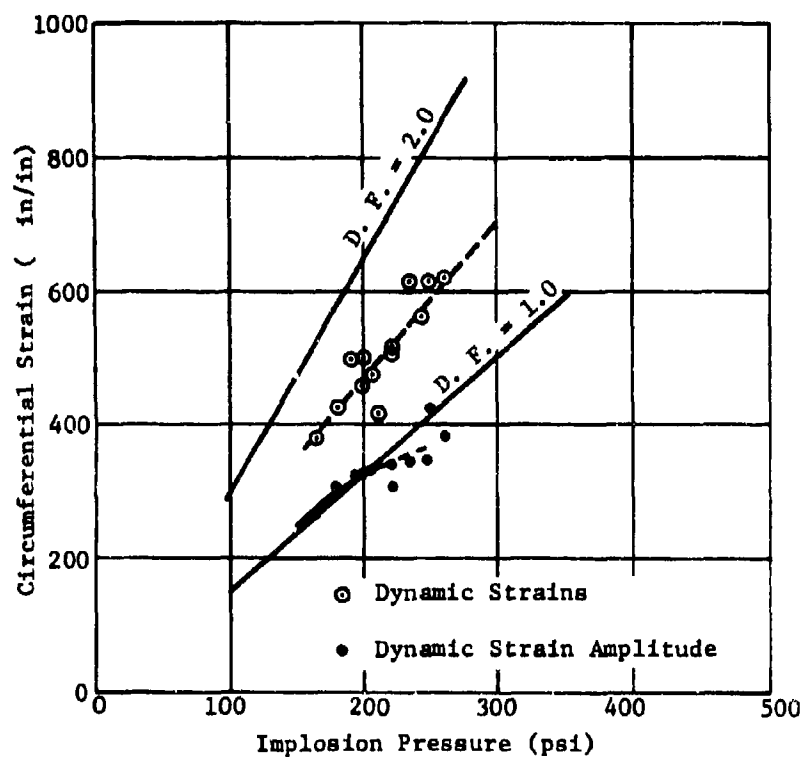
Figure 24a. Maximum dynamic circumferential
strains versus implosion pressures
of the aluminum cylinder tested with
2½-inch spheres.
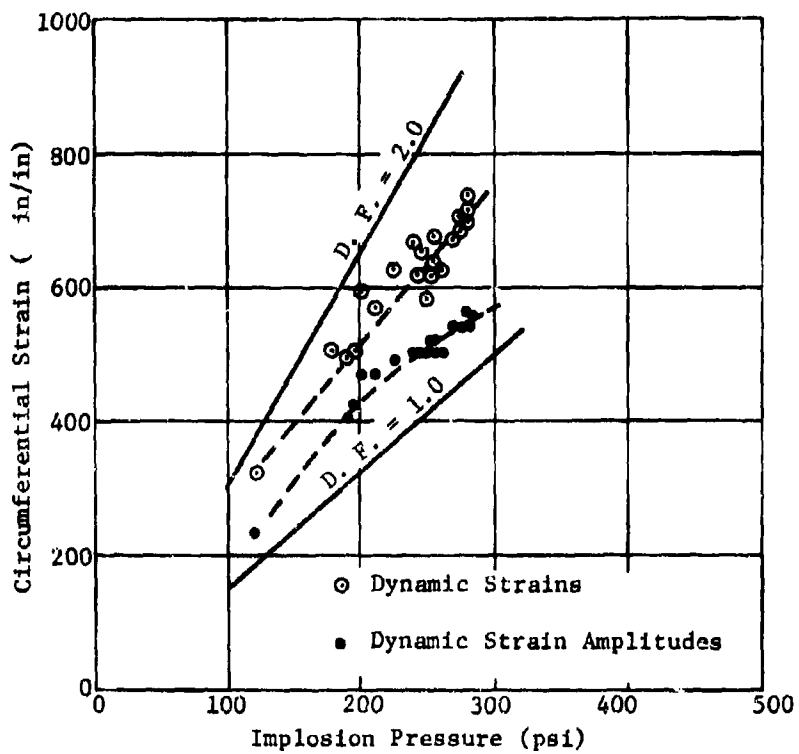
Figure 24b. Maximum dynamic circumferential strains
versus implosion pressures of the
aluminum cylinder tested with 2-5/8-
inch spheres.
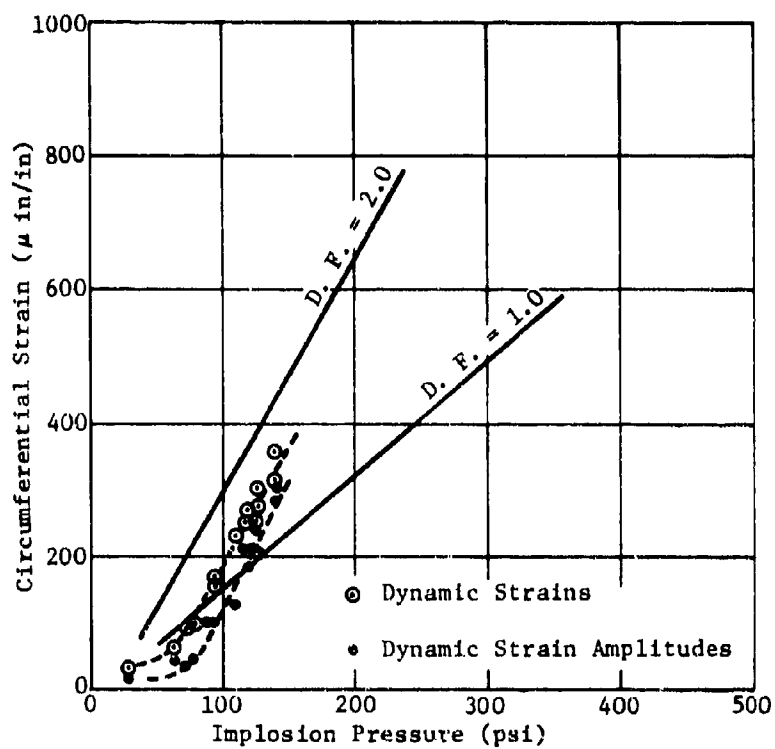
Figure 24c. Maximum dynamic circumferential strains versus implosion pressures of the aluminum cylinder tested with 3¼-inch spheres.
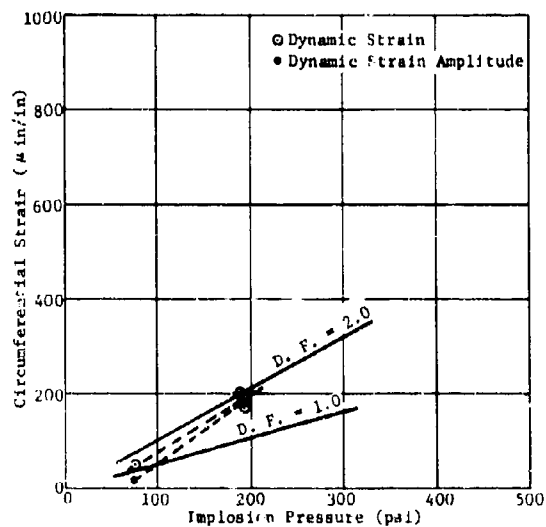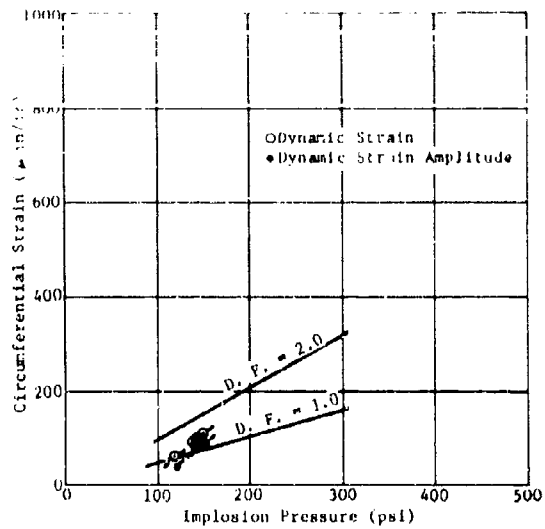
51
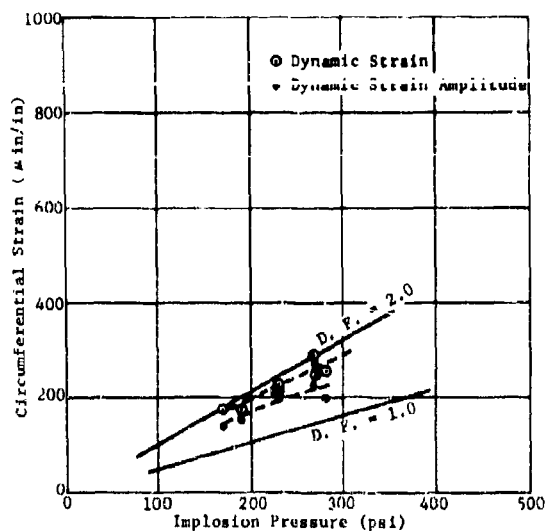
Figure 25a. Maximum dynamic circumferential strains
versus implosion pressures of the steel
cylinder tested with 2½-inch spheres.
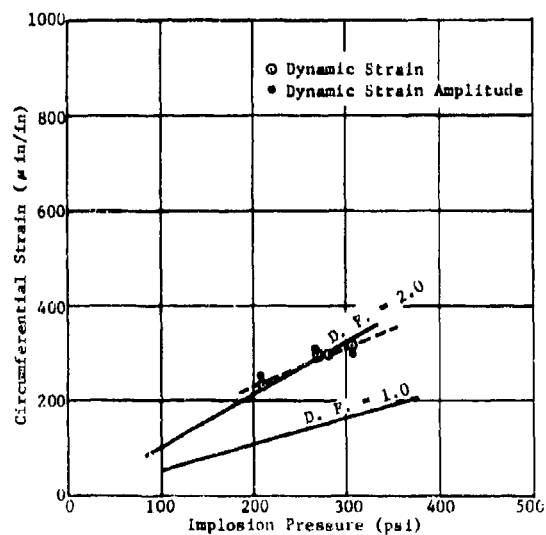
Figure 25b. Maximum dynamic circumferential strains
versus implosion pressures of the steel
cylinder tested with 2½-inch spheres.

Figure 25c. Maximum dynamic circumferential strains versus implosion pressures of the steel cylinder tested with 2-5/8-inch spheres.

Figure 25d. Maximum dynamic circumferential strains versus implosion pressures of the steel cylinder tested with 3-inch spheres.

Figure 25e. Maximum dynamic circumferential strains
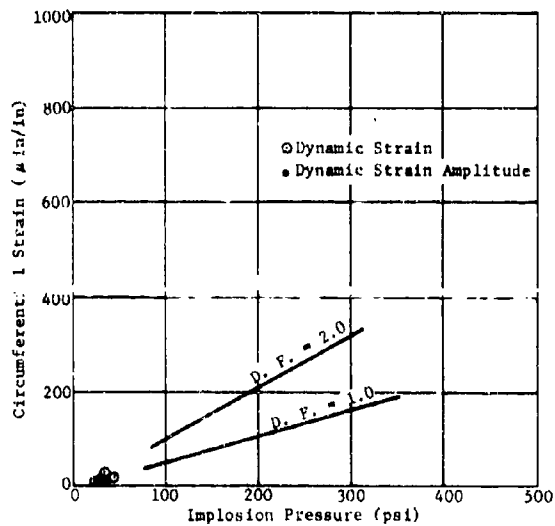versus implosion pressures of the steel
cylinder tested with 3¼-inch spheres.

Figure 25f. Maximum dynamic circumferential strains
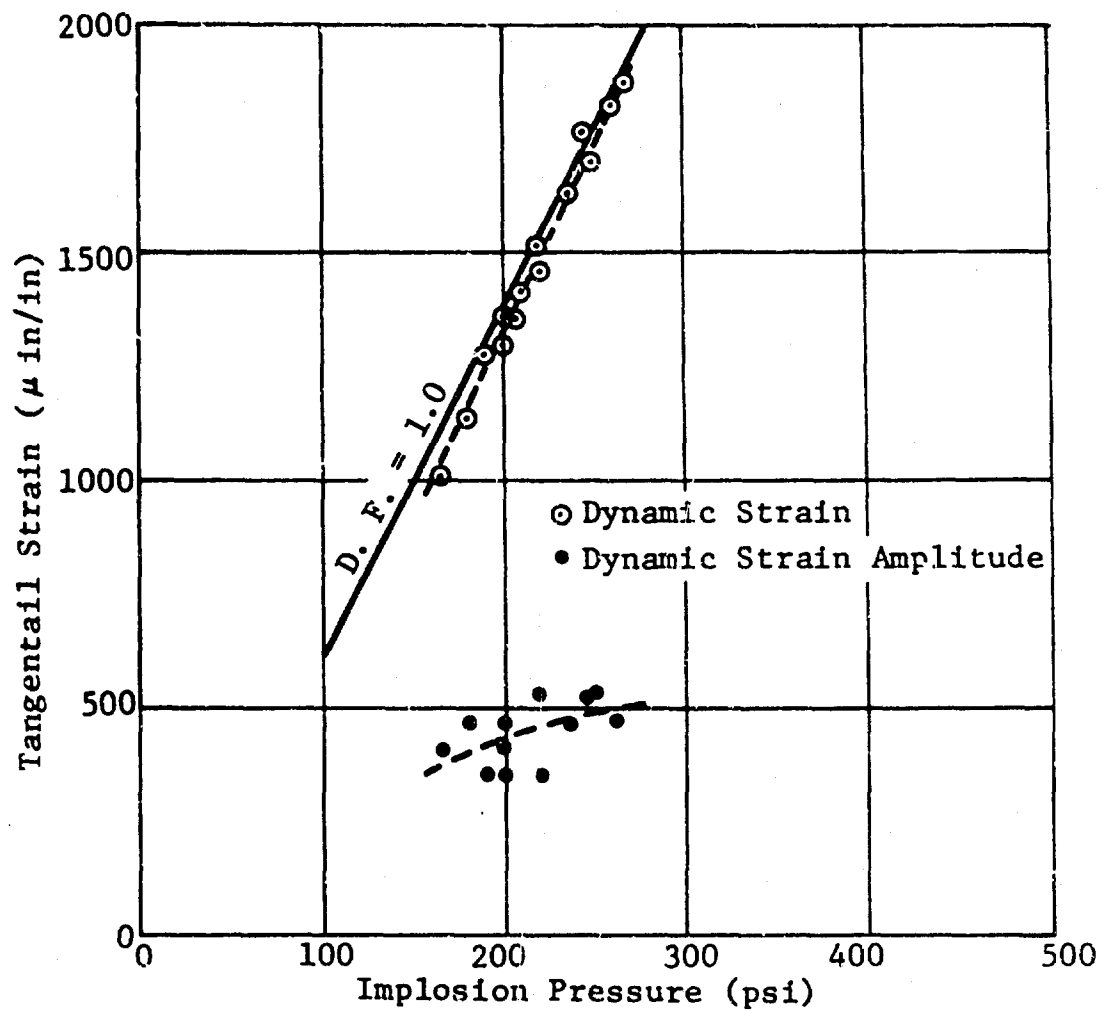versus implosion pressures of the steel
cylinder tested with 4-inch spheres.

52

Figure 26a. Maximum dynamic tangential strains versus implosion pressures of the top cover plate tested with 2¼-inch spheres.
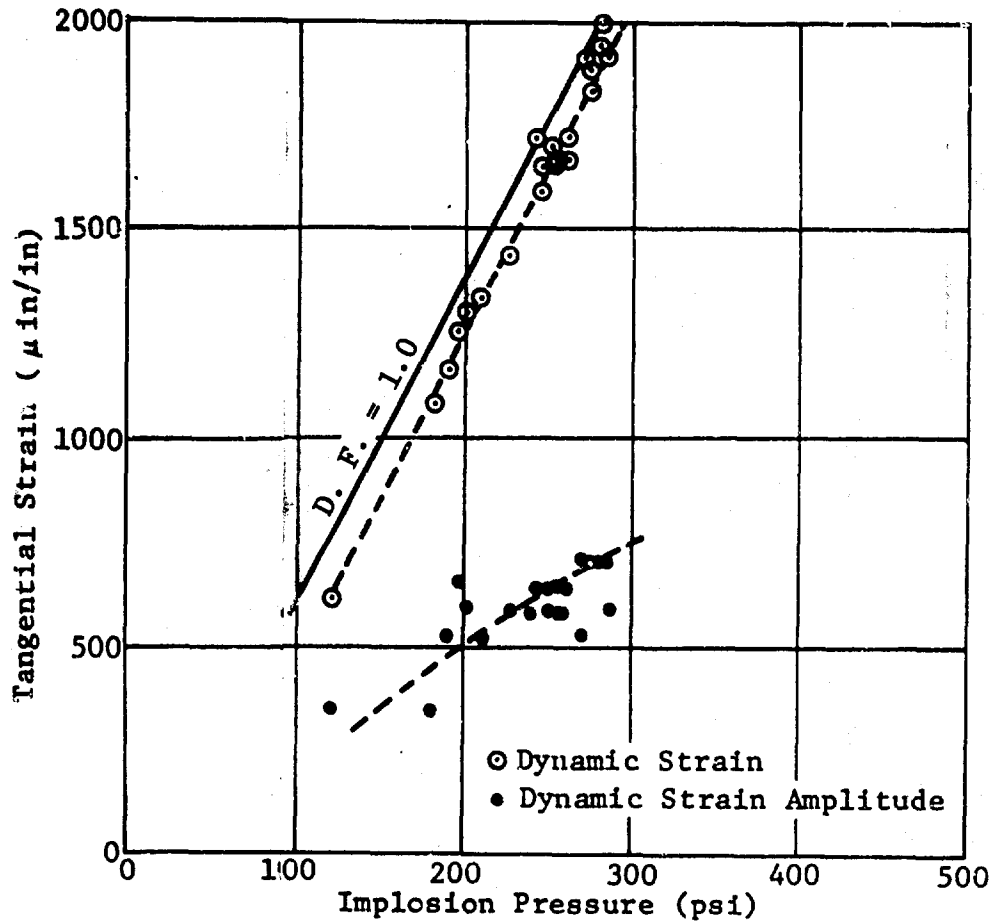
Figure 26b. Maximum dynamic tangential strains versus implosion pressures of the top cover plate tested with 2-5/8-inch spheres.
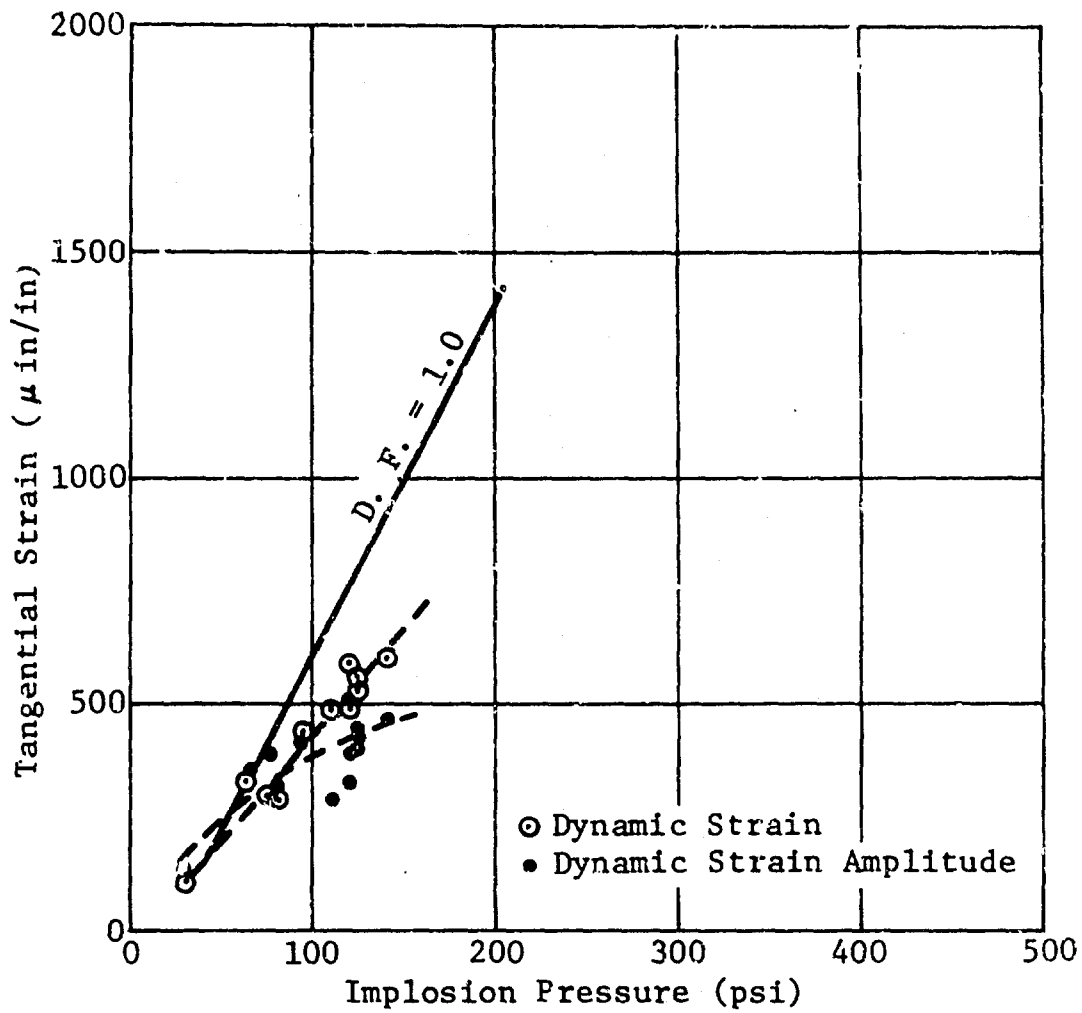
B.

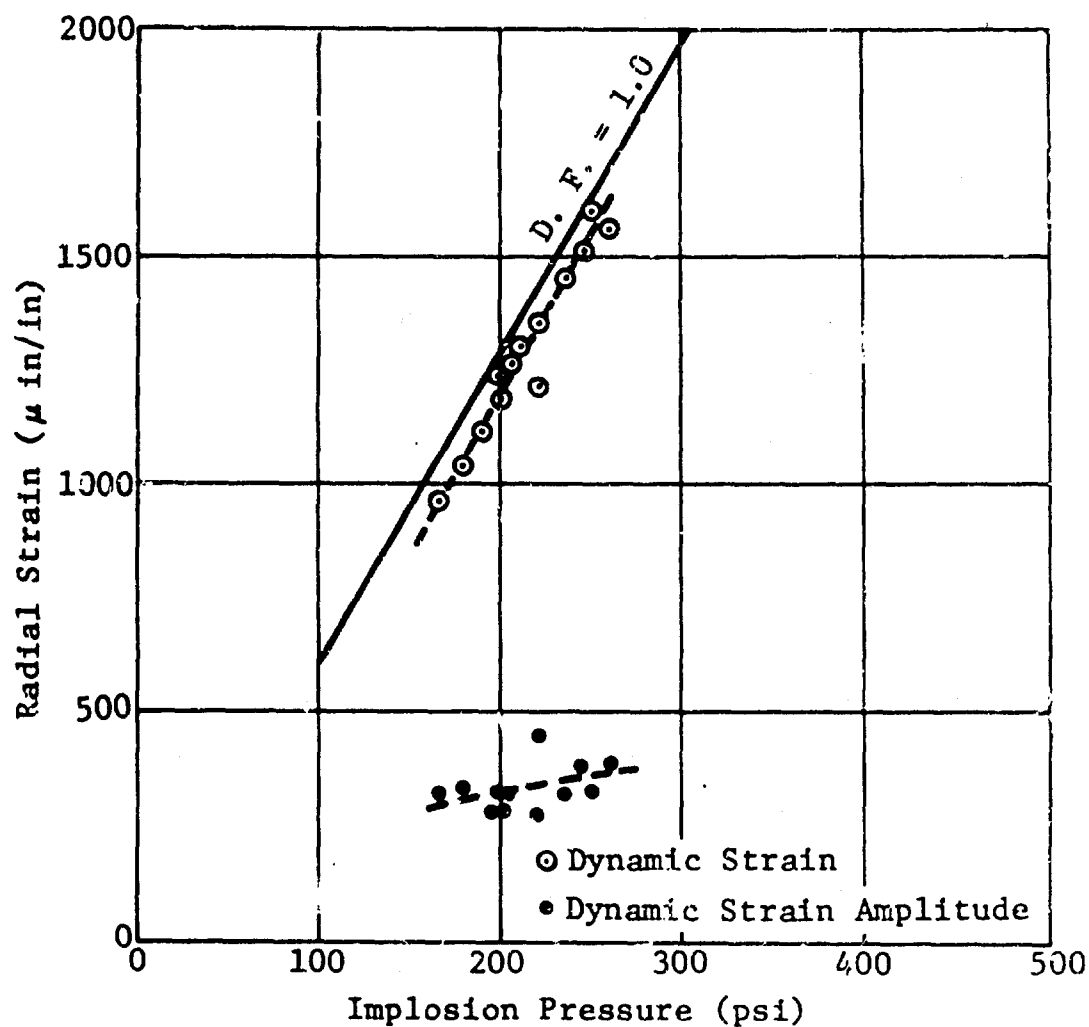Figure 26c. Maximum dynamic tangential strains versus implosion pressures of the top cover plate tested with 3¼-inch spheres.

Figure 27a. Maximum dynamic radial strains versus implosion pressures of the top cover plate tested with 2½-inch spheres.
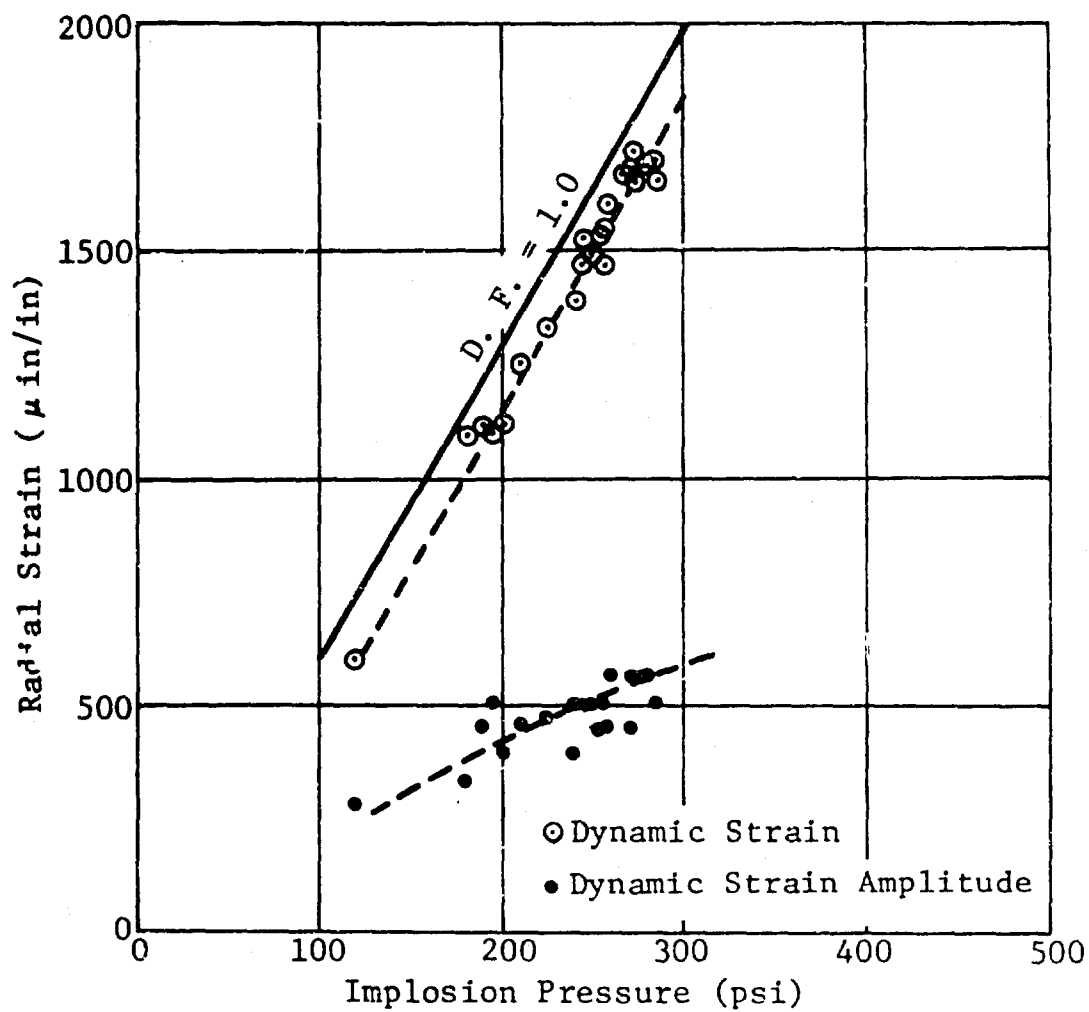
Figure 27b. Maximum dynamic radial strains versus implosion pressures of the top cover plate tested with 2-5/8-inch spheres.
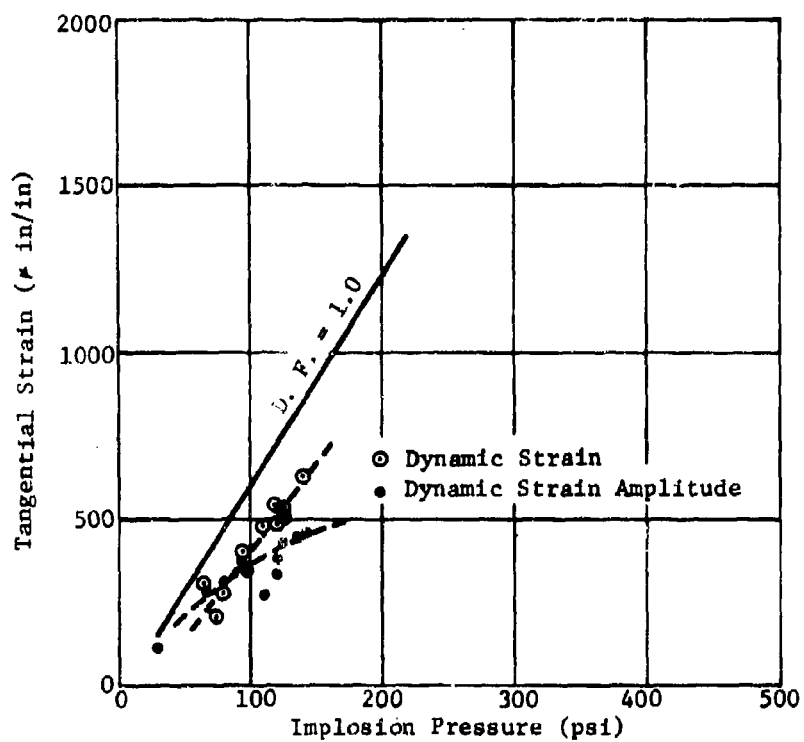
Figure 27c. Maximum dynamic radial strains versus implosion pressures of the top cover plate tested with 2-5/3-inch spheres.
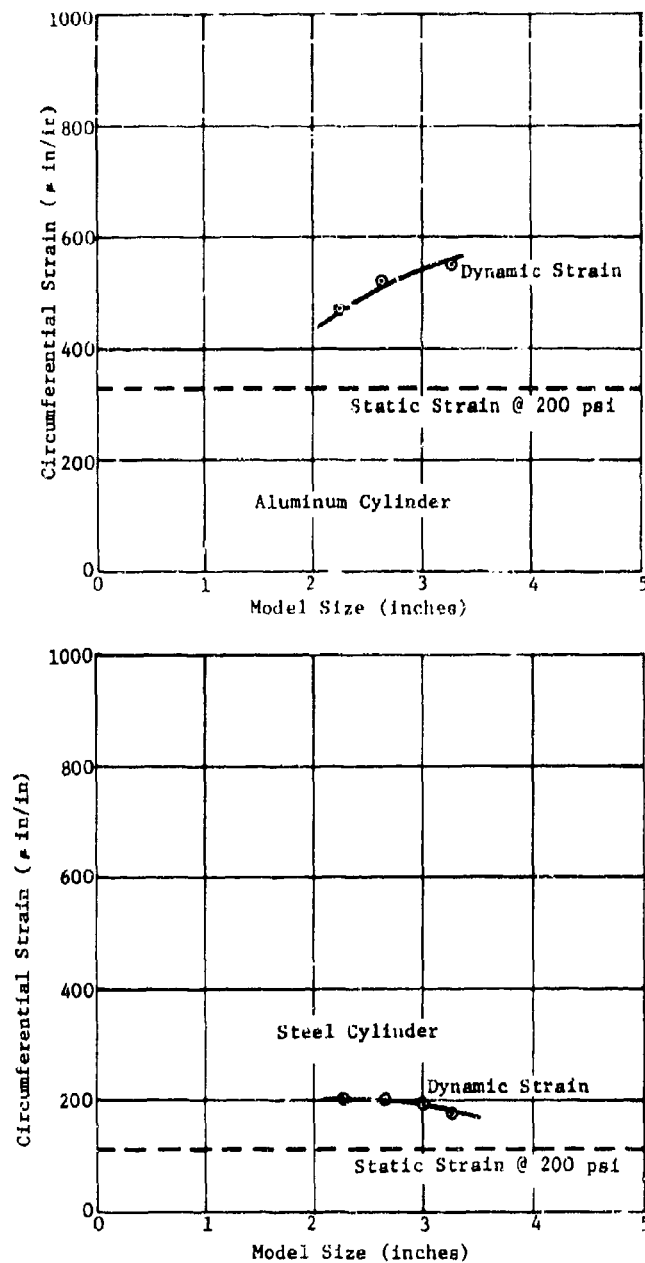
54

Figure 28. Maximum dynamic circumferential strains versus model sizes for aluminum and steel cylinders (implosion pressure of 200 psi).

55
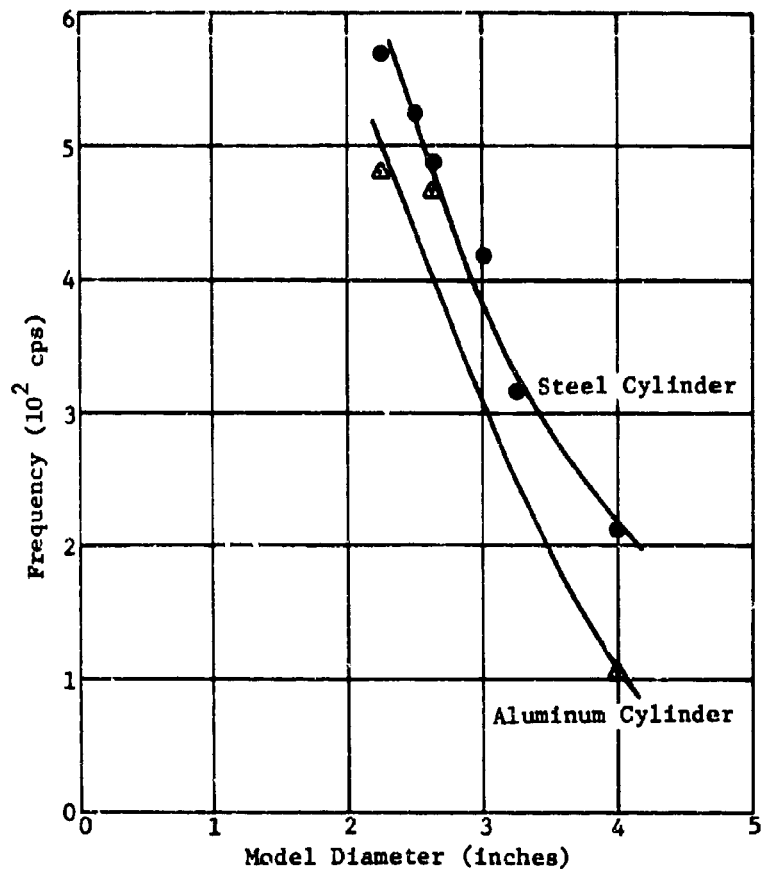
Figure 29. Circumferential strain frequency versus model size.
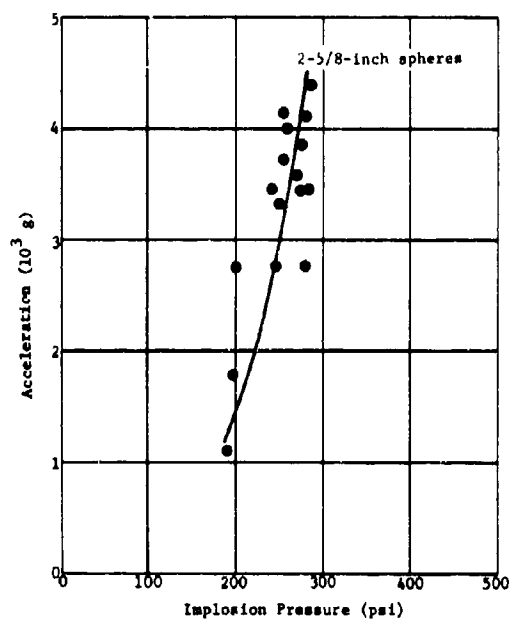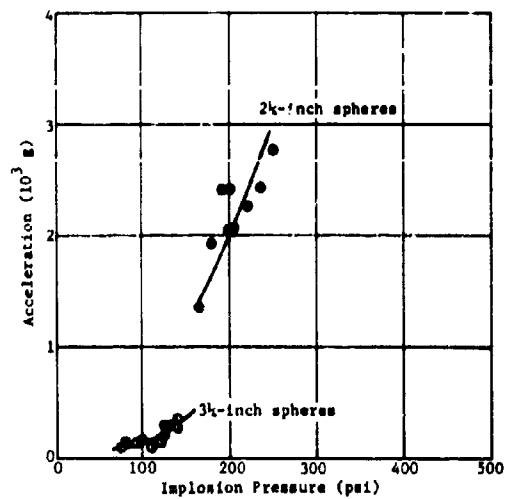
Figure 30. Peak-to-peak acceleration of the aluminum cylinder during implosions of 2¼, 2-5/8, and 3¼-inch spheres.

Figure 31. Peak-to-peak acceleration of the steel cylinder during
implosions of 2-1/4, 2-5/8, and 3-1/4-inch spheres
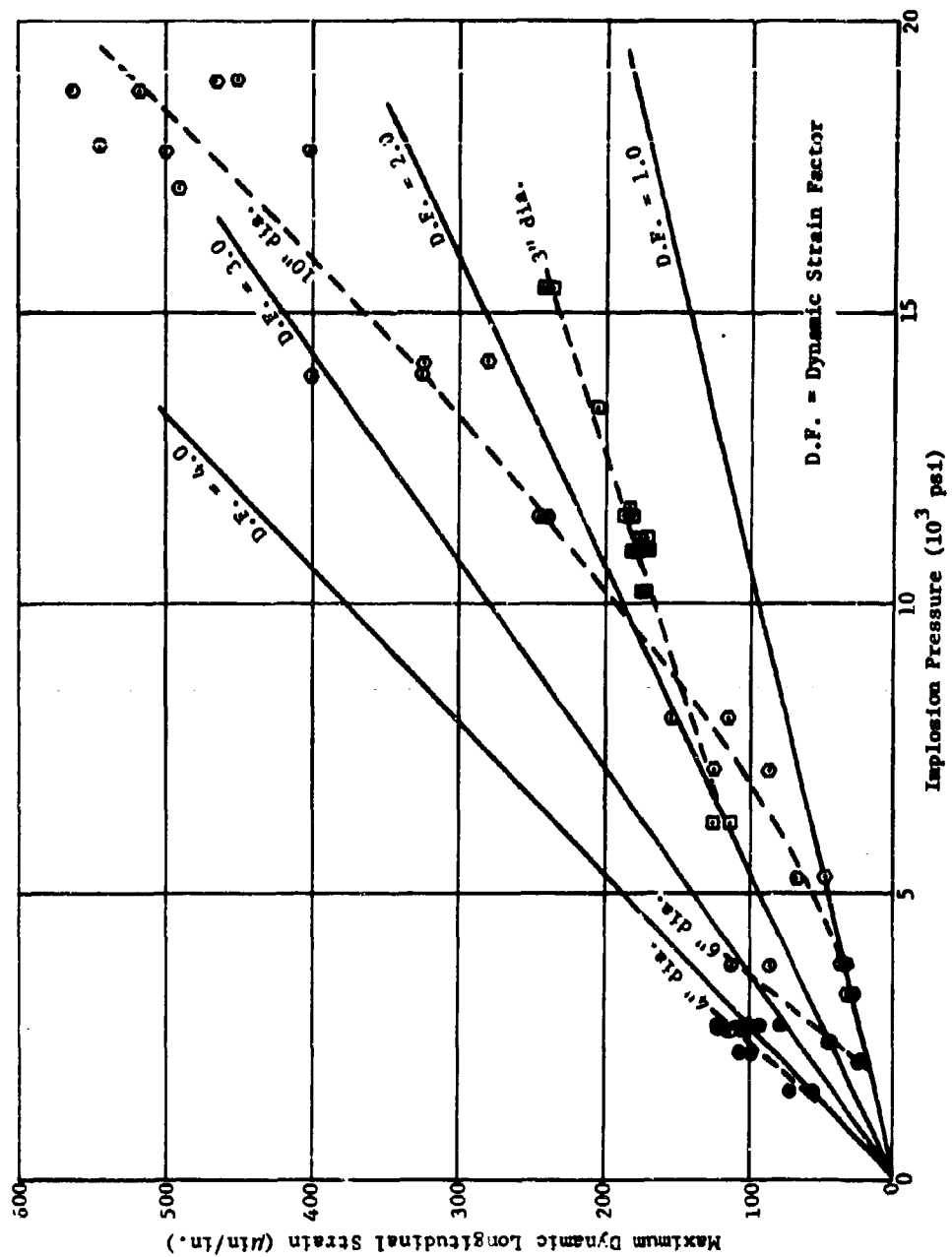
Figure 32. Maximum dynamic longitudinal strain versus the implosion pressure for various size models.

59
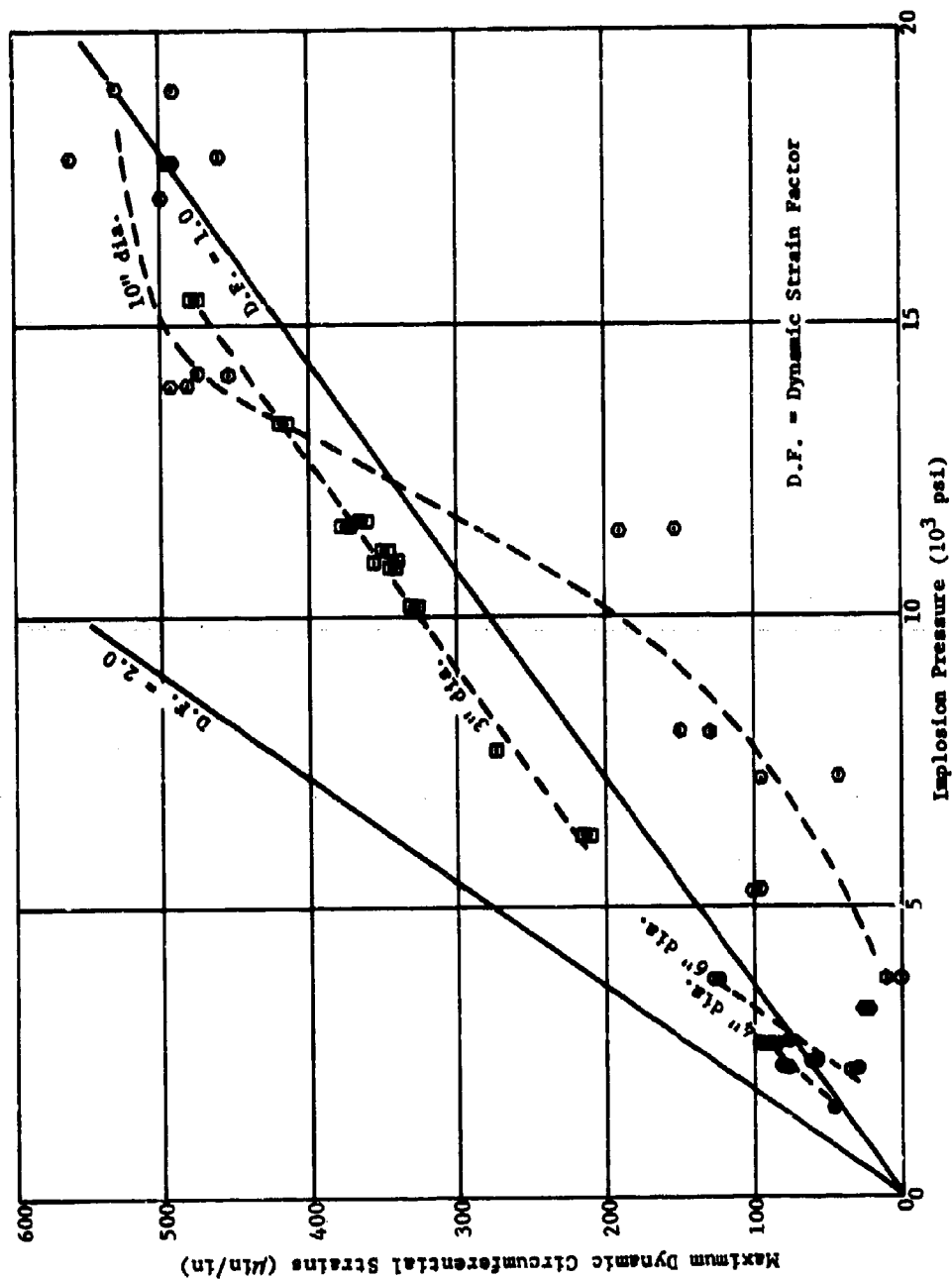
Figure 33. Maximum dynamic circumferential strain versus implosion pressure for various size models.

60
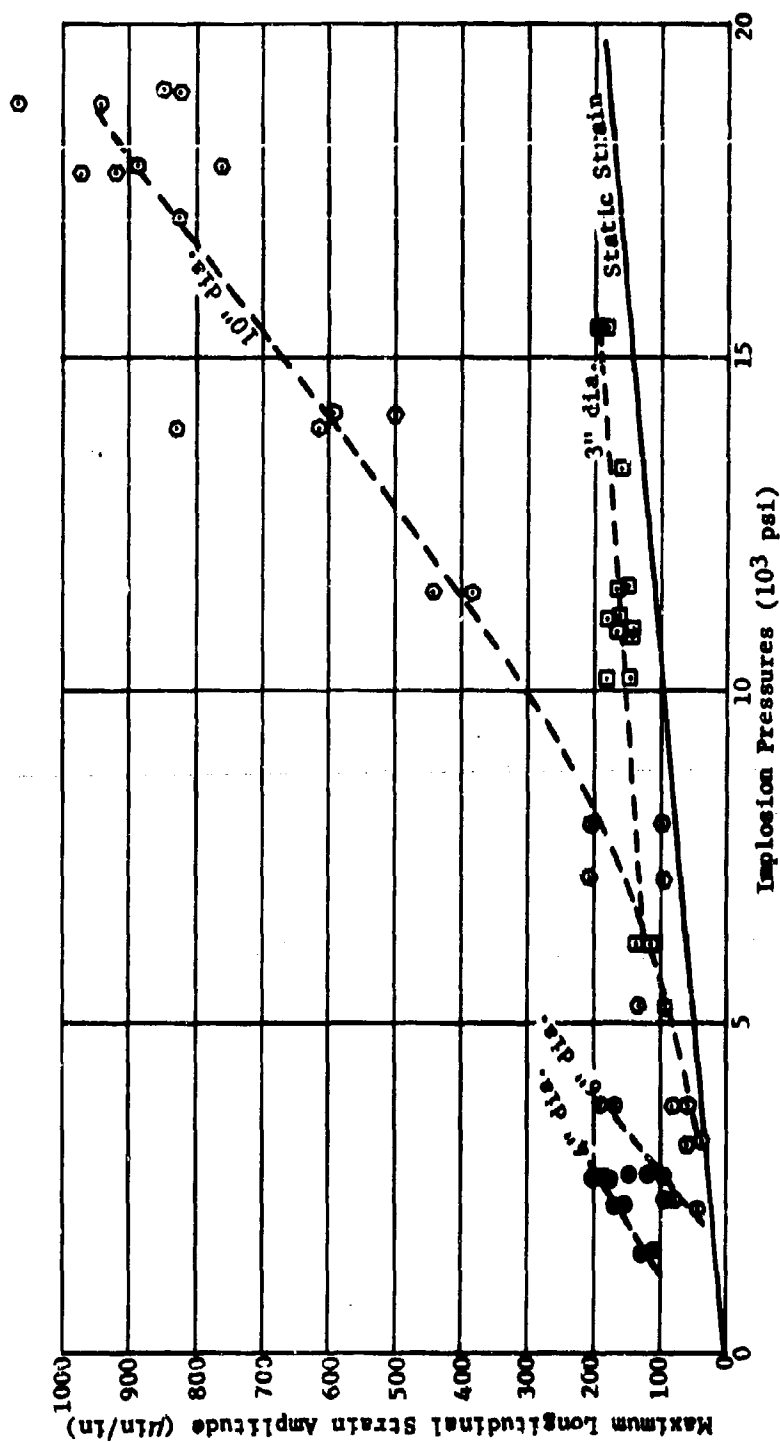
Figure 34. Maximum longitudinal strain amplitudes versus implosion pressure for various size models.

61
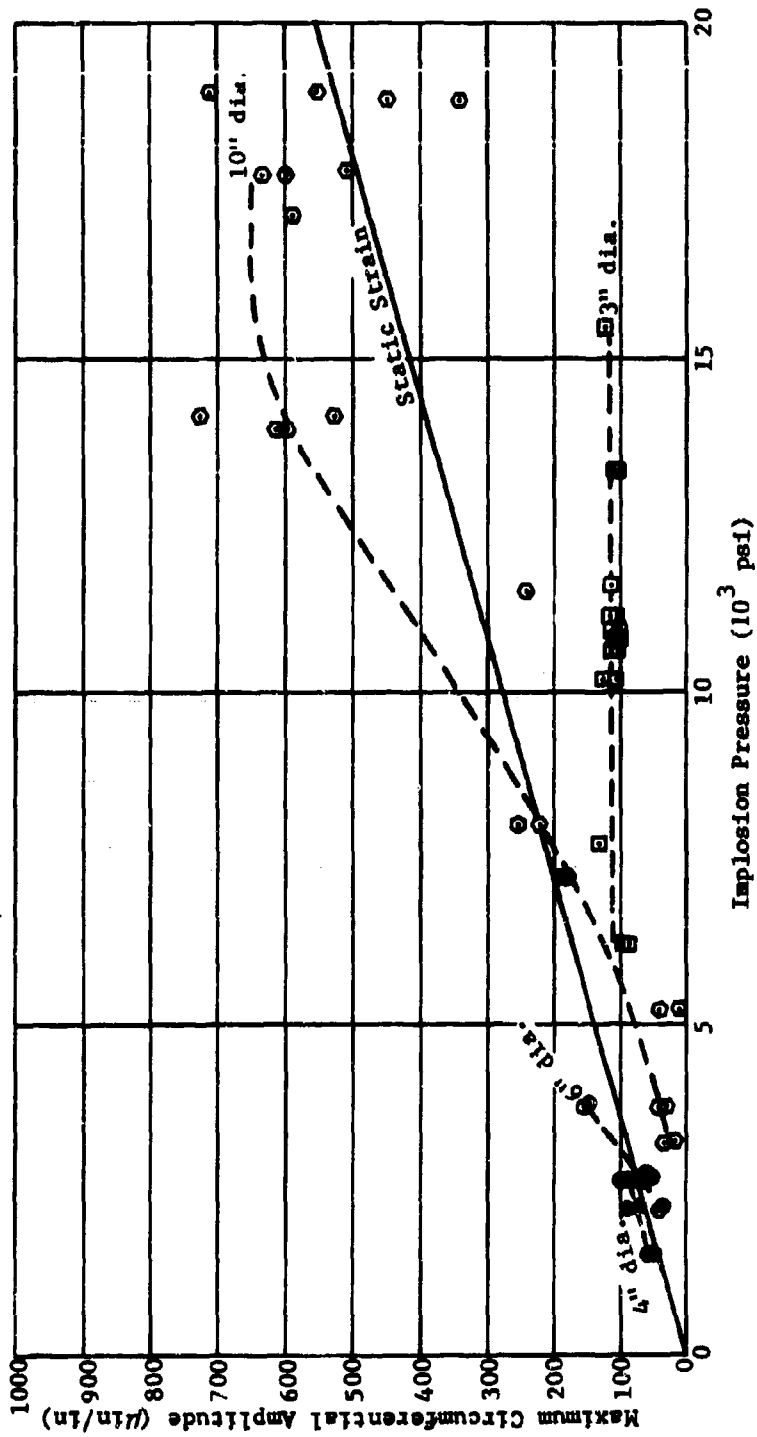
Figure 35. Maximum circumferential strain amplitudes versus implosion pressure for various size models.
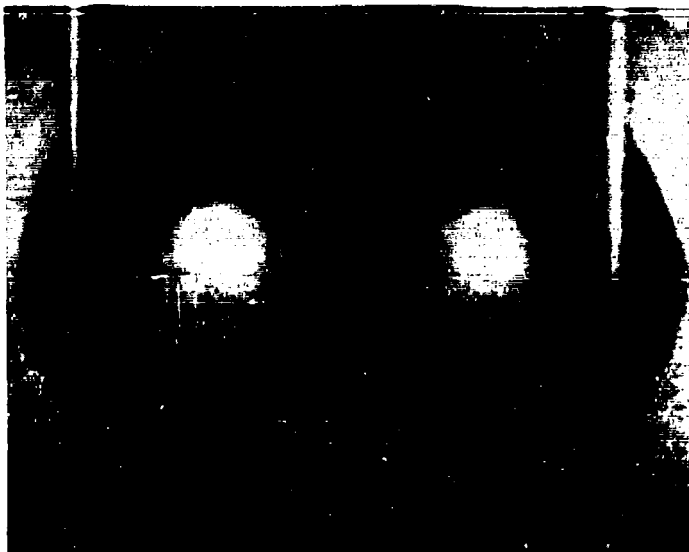
Frame 0
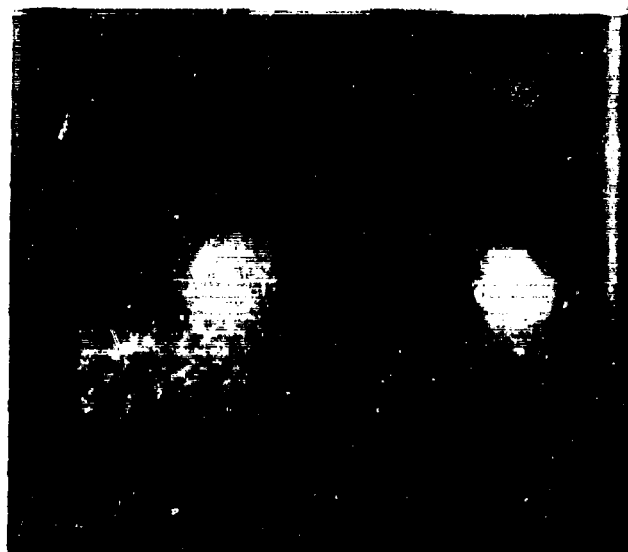
Frame 3

Frame 18

Frame 27

Figure 36. Typical collapse sequence of a 4-inch model at 3,000 frames/sec.

A.

Frame 3

Frame 9
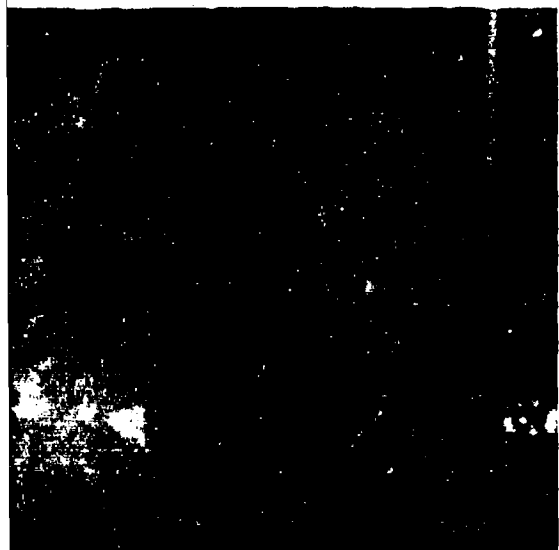
Frame 27
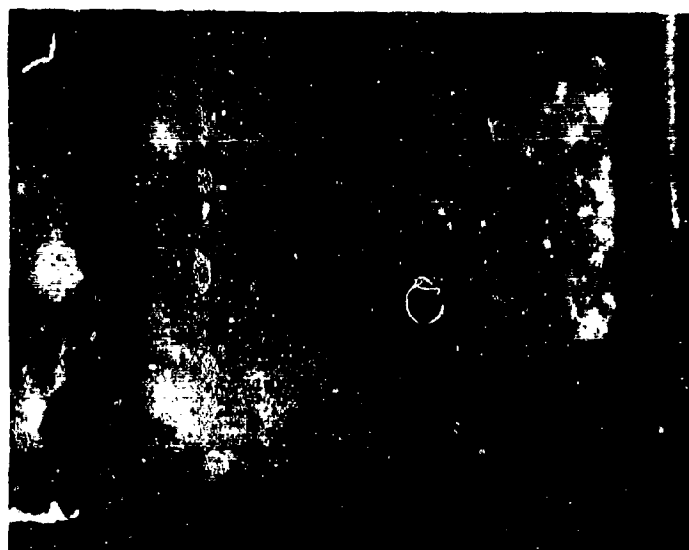
Frame 50

ollapse sequence of a 4-inch model; camera speed
frames/sec.

B.
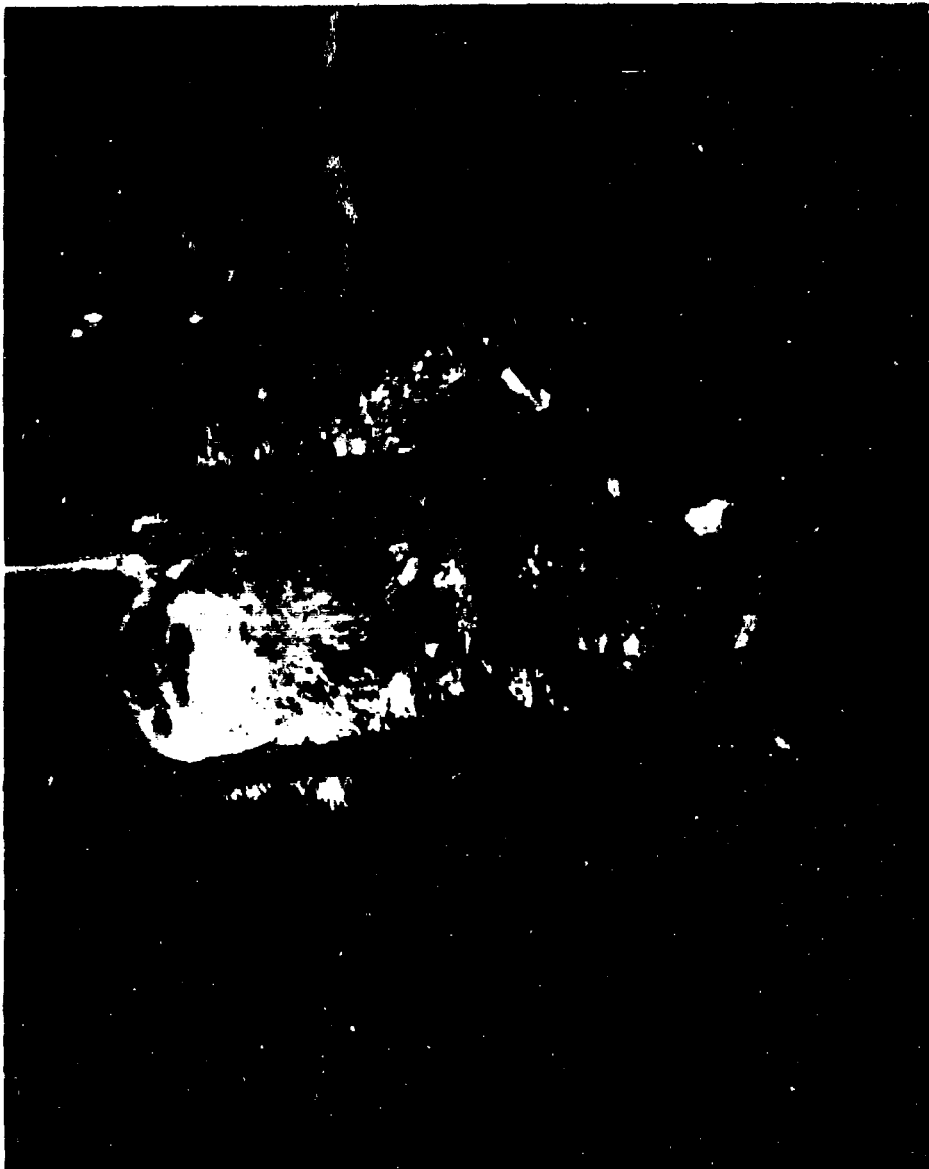
Figure 37 A typical defective implosion.

65

Figure 38. A typical close-up view of the fractured shells.

66

Figure 39. Loose pipe connections causing water to leak from the pressure vessel.

Figure 40.   Damaged o-rings of the top cover plug.

Figure 41.   Damaged o-rings of the pressure transducer probe.

Figure 42. Aluminum rods sheared off from the top cover plug.
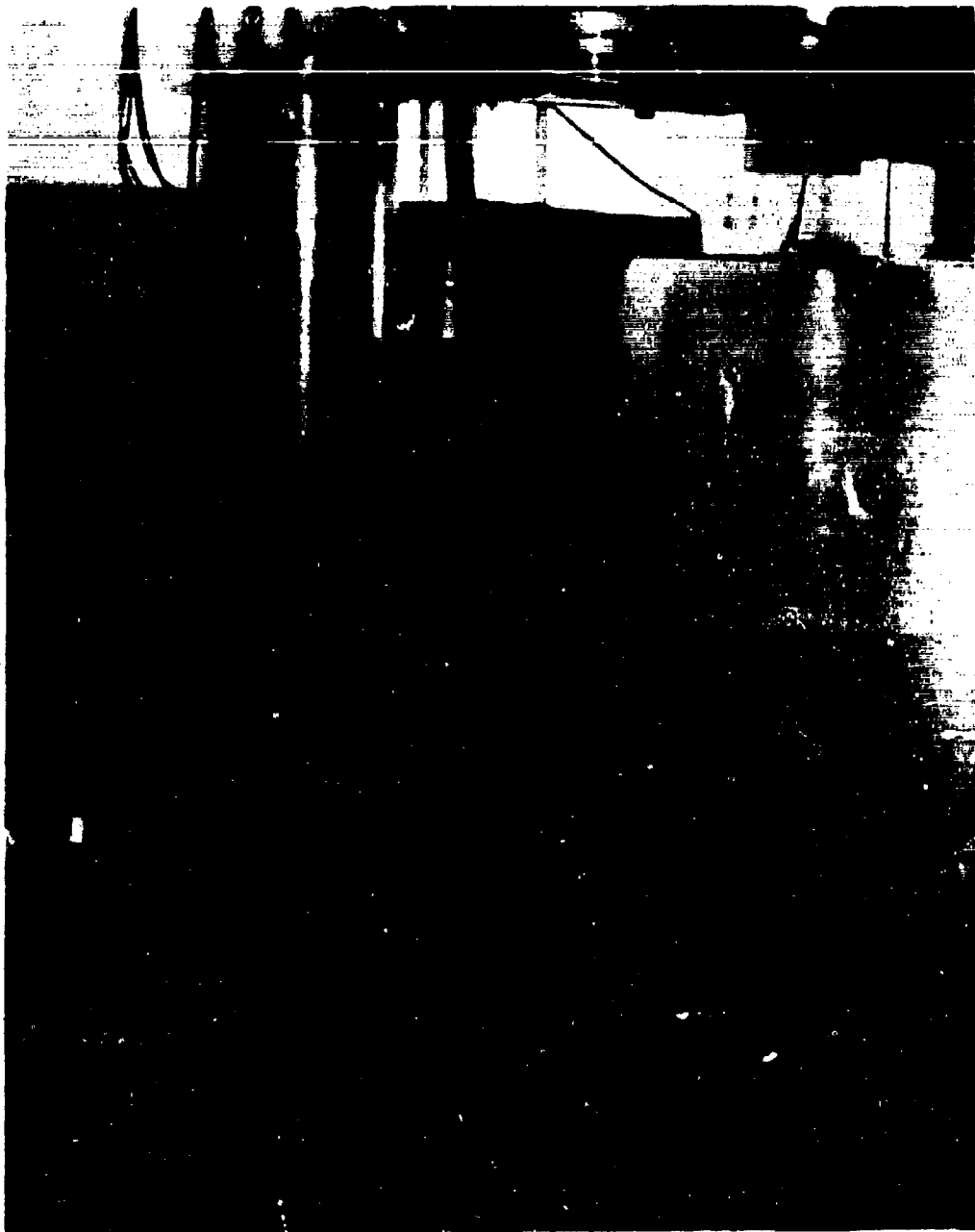
Figure 43. Aluminum frames damaged by the implosions.

Appendix

Implosion Method

To generate implosions at designated hydrostatic pressures, the ball-breaker method (Figure A-1) was tested in the glass cylinder. The method consisted of a sharp pin driven upward by a remote battery-activated solenoid. After several trials, this method was considered unsatisfactory primarily because penetration did not always cause an implosion or penetration was not always possible. The alternate method employed was to pressurize the vessel until implosion occurred.

Sealing Method

The sealing method for the glass and steel cylinders consisted a hard rubber gasket at both ends of the cylinder. Major difficulties encountered are summarized as follows:

1. Between tests, sealing materials had to be applied along the inner radius of the gasket to prevent minor leaks.

2. Considerable time had to be spent compressing the cover plates to attain maximum sealing pressures.

3. The gaskets had to be replaced after several tests.

The rubber gaskets were replaced by O-rings for the final series of tests conducted in the aluminum cylinder; no major difficulties were then encountered.

Triggering of Oscilloscopes

To record the initial phase of the dynamic response, it was necessary to trigger the oscilloscopes an instant before the implosion occurred. Since the implosion pressure was unpredictable and more sophisticated instrumentation was not available, it was difficult to trigger the oscilloscopes as desired. Therefore, a stress-induced signal from one of the transducers was employed to trigger one scope; the gate output of that scope triggered the other scopes. The result was that the pre-implosion static pressure and strains were difficult to determine from the photographed traces since some of the initial traces were generally not recorded. Therefore, the static measurements of the pressure gage and the pressure-strain calibration curves were used.

71

The transducer used for triggering the oscilloscopes was either the (1) strain gage, (2) accelerometer, or (3) pressure transducer. All three transducers presented difficulties: (1) premature triggerings occurred frequently due to sporadic high noise signals, (2) the induced signals failed many times to trigger the oscilloscopes, and (3) the triggering sensitiveness of the oscilloscope was difficult to adjust.

In a later series of low-pressure tests, the conductive paint method was finally tried. A narrow strip of conductive paint was applied to the model, with electrical leads attached and circuited to the oscilloscope. When the implosion occurred, the break in the circuit triggered the oscilloscopes; this method was more successful.

For tests conducted in the 20,000-psi pressure vessel, the conductive paint method was not used because electrical circuit connections (via the top cover to the model) could not be made easily. Instead, the strain-induced signal from one of the strain gages was employed to trigger the oscilloscopes.

Drifting Signals

The trace signals drifted during the pressurization. For the low-pressure tests, drifting of the various trace signals was tolerable; the drifting error was corrected by shifting the zero condition line until either the initial or final hydrodynamic conditions coincided approximately with the initial or final static conditions. The implosion pressure was recorded directly from the pressure gages; the static strains were determined from the pressure-strain curves.

The causes for signal drifting are not exactly known, but changes in environmental temperatures may have been a contributing factor. Other factors may be the inherent electrical drifting in the oscilloscopes, the ineffectiveness of the temperature-compensating strain gages, and the instability of the power sources.

In tests in the 20,000-psi pressure, the trace signals of the strain gages drifted completely out of the scopes, primarily because of the longer time required to attain the high collapsing pressures. To eliminate drifting, the AC stability feature of the scope was employed. This feature allows the trace to remain at constant position for a slow change in the strains. At implosion, the trace would deflect corresponding to the dynamic strains. The method of measuring implosion pressures and static strains was similar to that used in low-pressure tests.
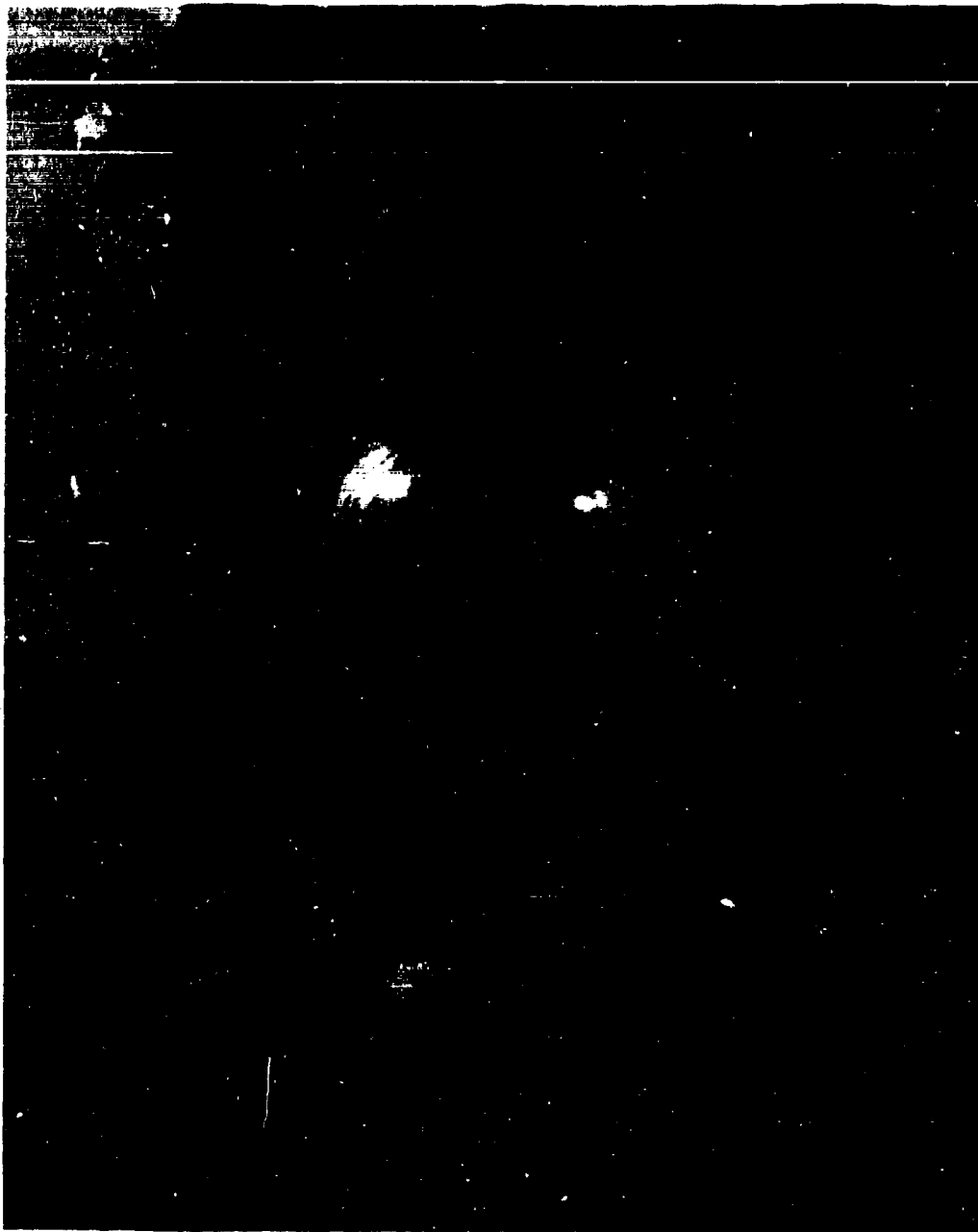
Figure A-1. The ball-breaker method.

73

Bibliography

1. Benjamin, T. B., "Pressure Waves from Collapsing Cavities," Second Symposium on Naval Hydrodynamics, September 24-28, 1956 Publication 515, pp. 325-352.

2. Boyer, D. W., "Spherical Explosions and Implosions," Institute of Aerophysics, UTIA Report No. 28, University of Toronto, November 1959.

3. Cinelli, G., "Dynamic Vibrations and Stresses in Elastic Cylinders and Spheres," Journal of Applied Mechanics, Vol. 33, No. 4, December 1966, pp. 825-830.

4. Costantino, C. J., "The Strength of Thin-Walled Cylinders Subjected to Dynamic Internal Pressures," Journal of Applied Mechanics, Vol. 32, No. 1, March 1965, pp. 104-108.

5. Hickling, R., "Some Physical Effects of Cavity Collapse in Liquids," Journal of Basic Engineering, Vol. 88, No. 1, March 1966, pp. 229-235.

6. Hunter, C., "On the Collapse of an Empty Cavity in Water," Journal of Fluid Mechanics, Vol. 8, June 1960, pp. 241-263.

7. Jones, I. R. and Edwards, D. H., "An Experimental Study of the Forces Generated by the Collapse of Transient Cavities in Water," Journal of Fluid Mechanics, Vol. 7, April 1960, pp. 596-609.

8. Kim, Y. C. and Binder, R. C., "Response of Models to Water-Shock Loading," Journal of the Engineering Mechanics, ASCE, December 1965, pp. 67-89.

9. Klein, B., "Additional Information on the Collapse of Pressure Loaded Spherical Shells," Journal of the Royal Aeronautical Society, Vol. 68, No. 645, September 1964, pp. 631-633.

10. Klein, B., "Parameters Predicting the Initial and Final Collapse Pressures of Uniformly Loaded Spherical Shells," Journal of the Aeronautical Sciences, Vol. 22, 1955, pp. 69-70.

11. Kraus, H., Thin Elastic Shells, New York, Wiley & Sons, 1967.

12. Lord Rayleigh, "On the Pressure Developed in a Liquid During the Collapse of a Spherical Cavity," Philosophical Magazine, Vol. 34, No. 200, August 1917, pp. 94-98.

13. Mellan, R. H., "An Experimental Study of the Collapse of a Spherical Cavity in Water." The Journal of the Acoustical Society of America, Vol. 28, No. 3, May 1956, pp. 447-454.

14. Nachbar, W., "The Effect of Finite Pressure-Pulse Duration on the Uniform Deformation of a Long Cylindrical Shell," Journal of Applied Mechanics, Vol. 32, No. 2, June 1965, pp. 331-336.

15. Zobell, C. E., "Some Effects of High Hydrostatic Pressures on Apparatus Observed on the Danish Galathea Deep-Sea Expedition," Deep Sea Research, Vol. 2, 1954, pp. 24-32.

DOCUMENT CONTROL DATA - R&D

(Security classification of title, body of abstract and indexing annotation must be entered when the overall report is classified)

1. ORIGINATING ACTIVITY (Corporate author)	2a. REPORT SECURITY CLASSIFICATION
Naval Civil Engineering Laboratory Port Hueneme, California 93041	Unclassified
	2b. GROUP

3. REPORT TITLE

IMPLOSIONS IN PRESSURE VESSELS, EXPERIMENTAL RESULTS

4. DESCRIPTIVE NOTES (Type of report and inclusive dates)

Final: July 1965 - June 1966

5. AUTHOR(S) (Last name, first name, initial)

Harold M. Kusano

6. REPORT DATE	7a. TOTAL NO. OF PAGES	7b. NO. OF REFS
February 1970	76	15

8a. CONTRACT OR GRANT NO.	9a. ORIGINATOR'S REPORT NUMBER(S)
b. PROJECT NO. Y-R009-03-01-004	TN-1059
c.	9b. OTHER REPORT NO(S) (Any other numbers that may be assigned this report)
d.	

10. AVAILABILITY/LIMITATION NOTICES

This document has been approved for public release and sale; its distribution is unlimited.

11. SUPPLEMENTARY NOTES	12. SPONSORING MILITARY ACTIVITY
	Naval Facilities Engineering Command

13. ABSTRACT

Pressure vessels were subjected to implosion-generated hydrodynamic pressures/impulses. The experimental results indicate the hydrodynamic pressure and the dynamic response of the pressure vessel vary, depending upon (1) model size, (2) implosion pressure, and/or (3) distance from implosion; graphs showing these relationships are presented.

Implosion pressures up to 19,000-psi were obtained. The higher implosion pressures occurred in the 20,000 psi pressure vessel and caused damage to O-rings and mounting facilities inside the pressure vessel, and loosened pipe connections from the top cover plug. High-speed motion pictures showed that the collapse of air cavities was generally asymmetric and inconsistent. The critical model sizes for maximum pressure drop or energy release in pressure vessels were determined. The effects of implosion on pressure vessels can be reduced greatly by filling the test sphere with water.

DD FORM 1473 0101-807-6800

14. KEY WORDS	LINK A		LINK B		LINK C	
	ROLE	WT	ROLE	WT	ROLE	WT
Pressure vessels						
Hydrodynamics						
Implosions						
Pressure						
Tests						
Damage						
O-ring seals						
Pipe fittings						
Collapse						
Shock wave						

INSTRUCTIONS

1. ORIGINATING ACTIVITY: Enter the name and address of the contractor, subcontractor, grantee, Department of Defense activity or other organization (corporate author) issuing the report.

2a. REPORT SECURITY CLASSIFICATION: Enter the overall security classification of the report. Indicate whether "Restricted Data" is included. Marking is to be in accordance with appropriate security regulations.

2b. GROUP: Automatic downgrading is specified in DoD Directive 5200.10 and Armed Forces Industrial Manual. Enter the group number. Also, when applicable, show that optional markings have been used for Group 3 and Group 4 as authorized.

3. REPORT TITLE: Enter the complete report title in all capital letters. Titles in all cases should be unclassified. If a meaningful title cannot be selected without classification, show title classification in all capitals in parenthesis immediately following the title.

4. DESCRIPTIVE NOTES: If appropriate, enter the type of report, e.g., interim, progress, summary, annual, or final. Give the inclusive dates when a specific reporting period is covered.

5. AUTHOR(S): Enter the name(s) of author(s) as shown on or in the report. Enter last name, first name, middle initial. If military, show rank and branch of service. The name of the principal author is an absolute minimum requirement.

6. REPORT DATE: Enter the date of the report as day, month, year; or month, year. If more than one date appears on the report, use date of publication.

7a. TOTAL NUMBER OF PAGES: The total page count should follow normal pagination procedures, i.e., enter the number of pages containing information.

7b. NUMBER OF REFERENCES: Enter the total number of references cited in the report.

8a. CONTRACT OR GRANT NUMBER: If appropriate, enter the applicable number of the contract or grant under which the report was written.

8b, 8c, & 8d. PROJECT NUMBER: Enter the appropriate military department identification, such as project number, subproject number, system numbers, task number, etc.

9a. ORIGINATOR'S REPORT NUMBER(S): Enter the official report number by which the document will be identified and controlled by the originating activity. This number must be unique to this report.

9b. OTHER REPORT NUMBER(S): If the report has been assigned any other report numbers (either by the originator or by the sponsor), also enter this number(s).

10. AVAILABILITY/LIMITATION NOTICES: Enter any limitations on further dissemination of the report, other than those imposed by security classification, using standard statements such as:

(1) "Qualified requesters may obtain copies of this report from DDC."

(2) "Foreign announcement and dissemination of this report by DDC is not authorized."

(3) "U. S. Government agencies may obtain copies of this report directly from DDC. Other qualified DDC users shall request through

."

(4) "U. S. military agencies may obtain copies of this report directly from DDC. Other qualified users shall request through

."

(5) "All distribution of this report is controlled. Qualified DDC users shall request through

."

If the report has been furnished to the Office of Technical Services, Department of Commerce, for sale to the public, indicate this fact and enter the price, if known.

11. SUPPLEMENTARY NOTES: Use for additional explanatory notes.

12. SPONSORING MILITARY ACTIVITY: Enter the name of the departmental project office or laboratory sponsoring (paying for) the research and development. Include address.

13. ABSTRACT: Enter an abstract giving a brief and factual summary of the document indicative of the report, even though it may also appear elsewhere in the body of the technical report. If additional space is required, a continuation sheet shall be attached.

It is highly desirable that the abstract of classified reports be unclassified. Each paragraph of the abstract shall end with an indication of the military security classification of the information in the paragraph, represented as (TS), (S), (C), or (U).

There is no limitation on the length of the abstract. However, the suggested length is from 150 to 225 words.

14. KEY WORDS: Key words are technically meaningful terms or short phrases that characterize a report and may be used as index entries for cataloging the report. Key words must be selected so that no security classification is required. Identifiers, such as equipment model designation, trade name, military project code name, geographic location, may be used as key words but will be followed by an indication of technical context. The assignment of links, rules, and weights is optional.